crystals

MDPI

Review

Metal Hydrides for Hydrogen Storage: Mechanisms, Advances, and Applications

Zeynep Erdem [1,*], Battal Doğan [2] and Ahmet Güral [3]

[1] Department of Metallurgy and Materials Engineering, Faculty of Engineering and Natural Sciences, Ankara Yıldırım Beyazıt University, Ankara 06010, Turkey
[2] Department of Energy Systems Engineering, Faculty of Technology, Gazi University, Ankara 06560, Turkey; battaldogan@gazi.edu.tr
[3] Department of Metallurgy and Materials Engineering, Faculty of Technology, Gazi University, Ankara 06560, Turkey; agural@gazi.edu.tr
* Correspondence: zeynep.erdem@aybu.edu.tr

Abstract

Hydrogen is an important energy carrier for a low-carbon energy system, but its storage remains a major challenge because of its low volumetric density. Metal hydrides have been widely studied as solid-state hydrogen storage materials due to their high volumetric hydrogen density, improved safety, and ability to operate at relatively low pressures. This review examines the mechanisms and material classes used in metal hydride-based hydrogen storage systems. The fundamental processes of hydrogen absorption and desorption in metal lattices are first described. Major hydride groups are then evaluated, including intermetallic hydrides, light metal hydrides, complex hydrides, and emerging high-entropy hydrides. Particular attention is given to complex hydride subgroups such as alanates, borohydrides, amides and imides, together with the closely related metal ammine complexes and nitride-based systems. These materials offer high hydrogen storage capacities but often show limitations such as high desorption temperatures and slow reaction kinetics. Recent strategies to address these limitations are reviewed, including catalyst addition, nanostructuring, ion substitution, and composite formation. Although significant progress has been made in improving the performance of these materials, challenges related to thermodynamics, kinetics, and practical implementation remain. Continued material development and system optimization are required to enable the broader application of metal hydrides in hydrogen storage technologies.

Keywords: metal hydrides; hydrogen storage; energy storage; solid-state hydrogen storage; hydrogen economy; material optimization

Check for updates

Academic Editor:
Jesús Sanmartín-Matalobos

Received: 1 September 2026
Revised: 26 October 2026
Accepted: 27 October 2026
Published: 18 November 2026

Copyright: © 2026 by the authors. Licensee MDPI, Basel, Switzerland. This article is an open access article distributed under the terms and conditions of the Creative Commons Attribution (CC BY) license.

1. Introduction

The intermittency of renewable electricity sources such as solar and wind requires large-scale energy storage, and hydrogen produced by water electrolysis is increasingly considered as a carbon-free secondary energy carrier that releases only water when it is converted in a fuel cell [1,2].

Hydrogen offers a solution to the long charging times encountered in electric vehicles, providing sustainable solutions without requiring users to change their habits. Hydrogen technologies resemble the rapid fuel supply that users have previously experienced and are therefore considered to have higher commercialisation potential. The unit energy value of hydrogen is considerably higher than that of existing fossil fuels, and the minimisation of

emission levels increases hydrogen's appeal. At 25 °C and 1 atm, hydrogen's lower heating value per unit mass is approximately 119.96 kJ·g^{-1} [3], which is considerably higher than that of petrol (43.4 kJ·g^{-1}); this means that more energy can be obtained per unit mass. However, the volumetric energy density of hydrogen strongly depends on its physical state and storage conditions. At 25 °C and 1 atm, gaseous hydrogen has a volumetric lower heating value of approximately 0.010 MJ·L^{-1}, whereas liquid hydrogen near its normal boiling point (approximately −253 °C at 1 atm) has a value of approximately 8.5 MJ·L^{-1}. Even in the liquid state, this value remains considerably lower than the volumetric lower heating value of liquid petrol (31.8 MJ·L^{-1}), highlighting the technical challenges associated with hydrogen storage and transport [4]. Hydrogen exhibits a high gravimetric energy density, but a relatively low volumetric energy density compared to conventional fuels. On the left of Figure 1, the electrochemical conversion of hydrogen in a fuel cell is schematically illustrated, producing electricity and heat with water as the only by-product. In the centre of Figure 1, a net-zero-based hydrogen energy cycle is presented, including renewable energy-driven electrolysis, hydrogen production, storage, and utilization pathways. The main disadvantage of hydrogen, the primary energy source for fuel cells, is the storage difficulties arising from its low density. Hydrogen can be stored using various methods, such as compressed gas, liquefied form, cryogenic compression or chemical adsorption. Although the storage method varies depending on the area where hydrogen will be applied, fuel tanks in transport vehicles must be lightweight yet durable. However, the large storage volumes of hydrogen cause compressed storage tanks to become excessively large, preventing vehicles from achieving the desired dimensions and fuel capacity. For this reason, storing hydrogen by absorbing it into specific materials, rather than storing it directly, has been accepted as an effective solution to hydrogen's low density. This study schematically illustrates hydrogen's high gravimetric energy density and its role in the sustainable energy cycle in Figure 1.

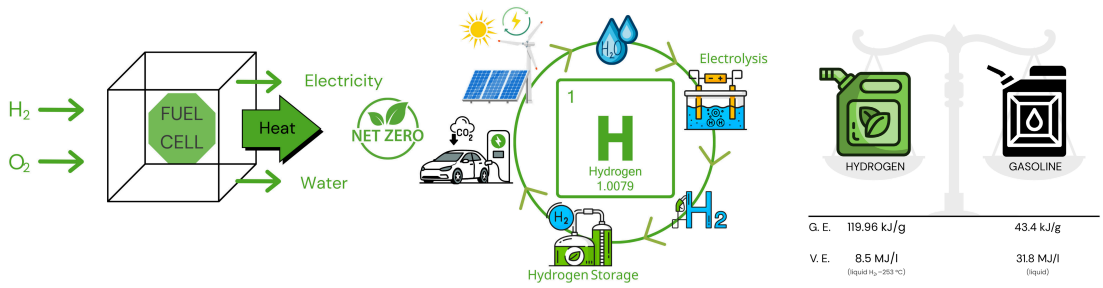


Figure 1. Fundamental energy characteristics of hydrogen and its role within a sustainable energy cycle. (**Left**) Electrochemical conversion of hydrogen in a fuel cell, producing electricity and heat with water as the only by-product. (**Centre**) Net-zero hydrogen energy cycle: renewable-powered electrolysis, hydrogen production, storage and use. (**Right**) Gravimetric (G.E.) and volumetric (V.E.) energy densities (lower heating values) of hydrogen and petrol; the V.E. of hydrogen refers to liquid hydrogen at −253 °C and 1 atm (gaseous hydrogen at 25 °C and 1 atm: about 0.010 MJ·L^{-1}).

Although Robert Boyle produced a flammable gas by dissolving iron in dilute acid as early as 1671, hydrogen was first recognised as a distinct element by Henry Cavendish in 1766 [5,6].

Molecular hydrogen produces water and heat energy through a chemical reaction with air:

$$H_2(g) + O_2(g) \rightarrow H_2O(l) \quad \Delta H^\circ = -286\ \text{kJ} \cdot \text{mol}^{-1} \tag{1}$$

The energy of −286 kJ mol^{-1} in Equation (1) is the standard reaction enthalpy with liquid water as the product and therefore corresponds to the higher heating value (HHV) of hydrogen, 141.8 kJ g^{-1}; with water vapour as the product, the corresponding lower heating value (LHV) is about 120 kJ g^{-1} [3]. Unless stated otherwise, energy densities in this review

are lower heating values. This chemical reaction can be carried out in a hydrogen fuel cell to generate electrical energy instead of heat. The energy obtained from the combustion of hydrogen can be used to power cars. This way, instead of polluting emissions, only water and heat are released [7].

The basic atomic and molecular constants of protium and deuterium are summarised in Table 1 for reference [7–9]; isotope effects are not discussed further in this review.

Table 1. Some properties of Protium and Deuterium [7,9].

Atomic Hydrogen	**Protium**	**Deuterium**
Atomic number	1	1
Atomic weight	1.0080 u	2.0141 u
Ionisation potential	13.595 eV	13.600 eV
Electron affinity	0.7542 eV	0.754 eV
Nuclear spin	1/2	1
Nuclear magnetic moment (nuclear magneton)	2.7927	0.8574
Nuclear quadrupole moments	0	2.77×10^{-27} cm^2
Electronegativity (Pauling)	2.1	~2.1
Molecular Hydrogen		
Bond length	0.7416 Å	0.7416 Å
Dissociation energy (25 °C)	104.19 kcal/mol	105.97 kcal/mol
Ionisation potential	15.427 eV	15.457 eV
Solid density	0.08671 g/cm^3	0.1967 g/cm^3
Melting heat	28 cal/mol	47 cal/mol
Liquid density	0.07099 g/cm^3 (–252.78 °C)	0.1630 g/cm^3 (–249.75 °C)
Boiling point	–252.77 °C	–249.49 °C
Vaporisation heat	216 cal/mol	293 cal/mol
Critical density	0.0310 g/cm^3	0.0668 g/cm^3
Heat of combustion to gaseous water (per mole)	–57.796 kcal/mol	–59.564 kcal/mol

Table 2 summarises the main thermophysical properties of hydrogen [7]. Because its critical temperature is about −240 °C, hydrogen cannot be liquefied by compression at room temperature, and liquid storage therefore requires cryogenic operation.

Table 2. Thermodynamic properties of hydrogen at 25 °C and 1 atm pressure [7].

Feature	**Value**
Specific volume (m^3/kg)	12.1
Liquid density at atmospheric pressure (kg/m^3)	71.0
Absolute viscosity (centipoises)	0.009
Sound velocity in gas (m/s)	1315
Specific heat, c_p (kJ/kgK)	14.310
Specific heat ratio, c_p/c_v	1.405
Gas constant, R (kJ/kg °C)	4.126
Thermal conductivity (W/m°C)	0.182
Boiling point (1 atm) (K)	20.4
Heat of vaporisation at boiling point (kJ/kg)	447
Freezing point (1 atm) (°C)	–259.1

Table 2. *Cont.*

Feature	Value
Freezing heat (J/kg)	58,000
Critical temperature (°C)	–240.0
Critical pressure (MN/m^2)	1.30
Critical volume (m^3/kg)	0.033
Higher heating value (kJ/kg)	141,800 [a]

[a] Higher heating value calculated from the standard enthalpy of formation of liquid water, $\Delta fH° = -285.83$ kJ mol^{-1} [3], i.e., 285.83 kJ mol^{-1}/2.016 g mol^{-1} ≈ 141.8 kJ g^{-1}. Ref. [7] lists a heat of combustion of 144,000 kJ/kg.

Hydrogen is often labelled with a colour code according to its production route (Figure 2) [10–15]: grey hydrogen is produced from fossil fuels by steam methane reforming or coal gasification, blue hydrogen is grey hydrogen combined with carbon capture and storage, turquoise hydrogen is produced by methane pyrolysis, in which the carbon is obtained as solid carbon black, and green hydrogen is produced by water electrolysis with renewable electricity [16]. Because real production routes do not always fit a single colour, policy decisions should rather be based on life-cycle greenhouse-gas emissions [16].



Figure 2. Different hydrogen production methods, classified by the colour code commonly used in the literature, with a short description and the main reaction(s) of each pathway.

Figure 3 shows a comparative overview of the hydrogen storage capacities of adsorbents, metal hydrides and chemical hydrogen carriers, along with their hydrogen absorption/desorption temperatures. Although adsorbent materials can operate at low temperatures, they generally fall short of Department of Energy (DOE) system targets. Metal hydrides offer moderate gravimetric capacity but mostly require high hydrogen desorption temperatures. Chemical hydrogen carriers, on the other hand, have high capacities approaching DOE final targets but have limitations in terms of reversibility and system integration [12,17,18]. The figure was drawn by the authors from the material-level experimental capacities compiled in the Table 3, Table 4 and Table 6 and from representative adsorbent data [18]; the dashed lines mark the DOE gravimetric system targets of 5.5 wt.% for 2025 and 6.5 wt.% (ultimate) [17]. Because these targets refer to the complete storage system, a material must exceed them by a considerable margin (Section 3.2).

Table 3. Comparison of the properties of selected light metal hydrides (n/a: not available). Experimental capacities are marked (R) for reversible capacities measured on rehydrogenation or cycling and (D) for hydrogen released on the first decomposition only; abbreviations and definitions are given below the table.

Hydride Class	Metal/ Alloy	Hydride	Synthesis Method	Synthesis Conditions	Character-isation	Activation	T_{abs} (°C)	p_{abs} (MPa)	T_{des} (°C)	p_{des} (MPa)	ΔH_{abs} (kJ mol^{-1} H_2)	ΔH_{des} (kJ mol^{-1} H_2)	w_{th} (wt.%)	w_{exp} (wt.%)	ρ_{th} (kg H_2 m^{-3})	ρ_{exp} (kg H_2 m^{-3})	Ref.
Light Metal Hydrides	Mg	MgH_2 (Comm.)	Direct Hydrogena-tion	400 °C 10 MPa	XRD	Slow kinetics	350	2	350	0.2	−74.5	74.5	7.6	7.6 (R)	110	110	[19]
Light Metal Hydrides	Mg	MgH_2 (Ball Milled)	Reactive Ball Milling	Milling under H_2 50 h	XRD SEM	Direct use	300	1	300	0.1	−74	74	7.6	7 (R)	110	100	[20]
Light Metal Hydrides	Mg	MgH_2 + 5wt.% Nb_2O_5	Catalysed Ball Milling	Nb_2O_5 additive	XRD XPS	Improved kinetics	250	1	250	0.1	−74	74	7.6	6.8 (R)	110	98	[21]
Light Metal Hydrides	Mg	MgH_2 + Graphene	Nanocom-posite	Milling with graphene	TEM Raman	Fast kinetics	200	1	250	0.1	−74	74	7.6	6.5 (R)	110	90	[22]
Light Metal Hydrides	Mg	MgH_2 + TiH_2	Composite	Ball milling MgH_2+TiH_2	XRD	Catalytic	250	1	300	0.1	−70	70	6.5	5.5 (R)	n/a	n/a	[23]
Light Metal Hydrides	Mg	MgH_2 + V	Composite	Ball milling with V	XRD	Catalytic	200	1	250	0.1	−74	74	7	6 (R)	110	95	[24]
Light Metal Hydrides	Mg	MgH_2 + Ni	Composite	Ball milling with Ni	XRD	Catalytic	250	1	300	0.1	−70	70	7	6.5 (R)	110	100	[25]
Light Metal Hydrides	Mg	MgH_2 + CNT	Composite	Carbon Nanotubes	SEM TEM	Catalytic	250	1	300	0.1	−74	74	7.6	6.5 (R)	110	90	[26]
Light Elemental Hydrides	Li	LiH	Direct Synthesis	700 °C	XRD	Stable	700	0.1	900	0.1	−180	180	12.7	12.5 (D)	97	95	[27]
Light Elemental Hydrides	Al	AlH_3 (Alane)	Chemical Synthesis	$LiAlH_4$ + $AlCl_3$	XRD TGA	Metastable	n/a	n/a	150	n/a	−7.6	7.6 (en-dothermic)	10.1	10 (D)	148	145	[28]

n/a: not available. T_{abs}, p_{abs}, T_{des}, p_{des}: temperature and hydrogen pressure of absorption and desorption; ΔH_{abs}, ΔH_{des}: absorption (formation) enthalpy, given as a negative value, and desorption (decomposition) enthalpy, given as a positive value; entries marked "exothermic" or "endothermic" indicate that only the sign of the heat effect was reported. w_{th}, ρ_{th}: theoretical gravimetric and volumetric capacities, calculated from the stoichiometry of the ideal hydride and referred to the mass or volume of the hydride. w_{exp}, ρ_{exp}: experimental capacities measured in the cited study; (R) denotes a reversible capacity measured on rehydrogenation or cycling, and (D) denotes hydrogen released on the first dehydrogenation, which is not claimed to be reversible under the stated conditions. The same definitions are used in all hydride tables of this review, and all capacities are material-level values (Section 7); system-level values are lower (Section 3.2).

Table 4. Comparison of physicochemical properties and hydrogen storage performance of selected metal hydrides (n/a: not available). Experimental capacities are marked (R) for reversible capacities and (D) for hydrogen released on the first decomposition only; other abbreviations and definitions as in Table 3.

Hydride Class	Metal/ Alloy	Hydride	Synthesis Method	Synthesis Conditions	Character-isation	Activation	T_{abs} (°C)	p_{abs} (MPa)	T_{des} (°C)	p_{des} (MPa)	ΔH_{abs} (kJ mol^{-1} H_2)	ΔH_{des} (kJ mol^{-1} H_2)	w_{th} (wt.%)	w_{exp} (wt.%)	ρ_{th} (kg H_2 m^{-3})	ρ_{exp} (kg H_2 m^{-3})	Ref.
Alanates	NaAl	$NaAlH_4$	Direct Synthesis	High pressure/temp	XRD	Slow	180	15	230	0.1	−37	37	7.4	3.0 (R)	n/a	n/a	[29]
Alanates	NaAl	$NaAlH_4$ + $TiCl_3$	Doped Ball Milling	2 mol% Ti catalyst	XRD	Fast	120	10	150	0.1	−37	37	7.4	4.9 (R)	n/a	n/a	[29]
Alanates	NaAl	$NaAlH_4$ + $ScCl_3$	Doped Ball Milling	Sc catalyst	XRD	Fast	100	10	140	0.1	−37	37	7.4	5 (R)	n/a	n/a	[30]
Alanates	LiAl	$LiAlH_4$	Schlesinger reaction (metathesis)	4LiH + $AlCl_3$ in ether	XRD	Not reversible at moderate conditions	n/a	n/a	150–200 (step 1); 200–270 (step 2)	n/a	n/a (irreversible)	−10 (step 1, exothermic); +25 (step 2)	10.6 (7.9 for steps 1 + 2)	7.9 (D)	n/a	n/a	[31, 32]
Alanates	KAl	$KAlH_4$	Direct Synthesis	K + Al + H_2	XRD	Moderate	250	10	300	0.1	n/a	n/a	5.7	4.5 (R)	n/a	n/a	[33]
Alanates	MgAl	$Mg(AlH_4)_2$	Metathesis	$MgCl_2$ + $NaAlH_4$	XRD	Unstable	n/a	n/a	140	n/a	n/a	Exothermic	9.3	7 (D)	n/a	n/a	[34]
Alanates	CaAl	$Ca(AlH_4)_2$	Metathesis	$CaCl_2$ + $NaAlH_4$	XRD	Unstable	n/a	n/a	130	n/a	n/a	Exothermic	7.7	5 (D)	n/a	n/a	[34]
Borohydrides	LiB	$LiBH_4$	Direct Synthesis	LiH + B + H_2 (High P)	XRD	High stability	350	10	400	0.1	−74	74	18.5	13.5 (D)	121	90	[35]
Borohydrides	LiB	$LiBH_4$ + SiO_2	Nanoconfinement	Melt infiltration in SBA-15	BET XRD	Lower Temp	300	5	300	0.1	−55	55	18.5	8.0 (D, per composite mass)	121	50	[36]
Borohydrides	MgB	$Mg(BH_4)_2$	Metathesis	$MgCl_2$ + $2LiBH_4$	XRD NMR	Complex	270	10	290	0.1	−39	39	14.8	11 (D)	112	85	[37]
Borohydrides	MgB	$Mg(BH_4)_2$ + $TiCl_3$	Doped	Ball Milling	XRD	Catalytic	200	10	250	0.1	−39	39	14.8	10.5 (D)	112	80	[38]
Borohydrides	CaB	$Ca(BH_4)_2$	Metathesis	$CaCl_2$ + $LiBH_4$	XRD	Moderate	350	20	360	0.1	−32	32	11.6	8.5 (D)	84	60	[39]
Borohydrides	Y	$Y(BH_4)_3$	Metathesis	YCl_3 + $LiBH_4$	XRD	Unstable	n/a	n/a	200	0.1	n/a	Endothermic	9	7.2 (D)	n/a	n/a	[40]
Borohydrides	Zn	$Zn(BH_4)_2$	Metathesis	$ZnCl_2$ + $NaBH_4$	XRD	Unstable	n/a	n/a	85	n/a	n/a	Exothermic	8.4	5 (D)	n/a	n/a	[41]
Complex Hydrides (RHC)	Li-Mg-B	$2LiBH_4$ + MgH_2	Ball Milling	2:1 molar ratio	XRD DSC	Coupled reaction	350	3	350	0.1	−46	46	11.4	9 (R)	n/a	n/a	[42, 43]
Complex Hydrides (RHC)	Ca-Mg-B	$Ca(BH_4)_2$ + MgH_2	Ball Milling	Molar ratio	XRD	Coupled	350	5	350	0.1	n/a	n/a	8.5	7 (D)	n/a	n/a	[44]

Table 4. *Cont.*

Hydride Class	Metal/ Alloy	Hydride	Synthesis Method	Synthesis Conditions	Character-isation	Activation	T_{abs} (°C)	p_{abs} (MPa)	T_{des} (°C)	p_{des} (MPa)	ΔH_{abs} (kJ mol^{-1} H_2)	ΔH_{des} (kJ mol^{-1} H_2)	w_{th} (wt.%)	w_{exp} (wt.%)	ρ_{th} (kg H_2 m^{-3})	ρ_{exp} (kg H_2 m^{-3})	Ref.
Complex Hydrides (RHC)	Li-Mg-B	$LiBH_4$ + $0.5MgH_2$	Ball Milling	Composite	DSC	Coupled	350	4	350	0.1	n/a	n/a	10	8 (R)	n/a	n/a	[42]
Nitride-based (related group)	Li	Li_3N	Direct Synthesis	Li + N_2	XRD	Reversible	200	0.1	250	0.1	−165	165	10.4	5.0 (R)	n/a	n/a	[45]
Complex Hydrides (Amide)	LiN	$LiNH_2$ + LiH	Ball Milling	Mixture	XRD	Standard	n/a	n/a	n/a	n/a	n/a	n/a	6.5	n/a	n/a	n/a	[45]
Complex Hydrides (Amide)	MgN	$Mg(NH_2)_2$	Ball milling under NH_3	Metal hydride + NH_3, room temperature	XRD	–	n/a	n/a	releases NH_3 (not H_2) on heating	n/a	n/a	n/a	7.1	n/a (NH_3 release)	n/a	n/a	[46]
Complex Hydrides (Composite)	Li-Mg-N	$2LiNH_2$ + MgH_2	Ball Milling	Post-milling	XRD	Interaction	180	5	200	0.1	−40	40	5.6	4.5 (R)	n/a	n/a	[47]
Nitride-based (related group)	Ca	Ca_2NH	Hydrogenation	Ca_3N_2 + H_2	XRD	High Temp	400	10	500	0.1	n/a	n/a	2.1	1.8 (D)	n/a	n/a	[48]
B–N Chemical Hydride (metal-free)	NH_3B	NH_3BH_3 (Ammonia Borane)	Chemical	Metathesis	NMR	Irreversible	n/a	n/a	100	n/a	n/a	Exothermic	19.6	14 (D)	145	100	[49]
Metal Amidoboranes (B–N compounds)	Li-N-B	$LiNH_2BH_3$	Ball Milling	$LiNH_2$ + BH_3	XRD	Unstable	90	n/a	95	n/a	n/a	Exothermic	10.9	7 (D)	n/a	n/a	[50]
Metal Amidoboranes (B–N compounds)	Na-N-B	$NaNH_2BH_3$	Ball Milling	$NaNH_2$ + BH_3	XRD	Unstable	80	n/a	90	n/a	n/a	Exothermic	7.5	5 (D)	n/a	n/a	[50]
Metal Amidoboranes (B–N compounds)	Ca-N-B	$Ca(NH_2BH_3)_2$	Ball Milling	CaH_2 + AB	XRD	Unstable	80	n/a	100	n/a	n/a	Exothermic	8	6 (D)	n/a	n/a	[51]

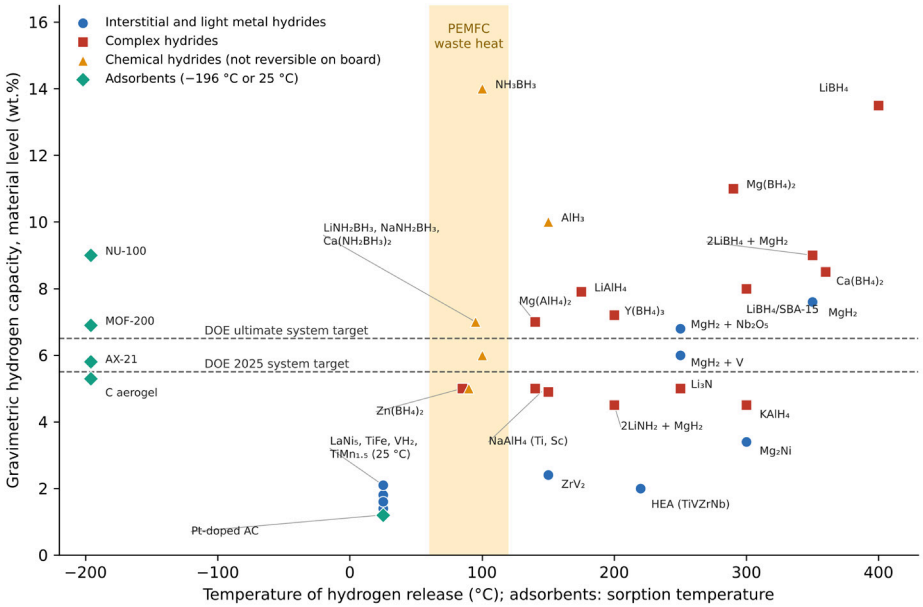


Figure 3. Material-level gravimetric hydrogen capacities of representative metal hydrides, complex hydrides, chemical hydrides and adsorbents as a function of the temperature of hydrogen release (for adsorbents, the sorption temperature), compared with the DOE system targets. Drawn by the authors.

2. The Working Principle of Metal Hydrides

The tendency of metal hydrides to bond with hydrogen varies across the periodic table, as shown schematically in Figure 4 [52]. Green-coloured elements represent exothermic hydride formation ($\Delta H < 0$), blue-coloured elements represent endothermic hydride formation ($\Delta H > 0$), while yellow-coloured elements indicate elements that do not form hydrides or have weak hydride stability. The schematic scale provided below illustrates the relationship between the metal–hydrogen interaction and the binding enthalpy (ΔH, kJ/mol H), emphasising the thermodynamic nature of hydride stability.

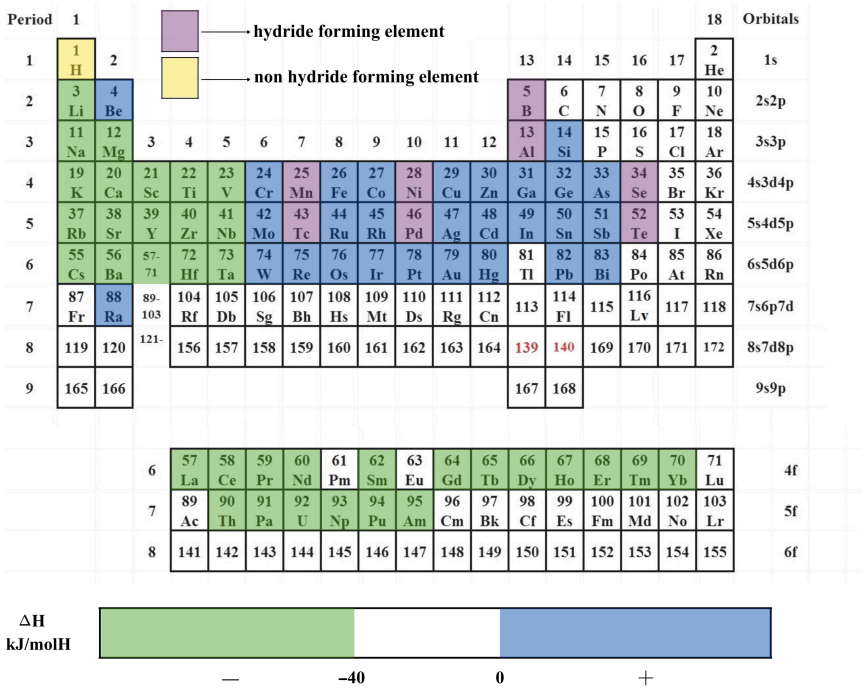


Figure 4. Distribution of elements in the periodic table that tend to form hydrides with hydrogen.

At low temperatures, hydrogen atoms diffuse into the metal lattice, leading to the formation of the hydride phase (absorption). As the temperature increases, the metal–hydrogen bonds weaken and hydrogen is released back into the gas phase (desorption) (Figure 5) [53,54]. This reversible process represents the fundamental mechanism that determines the thermodynamic equilibrium, kinetic behaviour, and cyclic stability properties of metal hydrides in hydrogen storage applications.

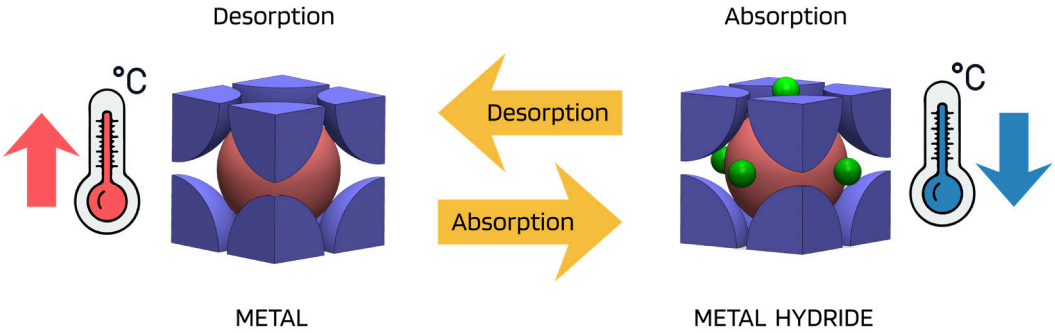


Figure 5. Illustration of hydrogen absorption and desorption behaviour in metal hydrides as a function of temperature.

As illustrated in Figure 6, hydrogen storage in metal hydrides involves the dissociation of hydrogen molecules into atomic hydrogen at the metal surface, followed by diffusion of hydrogen atoms into the interstitial sites of the metal lattice. The process begins at the metal's surface, which acts as a gateway where hydrogen molecules land and split apart (dissociate) into individual atoms. Hydrogen molecules dissociate at the metal surface, and the resulting atomic hydrogen diffuses into the lattice by occupying interstitial sites, leading to hydride formation [55,56]. This process leads to the formation of a metal–hydrogen solid solution and, at higher hydrogen concentrations, the development of a hydride phase within the structure.

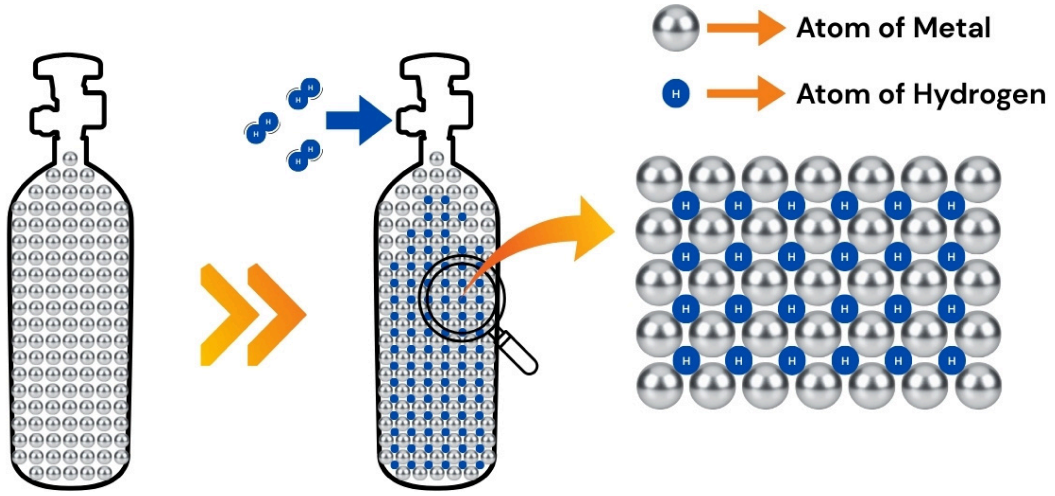


Figure 6. Schematic illustration of hydrogen absorption in a metal hydride system.

To place the reviewed topics in the context of the wider literature, a Scopus search was carried out with the query TITLE-ABS-KEY("metal hydride*" AND "hydrogen storage") for the publication years 1996–2026 (retrieved on 17 September 2026), and the retrieved records were analysed with the subject-area and keyword filters of the database. As shown in Figure 7, the records are concentrated in four subject areas of almost equal weight: Energy (2979 documents), Engineering (2848), Materials Science (2654) and Physics and

Astronomy (2581), followed by Chemistry (1614) and Chemical Engineering (887). This distribution shows that metal hydride storage is studied simultaneously as a materials problem and as an energy-engineering problem, which is why both material-level and system-level aspects are addressed in this review. Because Scopus may assign a document to more than one subject area, the values are non-exclusive document counts and are therefore not expressed as percentages.

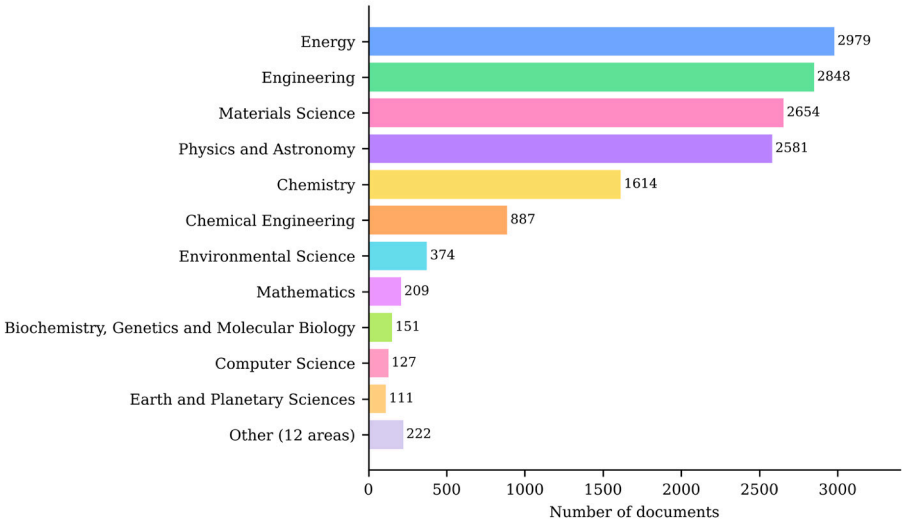


Figure 7. Distribution of documents on metal hydride-based hydrogen storage (1996–2026) by Scopus subject area. A document may be assigned to more than one subject area, so the values are non-exclusive document counts; data retrieved from Scopus on 17 September 2026.

The indexed keywords of the same record set (Figure 8) indicate how research effort is distributed among the topics discussed in this review. Keywords that merely restate the search concept, together with purely generic index terms, were excluded, and orthographic variants of the same term were merged before plotting. After this treatment, the most frequent keywords are dominated by material classes and by the fundamental description of the absorption–desorption reaction: hydrogen storage alloys (1406 documents), catalysis and catalysts (856), desorption (790), kinetics (782), X-ray diffraction (670) and hydrogen storage capacity (659). Magnesium-, lanthanum- and titanium-based systems are the most frequently indexed material families (622, 523 and 430 documents, respectively), which is consistent with the emphasis placed on MgH_2 and on AB_5- and AB_2-type intermetallics in Sections 3 and 4. Catalysis-related terms rank immediately after the material classes, and ball milling (410) is the most frequent synthesis-related term, which confirms that catalytic modification and mechanical processing remain the dominant strategies for improving sorption behaviour. System-level terms are present but clearly less frequent, the highest-ranked example being heat transfer (377); this is consistent with the observation, discussed in the Conclusions, that tank design and heat management have received less attention than material development. Terms such as fuel cells (614), electric discharges (374) and hydrogen production (343) show that part of the retrieved literature concerns adjacent applications, in particular nickel–metal hydride batteries, rather than gas-phase hydrogen storage. The assignment of keywords to the thematic groups shown in Figure 8 was made by the authors and should be read as an indication of relative research activity rather than as an exact partition of the literature.

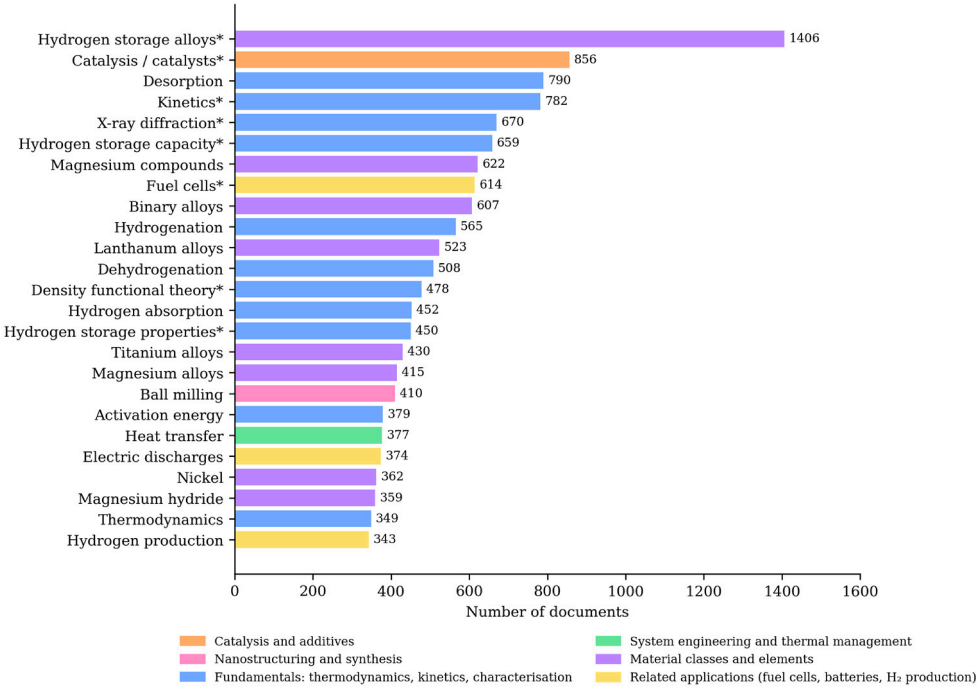


Figure 8. The twenty-five most frequent indexed keywords of the Scopus record set on metal hydride-based hydrogen storage (1996–2026). Keywords that restate the search concept (e.g., hydrogen storage, hydrides, metal hydrides) and generic index terms were excluded; asterisks denote entries for which orthographic variants were merged (e.g., kinetics and reaction kinetics; catalysis, catalysts and catalyst activity). Colours indicate the thematic group assigned by the authors. Values are non-exclusive document counts; data retrieved from Scopus on 17 September 2026.

In the performance characterisation of hydrogen storage technologies, the most fundamental criterion determining the system's efficiency and suitability for the application area is the concept of energy density. Solid-state storage solutions, particularly metal hydrides, provide strategic advantages in storage compared to traditional methods by optimising the amount of energy hydrogen provides per unit mass or volume [53]. In this context, the efficiency of hydrogen storage systems can be established within an academic framework based on two fundamental parameters: In Figure 9 gravimetric storage capacity (G) (wt.%) represents the system's mass energy density and is defined as the ratio of the mass of stored hydrogen to the total system mass [57]. Although light metal hydrides such as MgH_2 offer significant potential for mobile applications with high mass energy densities reaching 7.6 wt.%, the high desorption enthalpy required to release this energy presents thermal management challenges [58]. On the other hand, volumetric storage capacity (V) (kg/m^3) indicates the system's volumetric energy density by determining the amount of hydrogen stored per unit volume. Metal hydrides stand out for their ability to store hydrogen even more densely than in the liquid phase (71 kg/m^3); for example, $TiFeH_2$ and $LaNi_5$-based systems, despite their mass, deliver superior performance in fixed energy units with limited space thanks to the high volumetric density they offer. High volumetric efficiency allows for seamless integration into spatially restricted vehicle architectures [12,59]. The energy density in metal hydrides is not merely a static quantity; it is also directly related to the placement strategy of hydrogen atoms within the interstitial voids of the metal lattice structure and the thermodynamic nature of this process [57].

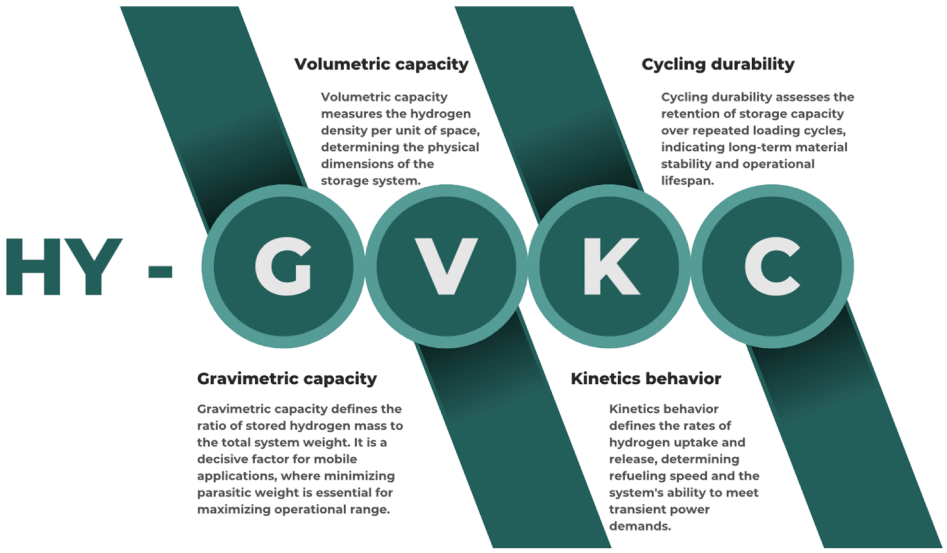


Figure 9. Hy-GVKC conceptual definitions for critical hydrogen storage parameters.

The kinetics (K) of the system include the rate-controlling steps of hydrogen adsorption and desorption, which define the rate at which the system can be refuelled or discharge the stored energy. Fast kinetics is required to provide a hydrogen supply rate sufficient to meet the changing demands of fuel cells while maintaining a rate of refuelling similar to conventional fuels [60]. The cycling durability (C) involves the structural and chemical integrity of the storage medium during repetitive hydrogenation and dehydrogenation reactions. The maintenance of a high capacity retention after thousands of cycles is a pre-requisite for reliability and reduction in life-cycle maintenance costs [61]. All these definitions are given in Figure 9.

Through improved microstructural control, advanced alloy design, and optimized thermal management strategies. Accordingly, metal hydride-based systems demonstrate significant potential particularly in stationary and niche hydrogen storage applications, with promising prospects for further development soon. The strengths, weaknesses, opportunities and threats of metal hydride storage summarised in this section are collected in Figure 10.

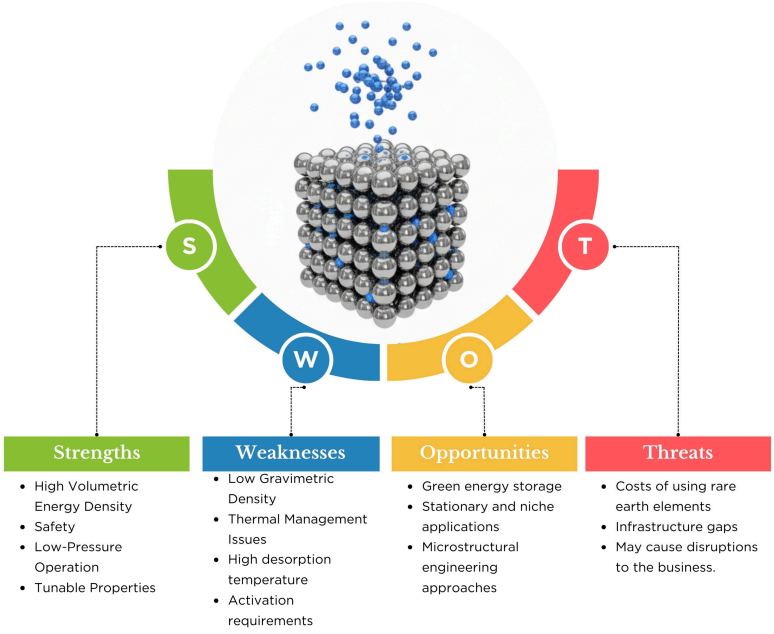


Figure 10. SWOT analysis of metal hydrides for solid-state hydrogen storage.

3. Light Metal Hydrides

Light metal hydrides are compounds containing alkali and alkaline earth metals with low atomic numbers. The most notable feature of these materials is their high hydrogen storage capacity by weight [53,54]. For example, magnesium hydride (MgH_2) can store approximately 7.6 per cent, lithium hydride (LiH) 12.7 per cent, and lithium borohydride ($LiBH_4$) approximately 18 per cent hydrogen [54,62]. These values are considerably higher than those of heavy metal hydrides and provide a significant advantage, particularly for portable energy systems. However, the main disadvantage of light metal hydrides is that relatively high temperatures are generally required to release hydrogen (300–400 °C for MgH_2) [63]. This is also the main difficulty limiting practical applications. Recent research has focused on methods such as nanostructuring, alloying and catalyst addition to overcome this problem [64,65]. Accordingly, the primary objective of current studies is to improve the kinetic properties of these materials and to enable hydrogen release at lower operating temperatures.

The classification adopted in this review follows the performance-oriented scheme of Alobaid et al. [66], in which metal hydrides are divided into heavy metal hydrides (transition metal, intermetallic and high-entropy hydrides) and light metal hydrides (light elemental and complex hydrides). The division rests on the atomic mass of the host elements, which determines the characteristic balance between gravimetric and volumetric capacity: light metal hydrides offer high gravimetric capacity and are mainly considered for mobile and onboard storage, whereas heavy metal hydrides offer high volumetric density, fast kinetics and good reversibility and are mainly considered for stationary and offboard storage [66]. Section 3 therefore covers hydrides in which hydrogen is bound predominantly to light elements (Li, Na, Mg, Ca, B, Al, N); this includes both the binary light elemental hydrides (e.g., MgH_2, LiH, AlH_3) and the complex hydrides, whose cations and anion-forming central atoms are also light elements and whose high gravimetric capacities arise from this low host mass [53,57,62,66]. Section 4 covers hydrides in which hydrogen occupies interstitial sites of a transition-metal or rare-earth lattice; transition metal hydrides, intermetallic hydrides and high-entropy hydrides belong to this group because their principal constituents (Ti, V, Zr, Nb, Hf, Ta, Fe, Ni, La) are heavy elements and they share the interstitial, metallic-bonding storage mechanism [53,54,58,66]. In the same scheme, metal ammine complexes and nitride-based (amide/imide) systems are listed under complex hydrides [66]. In this review they are retained in the complex hydride section for consistency with that scheme; however, because they do not contain a complex $[MH_n]^-$ anion and thus do not satisfy the strict definition of a complex hydride, they are discussed in Sections 3.2.3 and 3.2.4 as related groups.

The scope of this review is limited accordingly. It covers interstitial metal hydrides (Section 4) and ionic or covalent light-metal and complex hydrides that can, at least in principle, be rehydrogenated from the gas phase (Section 3). Molecular and chemical hydrogen carriers, such as ammonia borane (NH_3BH_3), the metal amidoboranes and the metal ammine complexes, store hydrogen in covalent B–H and N–H bonds or as coordinated NH_3; they release hydrogen by largely irreversible decomposition and generally have to be regenerated chemically rather than by reaction with H_2 gas [49–51,67]. These compounds are mentioned in Section 3.2 and listed in Table 4 for comparison only, and they are not otherwise treated in this review.

3.1. Light Elemental Hydrides

Light elemental hydrides have long been investigated in the field of hydrogen storage due to their high gravimetric capacity potential. Light elemental hydrides are compounds

formed by hydrogen and the alkali metals (Group I), alkaline earth metals (Group II) and certain low atomic number elements in the periodic table.

This class mainly consists of hydrides formed by hydrogen with alkali metals (Li, Na, K, Rb, Cs), alkaline earth metals (Mg, Ca, Sr, Ba), and certain low atomic number elements such as Be and Al [54,68]. Among alkali metal hydrides, lithium hydride (LiH) is particularly notable. Although it possesses a high hydrogen capacity, its strong reactivity with moisture and associated safety concerns significantly limit its practical use [12]. Within the alkaline earth metal group, magnesium hydride (MgH_2) stands out with a hydrogen storage capacity of approximately 7.6 wt.%. However, its high desorption temperature (300–400 °C) and slow reaction kinetics are considered major limitations for practical applications [57,69]. Calcium hydride (CaH_2) is also known for its relatively high hydrogen capacity; however, it presents similar thermodynamic limitations. On the other hand, beryllium hydride (BeH_2), although theoretically attractive due to its low density and potential storage capacity, has received limited attention because of its toxicity [54]. Aluminium hydride (AlH_3) is considered a promising candidate with a hydrogen storage capacity of approximately 10.1 wt.%. However, its low thermodynamic stability leads to disadvantages under practical storage conditions [70]. Overall, although these hydrides offer the advantage of high hydrogen storage capacity, they require further development due to high temperature requirements, stability issues, and safety concerns.

The potential of light elemental hydrides in hydrogen storage is constrained by several structural and thermodynamic limitations, despite their high gravimetric capacities. Their high desorption enthalpy necessitates elevated temperatures for hydrogen release. In addition, slow reaction kinetics and surface sensitivity to oxygen and moisture further restrict their practical performance [63,69]. In recent years, various approaches have been developed to overcome these challenges, and these strategies have been extensively addressed in the literature.

Nanostructuring and particle size reduction are among the most widely applied strategies for improving the performance of light hydrides. Owing to the increased surface-to-volume ratio and shortened diffusion pathways, hydrogen transport is enhanced and the activation energy is reduced. This approach has been implemented particularly through high-energy ball milling and nanoconfinement techniques. As a result, the desorption kinetics of MgH_2 and the reversibility of complex hydrides such as $LiBH_4$ have been significantly improved [25,64].

Another widely applied strategy is the use of transition metals or their compounds as catalytic additives. Titanium- and niobium-based additives have been shown to transform into in situ active phases during the reaction, thereby facilitating hydrogen dissociation and recombination processes. Through these catalytic effects, significant reductions in desorption temperature and marked improvements in reaction kinetics have been reported for systems such as MgH_2 [21,71,72].

Mechanical activation methods have also shown effective results. Techniques such as high-energy ball milling and severe plastic deformation (e.g., HPT and ECAP) decrease particle size and increase the number of structural defects, which in turn facilitate hydrogen diffusion. As a result, the hydrogen release temperature of Mg-based hydrides can be reduced by up to about 100 °C. However, during scale-up, concerns related to high energy consumption and long-term stability have become important issues that require further investigation [25,73,74].

Thermodynamic destabilization is achieved by combining different hydrides within a single system. In Reactive Hydride Composite (RHC) systems, such as $LiBH_4$–MgH_2 [42] or $LiBH_4$–CeH_2 [75] mixtures, new reaction pathways with lower enthalpy than the individual

components can be formed. This enables hydrogen release at lower temperatures compared to the single hydrides [52,76].

However, in some systems, the formation of by-products and the associated loss of capacity are considered important limitations of this approach [76].

The nanoconfinement strategy has gained particular attention in complex hydrides. In this approach, hydrides are incorporated into porous carbon materials, MOF-derived structures, or silica matrices. This limits particle agglomeration and improves cyclic stability. For materials such as $LiBH_4$, nanoconfinement has led to reduced desorption temperatures and improved reversibility [62,77].

Surface coating and encapsulation methods embed hydride particles in a secondary matrix or shell, such as graphene, reduced graphene oxide, polymers or core–shell structures. This barrier restricts particle growth and agglomeration during repeated absorption–desorption cycles and thus improves cyclic stability [64,65]; air-stable Mg nanoparticles of about 5 nm have also been reported [65].

Alloying is another approach used to reduce thermodynamic and kinetic limitations. Alloy systems such as Mg–Ni, Mg–Ti, and Mg–Li–Al can improve hydrogen storage properties through the formation of different intermetallic phases. For example, the Mg_2NiH_4 phase shows more favourable hydrogen release behaviour compared to pure MgH_2. However, alloying may also lead to certain disadvantages, including a reduction in gravimetric capacity and an increase in overall system weight [78,79].

Overall, the strategies developed to reduce the disadvantages of light elemental hydrides are complementary to each other. The literature emphasizes that the most successful results are generally achieved when approaches such as nanostructuring, catalytic additives, and surface modification are applied together [64,65,78].

Light metal hydrides summarized in Table 3 demonstrate the influence of synthesis route and catalytic modification on hydrogen storage performance. As shown in Table 3, ball milling, nanocomposite formation, and catalytic additives such as Nb_2O_5, V, Ni, and carbon-based materials significantly reduce the hydrogen desorption temperature of MgH_2 from 350 °C to nearly 200–250 °C, while maintaining comparable gravimetric capacities. In contrast, light elemental hydrides such as LiH and AlH_3 exhibit higher theoretical gravimetric capacities but require substantially higher temperatures or exhibit metastable behaviour. These comparisons clearly indicate that thermodynamic stability, reaction kinetics, and synthesis strategy collectively determine the practical applicability of light metal hydrides (Table 3).

3.2. Complex Hydrides

Complex hydrides are compounds derived from complex anionic structures formed by hydrogen atoms with metal or semi-metal centres. Therefore, the term “complex” refers to structures containing more than one central atom or ligand and exhibiting a bonding structure that is not only ionic but also covalent in character [53]. Complex hydrides are compounds formed by metal cations and complex anions, such as $[AlH_4]^-$, $[BH_4]^-$, and $[NH_2]^-$, and they are widely studied in solid-state hydrogen storage because they generally contain high amounts of hydrogen [80]. Unlike simple binary metal hydrides, these compounds exhibit more complex structures with ionic and/or covalent bonding characteristics. Accordingly, complex hydrides are generally based on light elements such as aluminum, boron, or nitrogen combined with alkali or alkaline earth metals [31]. One of the most important advantages of these materials is that they have a high gravimetric hydrogen capacity (for example, $NaAlH_4$ contains 7.4 wt.% H, of which 5.6 wt.% is released in the two decomposition steps below about 250 °C) [29,81]. Furthermore, thanks to the presence of different complex anions, the thermodynamic properties can be adjusted through compositional

and structural modifications [62]. However, the practical potential of complex hydrides remains limited. Hydrogen release generally requires elevated temperatures (100–300 °C), and kinetic barriers are often observed during reversible absorption–desorption processes. For this reason, current research focuses on reducing these limitations through strategies such as catalyst addition, nanostructuring, ion substitution, and composite formation. In particular, transition metal additives (e.g., Ti, Ni, and Fe) can modify reaction pathways and enable hydrogen release at lower energy barriers [62,81]. To evaluate the thermodynamic impact of these modifications, the relationship between hydrogen dissociation pressure and temperature is commonly analysed using Van't Hoff diagrams. These diagrams are widely employed to assess and compare the thermodynamic behaviour of metal hydrides (Figure 11) [56], providing insight into how material design influences hydrogen release conditions [62].

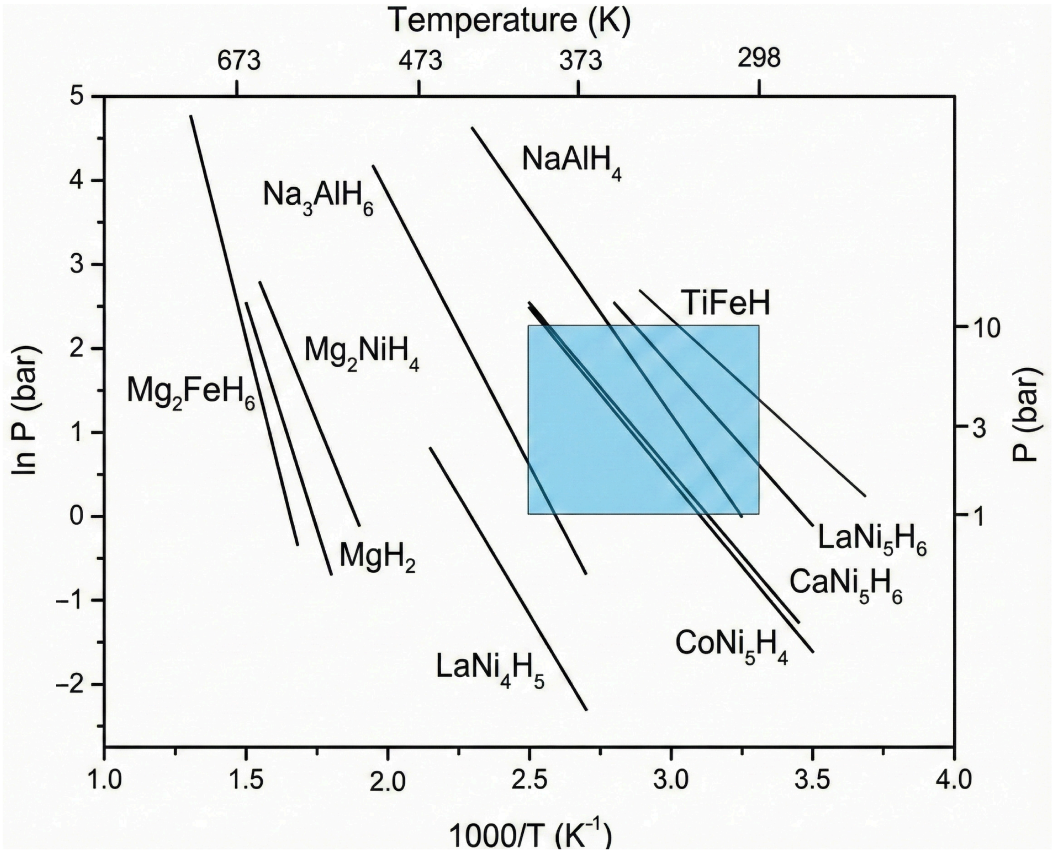


Figure 11. Van't Hoff graphs showing the hydrogen dissociation pressures and temperatures of various metal hydrides (the shaded area represents the desired operating conditions).

Complex hydrides are defined by the presence of a complex anion in which hydrogen is covalently bound to a central atom, and are classified accordingly into three classes: alanates, based on the $[AlH_4]^-$ anion, borohydrides, based on the $[BH_4]^-$ anion, and amides and imides, based on the $[NH_2]^-$ and $[NH]^{2-}$ anions (Figure 12) [82–84]. Metal ammine complexes, in which neutral ammonia molecules are coordinated to a metal centre, do not contain such an anion and are therefore treated in Section 3.2.3 as a closely related class of chemical hydrogen carriers rather than as complex hydrides in the strict sense. Binary nitrides such as Li_3N, in which nitrogen is present as N^{3-}, are likewise not complex hydrides; they are discussed in Section 3.2.4 as precursors to, and hybrid partners of, amide–hydride systems [54].

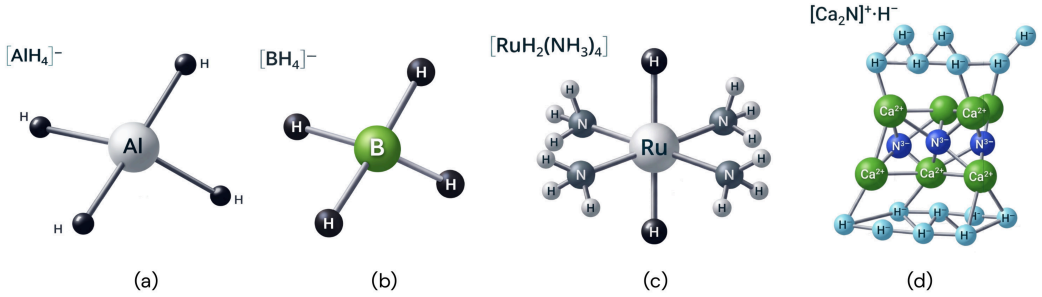


Figure 12. Examples of the main groups of complex hydrides: (**a**) alanates, (**b**) borohydrides, (**c**) metal ammine complexes, treated in this review as a related class of chemical hydrogen carriers, and (**d**) a representative nitride-based system.

- Alane compounds (e.g., $NaAlH_4$, $LiAlH_4$) are systems whose hydrogen recycling performance is improved, particularly with the addition of catalysts (such as Ti, Fe, Nb) [31,81].
- Borohydrides (e.g., $LiBH_4$, $Mg(BH_4)_2$, $Ca(BH_4)_2$) offer high hydrogen content (between 10 and 18 per cent) but tend to decompose at high temperatures [85].
- Metal ammine complexes are structures that carry hydrogen at the metal centre through ammonia coordination and are promising for hydrogen release under low pressure conditions [67].
- Amides and imides (e.g., $LiNH_2$ and the $LiNH_2$–LiH couple) store hydrogen through the reversible amide–imide conversion and offer high gravimetric capacities, whereas binary nitrides such as Li_3N act as precursors to these systems and as hybrid partners rather than as complex hydrides themselves [45,86,87].

Recent studies on complex hydrides show that their kinetic and thermodynamic performance can be significantly improved through nanoscale synthesis, ion doping, and composite formation approaches [88]. In this context, complex hydrides are considered a key material class for the future development of lightweight, high-capacity, and reversible hydrogen storage systems [53].

3.2.1. Alanates

Alanates derive their name from the aluminum-containing anionic unit $[AlH_4]^-$. This ion has a tetrahedral structure, with one central aluminum atom bonded to four hydrogen atoms. The term alanates is related to aluminate, reflecting its origin from aluminum-based hydride anions and emphasizing its complex structure containing both metal and hydrogen atoms. Alanates are complex hydrides that include the AlH_4^- anion and are typically combined with alkali or alkaline earth metals. In recent studies, approaches such as double-cation alanates, anion substitution, and reactive composites have gained attention to improve their kinetic and thermodynamic properties [31]. Alanates such as $NaAlH_4$, $LiAlH_4$, $KAlH_4$ and $Mg(AlH_4)_2$, including the high-pressure phases of the latter [34,89], are notable for their high hydrogen content and favourable reversibility. However, in their pure form, they exhibit high decomposition temperatures and slow kinetics, which limit their practical use. For this reason, recent research has focused on the thermodynamic destabilization of alanates through the incorporation of transition metal additives such as Ti, Ni, or Fe, with the aim of reducing hydrogen release temperatures [31,81].

3.2.2. Borohydrides

Borohydrides derive their name from the $[BH_4]^-$ ion, which has a boron (B) atom at its centre. The word borohydride is derived from the combination of the words boron and hydride. This group is extensively researched in hydrogen storage studies due to the high

hydrogen content and chemical bonding properties of the boron element [90]. However, high dehydrogenation temperatures and limited reversibility remain major barriers to practical application. Current research aims to reduce these limitations through approaches such as ion substitution, mechanical milling, catalyst addition (e.g., Ni_2B and $TiCl_3$), and composite formation. For example, a study by Liu et al. (2024) showed that the addition of Ni_2B destabilizes the thermodynamic equilibrium of $LiBH_4$ and enables hydrogen release at lower temperatures [91].

3.2.3. Metal Ammine Complexes

Metal ammine complexes derive their name from the term ammine, which refers to ammonia (NH_3) molecules coordinated to a central metal atom through coordinate bonds. In this terminology, "metal" denotes the central atom (e.g., Mg, Co, or Ni), while "ammine" indicates the presence of coordinated ammonia ligands. This naming convention is based on classical Werner coordination theory and highlights the coordination complex nature of these compounds [67]. Metal ammine complexes contain metal–ammonia coordination bonds and can act as a link between hydrogen storage systems and the ammonia economy. These materials store hydrogen in the form of ammonia and release it later through the decomposition of ammonia [92]. Their importance in hydrogen storage arises from the ability of ammonia molecules to function as chemical hydrogen carriers. Recent studies indicate that metal ammine complexes can provide safe hydrogen storage under low-pressure conditions and may serve as a bridge between the ammonia economy and the hydrogen economy [92].

3.2.4. Nitride-Based Systems (Related Group)

Nitride-based complexes derive their name from the nitride ion (N^{3-}), which originates from the nitrogen (N) element. These structures are generally used to improve hydrogen storage performance through the formation of mixed metal–hydride–nitride phases. The term nitride describes the bonding character formed between nitrogen and the metal species within the compound [45]. In recent years, nitride compounds have also been used as catalytic support materials, and terms such as complex nitride hydrides or nitride-supported hydrides are frequently reported in the literature. Nitrides are generally not classified as complex hydrides; instead, they function as catalytic additives or components in hybrid systems. However, some nitride structures have been investigated to enhance hydrogen storage efficiency and stability through metal nitride–hydride interfaces and hybrid composites. In addition, transition metal nitrides such as molybdenum nitride and tungsten nitride may contribute to hydrogen desorption mechanisms through catalytic activity or surface interactions. Although a clearly defined class of "established complex nitride hydrides" is not yet common, theoretical and modelling studies continue to explore this direction [93].

Table 4 presents a comparative overview of the physicochemical properties and hydrogen storage performance of different metal hydride classes. Upon examination of the data, it is evident that borohydrides ($LiBH_4$, 18.5%) and ammonia borane (NH_3BH_3, 19.6%) possess the highest theoretical gravimetric capacities. Ammonia borane and the metal amidoboranes are chemical hydrides outside the main scope of this review and are listed for comparison only (Section 3). It should be noted that ammonia borane contains no metal centre and is therefore listed in Table 4 as a metal-free B–N chemical hydride rather than as a metal ammine complex; the related $LiNH_2BH_3$, $NaNH_2BH_3$ and $Ca(NH_2BH_3)_2$ compounds are correspondingly grouped as metal amidoboranes. However, this high capacity is generally accompanied by disadvantages such as high desorption temperatures and limited reversibility.

Among light metal hydrides, MgH_2 offers a gravimetric capacity of approximately 7.6%. However, bulk MgH_2 releases hydrogen at practical rates only at about 350 °C (Table 3), well above the equilibrium temperature of about 285 °C at 0.1 MPa [69], because its kinetics are slow. When catalytic additives such as Nb_2O_5 or graphene are used, this temperature can be reduced to the range of 200–250 °C, and the reaction kinetics can be improved.

Intermetallic hydrides such as $LaNi_5$ and FeTi have lower gravimetric capacities in the range of 1.4–1.9%. Nevertheless, thanks to their low desorption enthalpies (28–31 kJ/mol H_2), they can perform rapid hydrogen exchange at conditions close to room temperature. Furthermore, due to their high volumetric capacities (92–115 kg/m^3), they are widely preferred in commercial applications. The table shows that there is a trade-off between high gravimetric capacity and the requirement for low-temperature operation. Current research focuses on nano-structuring approaches and multi-component hydride composites to improve this balance. It should also be emphasised that all capacities in the hydride tables of this review are material-level values. At system level, the mass and volume of the pressure vessel, heat exchanger, valves and thermal management units must be added, so that the gravimetric capacity of a complete metal hydride tank is typically only a fraction of that of the hydride powder itself [94]. For this reason, the DOE targets [17] are defined for the whole storage system, and a material meeting a given capacity value does not automatically meet the corresponding system target.

4. Heavy Metal Hydrides

Heavy metal hydrides are compounds formed by transition metals (Ti, Fe, Ni, Co, Pd, La, Zr, etc.) and hydrogen [66]. Although they have a lower gravimetric hydrogen capacity compared to light metal hydrides, they stand out due to their high thermodynamic stability, good reversibility and fast reaction kinetics [58]. These types of hydrides are formed by hydrogen atoms occupying the voids (interstitial positions) within the metal lattice and are therefore also referred to as interstitial hydrides [95]. Hydrogen atoms diffuse and settle into the tetrahedral or octahedral voids within the metal cage; the metallic host lattice is largely retained, but it expands on hydrogenation, by about 25% in unit-cell volume for $LaNi_5$ and about 18% for TiFe (Section Comparative Structure–Property–Performance Relationships of Metal Hydrides). Because hydrogen moves between interstitial sites, absorption and release are rapid. Although thermodynamically heavy metal hydrides have a lower hydrogen content (1–2% H_2) than light metal hydrides, their ability to achieve reversible storage at low temperatures and pressures makes them highly suitable for fuel cell supply units and hydrogen buffering systems [57]. For example, systems such as $LaNi_5H_6$, $TiFeH_2$ and ZrV_2H_x are frequently preferred in commercial metal hydride storage tanks due to their high reversibility under conditions close to room temperature [58,95].

These materials, which are also advantageous from a kinetic perspective, allow hydrogen to diffuse into and out of the metal lattice quite rapidly. However, some heavy metal hydrides may be sensitive to oxidation and therefore may require surface cleaning or activation processes [96]. In particular, TiFe-based alloys form a passivation layer on the surface when exposed to air; vacuuming and heat treatment methods are generally used to remove this layer [97,98]. Recent studies have focused on methods such as alloying, nanoscale sizing and catalyst doping to improve the performance of such materials. For example, adding elements such as Mn, V or Ni to the TiFe system significantly improves cycle stability by optimising the hydrogen absorption–desorption pressure ranges [57]. Although heavy metal hydrides have lower energy density than light metal hydrides, they are considered one of the most mature and reliable technologies in practical hydrogen storage systems due to their high cycle life, thermal stability and suitable operating conditions [53].

4.1. Transition Metal Hydrides

Transition metal hydrides are compounds formed between hydrogen and transition or rare earth metals such as Ti, Fe, Ni, Co, Pd, Zr, and La. These materials attract attention because of their high thermodynamic stability and relatively fast reaction kinetics [99,100]. Due to the wide variety of bonding tendencies exhibited by metal–hydrogen bonds (μ-hydride, σ-bond, dihydrogen complex, etc.), they possess a rather extensive range of chemical behaviour [101]. In these hydrides, hydrogen atoms typically occupy the tetrahedral or octahedral interstitial voids of the metal lattice, although ligand-supported complex bonds may also be observed in some cases [99]. Structurally, the electronic state of metal atoms, pore sizes, and metal-hydrogen bond energies in transition metal hydrides directly influence H absorption–desorption properties. Structurally, hydrogen atoms diffuse into the tetrahedral or octahedral interstitial sites (interstitial positions) of the metal lattice; therefore, they are often classified as interstitial hydrides [100].

Thermodynamically, the bond energies of transition metal hydrides have a wide range [102]. The free energy and enthalpy values of these hydrides are of critical importance in terms of both catalytic continuity and hydride stability. From a kinetic perspective, these materials also possess the ability to rapidly absorb and release hydrogen, which is advantageous in practical applications.

Some important examples in the literature are the use of metal–hydrogen complexes as models in catalytic reactions [103]. For example, McGrady's compilation comprehensively addresses the electronic structure, bond type and dynamic behaviour of transition metal hydrides [99]. In an early review, Libowitz showed that the hydride phases of the transition metals are definite chemical compounds with some ionic character rather than simple solid solutions, because most Group III A and IV A metals change their crystal structure on hydriding, and that their large deviations from stoichiometry can be explained by lattice defects [100]. X-ray and neutron diffraction studies summarised in the same review showed that, in the Group IV A hydrides, hydrogen occupies the tetrahedral sites of a cubic fluorite-type metal lattice, which becomes increasingly tetragonal as the H/M ratio approaches two [100].

This class of metal hydrides offers numerous advantages, including chemical diversity, flexible bonding properties, strong potential for catalytic applications, and generally fast reaction kinetics. However, some systems suffer from low thermodynamic stability or excessively strong bond energies, which can limit reversibility. Furthermore, some complex hydrides are prone to oxidation, creating difficulties in maintaining their structural stability.

4.2. High-Entropy Hydrides

High-entropy hydrides (HEHs) or high-entropy alloy (HEA)-based hydrides are defined as multi-component systems containing five or more principal metals; these materials can form single-phase solid solutions or stabilized microstructures due to their high configurational entropy and offer significant potential in terms of hydrogen storage capacity and kinetic performance. Marques et al. [104], in their evaluation of HEAs for hydrogen storage applications, highlighted that these alloys offer a very wide compositional range, yet the hydrogenation–dehydrogenation mechanisms are not fully understood. For instance, studies on a Ti–Zr–V–Cr–Ni-based HEA system reported a hydrogen storage capacity of approximately 1.78 wt.% [105], which is comparable to that of conventional AB and AB_2 alloys.

Following Alobaid et al. [66], high-entropy hydrides are placed in Section 4 because their principal elements are mainly early transition metals and because, like conventional transition metal and intermetallic hydrides, they store hydrogen interstitially in a BCC, FCC or Laves-type metallic lattice. Compared with these conventional alloys, the main advance

of recent studies is the possibility of tuning plateau pressure and hydride stability through the average valence-electron concentration and lattice distortion rather than through a single substituting element; several compositions show absorption within one minute at room temperature, and some retain their capacity over the limited number of cycles tested so far [66,104,106]. However, most reported compositions still show gravimetric capacities of roughly 0.6–2.8 wt.%, comparable to conventional BCC alloys, and the highest reported values, for a few Ti–V–Cr-based compositions, reach about 3.5 wt.% [66,104,107]. In addition, the need for several principal elements in near-equimolar ratios and precise compositional control increases raw-material and processing costs, which currently limits large-scale use [66]. In practice, high-entropy alloys therefore appear at least as promising as catalysts for MgH_2 as they are as stand-alone storage media [108].

However, the main advantages of HEHs lie in their wide structural design freedom, the tunability of thermodynamic stability, and the possibility to optimize kinetic properties through composition. On the other hand, high production costs, the analytical challenges of multi-component structures, the risk of phase separation, and insufficient cyclic stability hinder the transition of this material group to industrial applications [106]. Overall, high-entropy hydrides are regarded as a promising research area among next-generation hydrogen storage materials, yet further improvements are needed in terms of capacity, stability, and scalability.

4.3. Intermetallic Hydrides

Intermetallic hydrides are formed as a result of the interaction of hydrogen with compounds that have regular crystal structures formed by two or more metal elements in specific ratios. In these materials, hydrogen typically occupies the interstitial positions within the metal lattice, forming a stable hydride phase. The most studied systems include TiFe, $LaNi_5$, ZrV_2, and Mg_2Ni alloys. Although these intermetallic compounds have a lower gravimetric capacity (typically 1–2% H_2) compared to light metal hydrides in hydrogen storage applications, they offer advantages such as high reversibility, low operating pressure, good thermal stability, and long cycle life [109].

Structurally, hydrogen atoms in intermetallic hydrides occupy interstitial sites within the metal lattice, and hydrogen absorption may induce substantial lattice expansion and phase transformations. TiFe initially crystallizes in the ordered cubic B2 (CsCl-type) structure. During hydrogenation, hydrogen first dissolves in the B2 lattice to form an α solid-solution phase at low hydrogen concentrations. With increasing hydrogen content and pressure, hydride phases are formed, including the β monohydride (TiFeH) and, under appropriate conditions, the γ dihydride ($TiFeH_2$). These hydride phases involve changes in lattice parameters and crystal symmetry: the β monohydride is orthorhombic, whereas neutron diffraction of the γ deuteride $TiFeD_{1.93}$ showed a monoclinic structure (P2/m) [110], and formation of the γ phase increases the unit-cell volume by about 18% (Section Comparative Structure–Property–Performance Relationships of Metal Hydrides). The exact phase sequence and stability depend on hydrogen pressure, temperature, alloy composition, and sample history [96,98,109]. $LaNi_5$, on the other hand, retains its hexagonal $CaCu_5$-type structure on hydrogenation, with an increase in unit-cell volume of about 25% [111], and can rapidly absorb and release hydrogen at room temperature. Consequently, $LaNi_5$-derived systems are used on an industrial scale in hydrogen buffer tanks for fuel cells [112].

From a thermodynamic perspective, these systems can operate at low equilibrium pressures (0.1–1 MPa) and relatively low temperatures (20–80 °C). The TiFe alloy is notable for its high cycle stability and low cost; however, the initial activation process is difficult due to the passivation layer that forms on its surface. This situation is remedied by vacuuming, heat treatment or chemical activation techniques [98,113]. In contrast, Zr

and V based intermetallic systems offer kinetic advantages by providing higher hydrogen diffusion coefficients.

According to studies in the literature, the TiFe alloy exhibits approximately 1.8 wt.% H_2 storage capacity, while $LaNi_5$ exhibits approximately 1.4 wt.% H_2 and ZrV_2 can reach approximately 2.0 wt.% H_2 [58,96,114]. Although these values appear low gravimetrically, the systems' high cycle life (up to 10,000 cycles) and stable pressure–composition isotherms (PCIs) make them significant for practical hydrogen storage applications.

The main strengths of these materials are their high structural stability, reproducible hydrogen absorption–desorption behaviour, and fast kinetics at moderate temperatures. Their weaknesses include relatively low hydrogen capacity, difficulties in initial activation, and oxidation sensitivity in some systems. Current research focuses on overcoming these limitations through alloy engineering (e.g., TiFe-Mn or TiFe-Ni additions), nano scaling, and catalyst incorporation. These approaches aim to optimize both kinetic and thermodynamic parameters, enabling the development of more stable and high-performance intermetallic hydride systems [98,109]. As shown in Table 5, the hydrogen storage properties of different intermetallic compounds exhibit significant differences depending on the composition type, H/M ratio, mass hydrogen capacity, and desorption temperature. Critical parameters such as the atomic hydrogen binding ratio to metal compounds (H/M), the material's mass hydrogen capacity (%H_2), and the temperature at which hydrogen desorption occurs at 0.1 MPa pressure are provided.

4.3.1. AB_5

AB_5-type alloys, particularly $LaNi_5$ (Lanthanum-Nickel), are the interstitial hydride class that is considered a reference point in the history of hydrogen storage technologies and has been the subject of the most research in the literature. As noted in fundamental studies by Schlapbach and Züttel, these alloys have a hexagonal $CaCu_5$ crystal structure and can form hydrides up to the $LaNi_5H_6$ form by placing hydrogen atoms in the voids (interstitial) within the crystal lattice [53]. The most prominent feature of this class highlighted in the literature is its rapid absorption/desorption kinetics at room temperature, with a plateau pressure of about 0.15–0.2 MPa at 25 °C (Section Comparative Structure–Property–Performance Relationships of Metal Hydrides). As emphasised in Sandrock's work, $LaNi_5$ is comparatively easy to activate and shows low hysteresis (a small difference between absorption and desorption pressures) [58]; a few absorption–desorption cycles after a heat treatment are usually sufficient [112]. The volume increase of about 25% on hydrogenation, however, leads to decrepitation of the particles during the first cycles [58,111]. However, as detailed by Broom, $LaNi_5$'s gravimetric hydrogen storage capacity is limited to approximately 1.4–1.5 per cent by mass [115]. Furthermore, dependence on rare earth elements increases costs, while sensitivity to impurities in the hydrogen gas flow can lead to capacity loss during long-term cycles.

4.3.2. AB

The class that has attracted the most attention in the literature in terms of economic feasibility is the AB-type hydrides represented by the TiFe (Titanium-Iron) alloy. As has been known since the pioneering work of Reilly and Wiswall, the TiFe alloy has a CsCl-type (B2) cubic structure and, due to its composition of abundant, low-cost elements, is considered an ideal candidate for large-scale stationary storage applications [96]. However, the biggest obstacle to the commercialisation of this material is the situation referred to in the literature as the activation problem. As noted by Emami and colleagues, the passive oxide layer that forms on the TiFe surface when exposed to air prevents hydrogen diffusion;

therefore, the material must undergo heat treatment at 400 °C and high pressure for its initial use [113].

4.3.3. A_2B

A_2B-type interstitial hydrides typically contain a combination of transition metals and light metals, with Ti_2Ni being a characteristic example of this group. Although these alloys show structural similarities to light metal-based systems such as Mg_2Ni in the literature, Ti_2Ni is considered a transition metal hydride offering operating conditions closer to room temperature. In evaluations conducted by Züttel, it was noted that due to its high Ti content, this structure theoretically possesses a higher gravimetric capacity potential than AB and AB5 types, and that with appropriate modifications, the capacity could reach the range of 2.5–3.0% [54]. The Ti_2Ni phase reacts with hydrogen to form Ti_2NiH; however, one of the fundamental topics of debate in the literature is that the thermodynamic stability of these hydrides can sometimes be very high, requiring high temperatures for hydrogen desorption.

4.3.4. AB_2

AB_2-type alloys are referred to in the literature as "Laves Phases" and are typically found in C14 (hexagonal) or C15 (cubic) crystal structures. The most important representatives of this class are Zr- or Ti-based alloys such as $ZrFe_2$ and $TiMn_2$. AB_2 alloys have a higher hydrogen storage capacity (approximately 2.0% by mass) and higher discharge rates than AB_5 systems [114,116]. These properties make them a strong competitor to AB_5 alloys, particularly for the negative electrodes of Nickel-Metal Hydride (Ni-MH) batteries. As noted by Ovshinsky and colleagues, thanks to their structural flexibility, the stoichiometry of the elements in regions A and B can be altered (multi-component alloying), allowing the thermodynamic stability and equilibrium pressure of the hydride to be adjusted with great precision [116]. However, it has been reported in the literature that these alloys are difficult to activate and are more prone to mechanical fragmentation (pulverisation) due to lattice expansion during hydrogenation cycles.

4.3.5. AB_3

AB3-type alloys (e.g., $LaNi_3$, $CeNi_3$) are superlattice structures formed by the crystallographic stacking of AB_5 and AB_2 unit cells along the c-axis in a specific order. In studies pioneered by Kohno and colleagues, it is emphasised that these alloys aim to combine the excellent electrode kinetics of AB_5 alloys with the high capacity of AB_2 alloys [117]. According to literature data, AB_3-type hydrides offer a higher capacity than AB_5, ranging from 1.5% to 1.8% by mass. This increase in capacity stems from the presence of a greater number of interstitial voids capable of accommodating hydrogen within the structure. However, as noted by Willems, the main disadvantage of these materials is their cyclic stability; volumetric changes occurring in the crystal lattice during hydrogen insertion and extraction can compromise the material's mechanical integrity and shorten its cycle life [118].

4.3.6. Solid Solution

Solid solution hydrides typically refer to Vanadium (V)-based or Titanium–Chromium–Vanadium (Ti-Cr-V) alloys with a BCC (Body-Centred Cubic) crystal structure. Introduced to the literature by Akiba and Iba [119], these systems represent the group with the highest gravimetric capacity potential among interstitial hydrides. The BCC structure can accommodate many hydrogen atoms per metal atom, enabling a very high capacity ranging from 2.5 to 3.5 per cent by mass. Despite this high-capacity advantage, which is frequently emphasised in review articles, the fundamental problem with solid solution alloys is their "sloping plateau" and large hysteresis characteristics; that is, hydrogen is released not at

a constant pressure but over a variable pressure range. This is an important parameter affecting the efficiency of the system.

Table 5 presents a comparative overview of the hydrogen storage performance of intermetallic compounds with different crystal structures. AB and AB_5 type alloys (TiFe, $LaNi_5$, $MmNi_5$), despite their relatively low gravimetric capacities, offer advantages in practical hydrogen storage applications due to their low desorption temperatures and good reversibility the Mm notation used here refers to Misch metal, which is predominantly composed of the elements Ce, La, Nd, and Pr. Misch metal is a commercially available rare earth alloy widely used in hydrogen storage alloys to reduce costs and balance alloy performance. A typical composition in the literature is represented as Mm_5 (Ce + La + Nd + Pr). A_2B-type Mg-based alloys (Mg_2Ni and Mg_2Cu) exhibit higher gravimetric and volumetric hydrogen capacities but are disadvantageous in terms of energy requirements due to high desorption temperatures. AB_2 type alloys offer balanced performance with medium capacity and relatively low desorption temperatures. The binary hydride MgH_2, included in Table 5 as a reference, exhibits the highest gravimetric and volumetric capacity, but its high hydrogen release temperature limits its practical applications [56,63,120–122].

Table 5. Hydrogen storage properties of certain intermetallic compounds [56,63,120–122]. The temperature column gives the temperature at which the desorption equilibrium pressure reaches 0.1 MPa; capacities are theoretical values for the stated H/M ratio.

Type	Example Compound	H/M	Hydrogen Capacity at the Stated H/M (wt.%)	T (K) for p_{des} = 0.1 MPa	Volumetric Capacity (kg H_2 m^{-3})
AB	TiFe	0.975	1.86	265	96
AB	ZrNi	1.4	1.85	565	50
A_2B	Mg_2Ni	1.33	3.6	528	90
A_2B	Mg_2Cu	1.2	2.8	560	70
AB_2	$ZrMn_2$	1.2	1.77	440	45
AB_2	$TiMn_2$	1.5	1.9	310	50
AB_2	$TiV_{0.62}Mn_{1.5}$	1.14	2.15	267	55
AB_3	Ni_3Al	0.75	0.8	580	-
AB_5	$LaNi_5$	1.08	1.49	285	115
AB_5	$MmNi_5$ (Misch metal)	1.1	1.4	295	105
Binary hydride (reference)	MgH_2 (β-phase)	2.0	7.6	553	110

Representative literature values for the main hydride classes are compiled in Appendix A (Table A1), together with the conditions under which they were obtained. Because the properties vary widely within each class and the available data refer to different conditions (for example, theoretical and reversible capacities differ strongly for complex hydrides, and cycling data for high-entropy hydrides cover only 5–10 cycles), these values should be compared only where the conditions are similar. The comparison nevertheless shows that material selection in metal hydride-based hydrogen storage is a multi-parameter optimisation problem [53].

Light elemental hydrides (e.g., MgH_2) stand out in terms of gravimetric capacity (7.6 wt.% for MgH_2) and elemental abundance, but pure MgH_2 shows very slow kinetics, has to be activated at higher temperatures and pressures than those used in subsequent operation, and activated powders are often pyrophoric [57,69]. Complex hydrides (e.g., $LiBH_4$ and $NaAlH_4$) reach the highest theoretical gravimetric capacities (18.5 wt.% for $LiBH_4$), but rehydrogenation of $LiBH_4$ requires 873 K and 35 MPa, bulk $LiBH_4$ loses most of its capacity within a few cycles, and the release of diborane and the high reactivity of alanates

with air and water limit their safety [31,88]. Transition metal hydrides (e.g., TiH_2, VH_2 and PdH) reach high volumetric hydrogen densities, about 9.5×10^{22} H atoms cm^{-3} in TiH_2, whereas their reversible gravimetric capacity remains low, for example about 2 wt.% for the VH–VH_2 step [100,123]. High-entropy hydrides show fast kinetics, with equilibrium reached within about one minute at room temperature for TiZrNbTa, and gravimetric capacities of 0.59–3.5 wt.%; however, cycling data are still limited, and several compositions contain less abundant elements such as Nb, Hf and Ta [104]. Intermetallic hydrides, particularly AB_5- and AB-type alloys such as $LaNi_5$ and TiFe, offer stable reversible absorption and desorption at room temperature below 1 MPa and volumetric densities of about 115 kg H_2 m^{-3} for $LaNi_5$, but gravimetric capacities of only about 1.4 wt.% [54,112]; TiFe additionally requires activation cycles at high temperature and high hydrogen pressure [113].

The graph presented in Figure 13 compares the theoretical gravimetric and volumetric hydrogen storage potentials of different types of metal hydrides. The distribution obtained clearly demonstrates that intermetallic hydrides have the advantage of high volumetric capacity, whereas borohydrides and light metal hydrides exhibit superior performance in gravimetric terms.

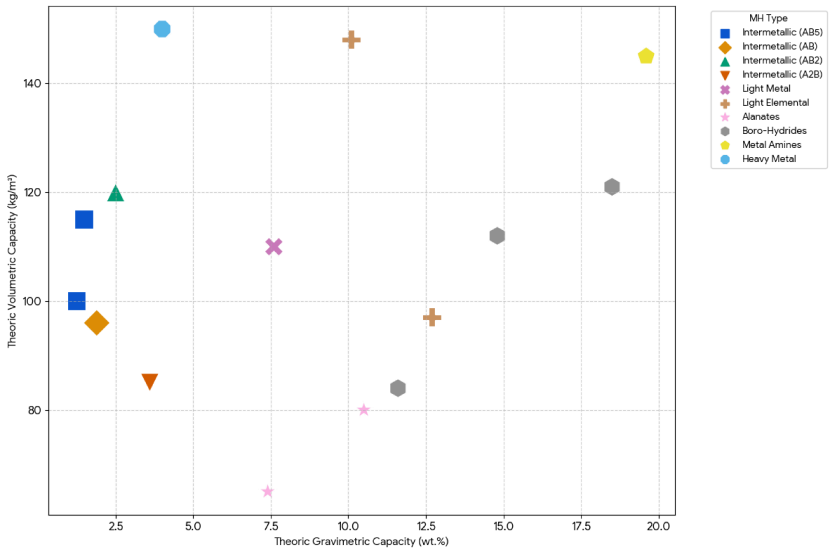


Figure 13. Comparison of theoretical volumetric (kg/m^3) and gravimetric (wt.%) hydrogen storage capacities of selected metal hydrides.

Table 6 summarizes the physicochemical properties and hydrogen storage performance of different metal hydride systems, including intermetallic (AB_5 and AB_2), transition metal, heavy metal, and high-entropy hydrides. The table compares synthesis routes such as arc melting, induction melting, ball milling, and gas-phase reactions, together with structural characterization methods like XRD, SEM, and DSC. In addition, key hydrogen storage parameters are presented, including activation conditions, absorption–desorption temperatures and pressures, reaction enthalpies, and both gravimetric (wt.%) and volumetric (kg/m^3) capacities. AB_5-type alloys, particularly $LaNi_5$-based systems, generally operate near room temperature and low pressures, offering good reversibility but limited gravimetric capacity (around 1.2–1.9 wt.%). AB_2-type alloys such as ZrV_2 and $TiMn_2$ show slightly higher theoretical capacities and good volumetric densities, although some require specific activation or higher operating temperatures.

Table 6. Comparison of physicochemical properties and hydrogen storage performance of selected metal hydrides (n/a: not available). Experimental capacities are marked (R) for reversible capacities and (D) for hydrogen released on the first decomposition only; ammonia borane and the metal amidoboranes are included for comparison only (see Section 3). Other abbreviations and definitions as in Table 3.

Hydride Class	Metal/ Alloy	Hydride	Synthesis Method	Synthesis Conditions	Character-isation	Activa-tion	T_{abs} (°C)	p_{abs} (MPa)	T_{des} (°C)	p_{des} (MPa)	ΔH_{abs} (kJ mol^{-1} H_2)	ΔH_{des} (kJ mol^{-1} H_2)	w_{th} (wt.%)	w_{exp} (wt.%)	ρ_{th} (kg H_2 m^{-3})	ρ_{exp} (kg H_2 m^{-3})	Ref.
Intermetal-lic Hydrides (AB_5)	$LaNi_5$	$LaNi_5H_{6.5}$	Arc Melting	Argon atm annealed 1000 °C 8 h	XRD PCT	RT cycles	25	0.2	25	0.15	−30.8	30.8	1.49	1.4 (R)	115	105	[124]
Intermetal-lic Hydrides (AB_5)	$LaNi_{4.5}Al_{0.5}$	$LaNi_{4.5}Al_{0.5}H_5$	Arc Melting	Substituted Ni with Al	XRD PCT	RT cycles	25	0.05	60	0.1	−38	38	1.20	1.2 (R)	100	90	[125]
Intermetal-lic Hydrides (AB_5)	$MmNi_5$ (Mis-chmetal)	$MmNi_5H_6$	Induction Melting	Industrial grade mischmetal	XRD	RT cycles	25	1.5	25	0.8	−26	26	1.4	1.3 (R)	105	100	[58]
Intermetal-lic Hydrides (AB_5)	$LaNi_{4.8}Co_{0.2}$	$LaNi_{4.8}Co_{0.2}H_6$	Arc Melting	Co substitution	XRD	Cycle	25	0.15	25	0.1	−32	32	1.4	1.45 (R)	105	100	[126]
Intermetal-lic Hydrides (AB_5)	$CaNi_5$	$CaNi_5H_6$	Arc Melting	Ca based	XRD	RT	25	0.5	25	0.4	−30	30	1.8	1.6 (R)	110	100	[127]
Intermetal-lic Hydrides (AB)	FeTi	$FeTiH_{1.95}$	Induction Melting	Annealed 900 °C	XRD SEM	450 °C Vacuum	25	2	25	0.5	−28.1	28.1	1.86	1.8 (R)	96	92	[96]
Intermetal-lic Hydrides (AB)	$TiFe_{0.9}Mn_{0.1}$	$TiFe_{0.9}Mn_{0.1}H_{1.9}$	Arc Melting	Doped with Mn	XRD	Easier activation	25	1.5	25	0.6	−29	29	1.8	1.8 (R)	98	95	[109]
Intermetal-lic Hydrides (AB)	$TiFe_{0.8}Ni_{0.2}$	$TiFe_{0.8}Ni_{0.2}H$	Arc Melting	Ni doped	XRD	RT	25	1.5	25	0.8	−27	27	1.8	1.6 (R)	95	90	[128]
Intermetal-lic Hydrides (AB_2)	ZrV_2	$ZrV_2H_{5.1}$	Arc Melting	Laves phase C15	XRD	Heat 300 °C	25	0.01	150	0.1	−45	45	2.5	2.4 (R)	120	115	[114]
Intermetal-lic Hydrides (AB_2)	$TiMn_{1.5}$	$TiMn_{1.5}H_{2.5}$	Arc Melting	C14 Laves phase	XRD	RT activation	25	3	25	0.5	−26	26	1.9	1.6 (R)	105	95	[129, 130]

Table 6. *Cont.*

Hydride Class	Metal/ Alloy	Hydride	Synthesis Method	Synthesis Conditions	Character-isation	Activa-tion	T_{abs} (°C)	p_{abs} (MPa)	T_{des} (°C)	p_{des} (MPa)	ΔH_{abs} (kJ mol^{-1} H_2)	ΔH_{des} (kJ mol^{-1} H_2)	w_{th} (wt.%)	w_{exp} (wt.%)	ρ_{th} (kg H_2 m^{-3})	ρ_{exp} (kg H_2 m^{-3})	Ref.
Intermetal-lic Hydrides (AB_2)	$ZrCr_2$	$ZrCr_2H_{3.8}$	Arc Melting	Laves phase	XRD	RT	25	0.01	25	0.1	−22	22	2	1.8 (R)	105	100	[131]
Intermetal-lic Hydrides (A_2B)	Mg_2Ni	Mg_2NiH_4	Mechani-cal Alloying	Ball milling 20h Ar	XRD DSC	350 °C 2 MPa	250	1	300	0.1	−64.5	64.5	3.6	3.4 (R)	85	81	[79]
Intermetal-lic Hydrides (A_2B)	Ti_2Ni	Ti_2NiH	Arc Melting	Amorphous-Nano	XRD	Heat	200	1	250	0.1	−55	55	3.2	2.5 (R)	115	100	[132]
Transition Metal Hydrides	Pd	$PdH_{0.6}$	Gas Ab-sorption	Ambient	XRD	Sponta-neous	25	0.02	25	0.01	−37	37	0.6	0.6 (R)	n/a	n/a	[133]
Transition Metal Hydrides	V	VH_2	Gas Ab-sorption	Ambient	XRD	Fast	25	0.1	25	0.05	−40	40	3.8	2.1 (R)	n/a	n/a	[123]
Actinide Hydrides	UH_3	UH_3	Direct Reaction	U + H_2	XRD	Py-rophoric	250	0.1	400	0.1	−84	84	1.3	1.3 (D)	n/a	n/a	[134]
Transition Metal Hydrides	TiH_2	TiH_2	Direct Reaction	Ti + H_2	XRD	Stable	400	0.1	600	0.1	−160	160	4	3.9 (D)	150	140	[135]
High-Entropy Hydrides	$Ti_{0.325}V_{0.275}Zr_{0.125}Nb_{0.275}$	bct dihydride (H/M ≈ 1.8)	Reactive ball milling	7 MPa H_2	XRD, ND, PCI, TDS	One desorp-tion/ab-sorption cycle	25	0.1–4	onset 185; peaks 220, 260 (TDS)	n/a	n/a	n/a	2.7	2.0 (R, after 3 cy-cles)	n/a	n/a	[136]
High-Entropy Hydrides	TiVZrNbHf	$TiVZrNbHfH_{12.5}$ (H/M = 2.5)	Arc Melting	Ball-milled, sieved < 50 µm	XRD, PCT, TDS	First hydro-genation at 400 °C, 2 MPa H_2	299	up to 5.3	onset ≈ 200; max > 400 (TDS)	n/a	n/a	n/a	2.7	2.7 (R)	n/a	n/a	[137]
High-Entropy Hydrides	MgZr-$TiFe_{0.5}Co_{0.5}Ni_{0.5}$	MgZr-$TiFe_{0.5}Co_{0.5}Ni_{0.5}H$	Ball Milling	Mix	XRD	Cycling	25	3	200	0.1	n/a	n/a	2	1.5 (D)	n/a	n/a	[138]

The table also shows that transition and heavy metal hydrides can reach higher theoretical hydrogen capacities. For example, TiH_2 and VH_2 exhibit capacities above 3 wt.%; however, these systems often require high desorption temperatures or involve safety concerns such as pyrophoric behaviour. High-entropy hydrides present moderate storage capacities (0.6–3.5 wt.% over the reported compositions [104]; 1.5–2.7 wt.%) and offer flexibility in tuning thermodynamic and kinetic properties through compositional design, although volumetric data are not always available. Overall, the comparison highlights the balance required between capacity, thermodynamics, kinetics, and safety. None of the listed systems fully meet all practical requirements, indicating that further material optimization is still necessary for efficient and scalable hydrogen storage applications.

5. Kinetics and Thermodynamics of Metal Hydrides

For hydrogen storage systems based on metal hydrides to gain practical relevance, the materials must be able to absorb and release hydrogen at sufficiently high rates; this behaviour is referred to as the kinetics of the metal hydride [81]. Therefore, reaction kinetics is of critical importance in determining whether the system can enable fast refuelling and provide sufficient hydrogen supply to feed a fuel cell or other end-use applications [139].

Thermodynamic properties determine the energy efficiency of the storage process, the storage efficiency, and the ideal operating temperature of the system. In particular, to utilise the waste heat from Proton Exchange Membrane Fuel Cells (PEM) for desorption (hydrogen release), materials should release hydrogen within the decomposition-temperature window of 60–120 °C specified by the DOE target [57]. However, high-capacity materials such as magnesium hydrides generally require high temperatures above 200 °C for hydrogen release due to their high thermodynamic stability [140].

The high enthalpy requirement leads to excessive energy expenditure for the decomposition of the hydride, thereby reducing overall energy efficiency [141]. To overcome these challenges, the adjustment of both kinetic and thermodynamic properties in MgH_2 systems and complex hydrides is an intensive area of research [142,143]. Figure 14 summarises the target range of metal–hydrogen bond strengths that permits hydrogen to be released at or close to room temperature [33,144]. Hydrides whose metal–hydrogen interaction is weaker than this window bind hydrogen too loosely and therefore require elevated pressures for absorption, whereas hydrides lying above the window, such as MgH_2 and most complex hydrides, are thermodynamically too stable and release hydrogen only at high temperatures. The shaded band thus represents the thermodynamic compromise that a practical storage material must satisfy, and it provides the framework within which the material classes reviewed in the following sections are compared.

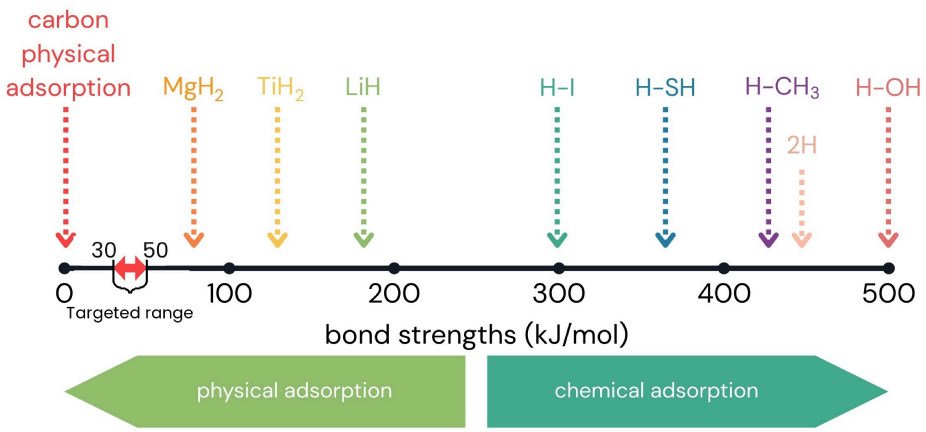


Figure 14. Target binding affinity range allowing hydrogen release at room temperature.

Thermodynamic properties primarily govern the operational temperatures required for hydrogen release and uptake. The equilibrium relationship between the pressure (P) and temperature (T) is described by the van't Hoff equation:

$$\ln P = \frac{\Delta H}{RT} - \frac{\Delta S}{R} \quad (2)$$

Here, ΔH and ΔS represent the enthalpy and entropy changes in the reaction and R is the universal gas constant. To achieve hydrogen release near or below 100 °C, the magnitude of the enthalpy of formation (ΔH) must be substantially reduced, typically aiming for values of about 30–50 kJ mol^{-1} H_2; with $\Delta S \approx 130$ J K^{-1} mol^{-1} H_2, Equation (2) places the temperature at which the equilibrium pressure reaches 0.1 MPa between about −40 and 110 °C for this range. This adjustment, known as thermodynamic destabilization, is achieved by ensuring that the dehydrogenated products form highly stable compounds, thereby lowering the overall reaction energy barrier [140].

Kinetic properties describe the rate at which a metal hydride absorbs or releases hydrogen. The kinetic rate is typically represented by the activation energy (E_a), which is the energy barrier that must be overcome for the reaction to occur. Thermodynamic properties, on the other hand, are related to the enthalpy (ΔH) and entropy (ΔS) values of hydride formation [63]. The magnitude of the formation enthalpy is the fundamental thermodynamic variable that determines the strength of the M–H bond: a more negative enthalpy corresponds to a more stable hydride and therefore to a higher desorption temperature [140]. The absorption of hydrogen by a metal/alloy (hydrogenation) consists of several sequential fundamental steps: (i) Physical adsorption of the H_2 molecule onto the surface, (ii) dissociation into atomic hydrogen (chemical adsorption), (iii) desorption of atomic hydrogen from the surface, (iv) diffusion within the bulk, and (v) formation of the hydride phase. Kinetic improvement aims to lower the activation barrier of the reaction without altering the thermodynamic structure, thereby preventing any of these steps from becoming the rate-limiting step [63].

When examining metal hydrides for their potential to meet high gravimetric capacity targets, their performance is generally evaluated in terms of kinetic and thermodynamic equilibria:

- Mg-based hydrides offer a high theoretical storage capacity of 7.6 wt.%. However, pure MgH_2 is thermodynamically very stable ($\Delta H \approx 75$ kJ/mol H_2) so that the equilibrium pressure reaches 1 bar only at about 285 °C [69]; in practice, bulk MgH_2 releases hydrogen at useful rates only above about 300 °C [141,142,145].
- The distribution of reported apparent activation energy (E_a) values in magnesium-based hydrides is quite broad, ranging from 66 kJ/mol to 308 kJ/mol [146]. These large variations are generally rationalised because of surface oxidation for MgH_2 dehydrogenation, amounting to approximately 200 kJ/mol.
- The high activation energy observed in inactive Mg samples, i.e., those that have not undergone the H_2 cycle, is related to the presence of a MgO shell surrounding the Mg particles. This MgO shell strongly inhibits hydrogen diffusion. In this case, the kinetics are limited by H_2 diffusion along MgO-rich surfaces [146].
- When samples are activated (after several cycles of hydrogen exchange) or alloyed, the MgO layer breaks down, the surface is cleaned, and the apparent activation energy decreases. In this case, the rate-limiting step of the reaction typically becomes H_2 decomposition on the surface rather than H diffusion in MgH_2 [146].
- Combining Mg with alloys such as Al, $MgCu_2$ or Mg_2Cu may result in lower activation energies compared to pure Mg [145,146].
- $LaNi_5$-based hydrides have a lower gravimetric capacity than MgH_2, with a value of approximately 1.28–1.49 wt.%, but have been commercially successful in several applications, such as NiMH batteries.

- $LaNi_5$ is less sensitive to surface contamination and oxidation. Consequently, the reported distribution of apparent activation energies is less pronounced than for MgH_2 and generally remains between 19 kJ/mol and 38 kJ/mol [146]. The intrinsic kinetics of $LaNi_5$ are generally fast [58].

Three main strategies are employed to overcome kinetic and thermodynamic constraints: adding suitable additives (catalysts), controlling particle size (nanostructuring), and designing new reactant combinations [141].

Catalyst Doping and Alloying:

- The addition of transition metals such as Ti, V, Nb and Ni to MgH_2 systems significantly reduces the activation energy for hydrogen desorption [72,143,147]. For example, the desorption activation energy (E_a) of pure MgH_2, which is approximately 120 kJ/mol, can be reduced to 71 kJ/mol with the addition of TiH_2 [63].
- Nb_2O_5 is considered one of the most effective catalysts and provides fast sorption kinetics for MgH_2 systems [21,71]. For Mg catalysed with mesoporous Nb_2O_5, hydrogen absorption has been observed even at −50 °C, with an activation energy of about 38 kJ mol^{-1} for absorption compared with about 70 kJ mol^{-1} for desorption [148,149]. This is a kinetic effect of the catalyst on hydrogen absorption; it does not mean that MgH_2 can release hydrogen at such temperatures, since the equilibrium temperature for desorption at 1 bar H_2 remains about 285 °C (Equation (2)) [69].
- Alloying Pd with Au significantly accelerates hydrogenation kinetics through both enhanced diffusion and reduced activation energy and can shorten reaction times by up to five times compared to Pd alone [150].
- In complex hydrides, Ti addition has led to a breakthrough improvement in the reversibility and kinetics of the $NaAlH_4$ system [81]. Doping with $ScCl_3$ increased both the hydrogenation rate, by a factor of about ten relative to Ti, and the reversible storage capacity of $NaAlH_4$, whereas $CeCl_3$- and $PrCl_3$-doped samples showed excellent cycle stability [30].

Nanostructuring:

- Reducing the particle size to the nanoscale increases the specific surface area and shortens hydrogen diffusion pathways [147]. This effect is particularly important for coarse-grained Mg, in which diffusion through the growing hydride layer limits the absorption rate [151].
- Theoretical studies indicate that, in MgH_2 nanoparticles, thermodynamic properties also change as the particle size decreases; however, the most pronounced thermodynamic effects are observed when the particle size falls below 10 nm [65].
- Nanostructuring can substantially reduce the apparent activation energy of MgH_2 and improve hydrogen desorption kinetics by shortening hydrogen diffusion pathways and increasing the available surface area [147,148]. For MgH_2 nanowires, an energy barrier of about 33.5–38.8 kJ mol^{-1} has been reported, compared with 120–142 kJ mol^{-1} for bulk MgH_2 [148] (Table 7). This is a kinetic effect: it lowers the temperature at which desorption becomes fast, but the equilibrium temperature of about 285 °C at 0.1 MPa changes appreciably only for particles smaller than about 10 nm [65]. However, the extent of the reduction in desorption temperature strongly depends on particle size, catalyst addition, and experimental conditions.

Table 7. Comparison of kinetic and thermodynamic properties in metal hydrides.

Category	MH	Parameter	Value	Ref.
Thermodynamic barriers	MgH_2 (Bulk)	Formation Enthalpy (ΔH)	−75 kJ/mol H_2 (formation); +75 kJ/mol H_2 (desorption)	[141]
	MgH_2 (Bulk)	Apparent Activation Energy ($E_{a,app}$)	66–308 kJ/mol (range of reported values)	[146]
	$LaNi_5$	Apparent Activation Energy ($E_{a,app}$)	19–38 kJ/mol	[146]
Kinetic improvement	MgH_2 nanowires	Desorption Activation Energy (E_a)	33.5–38.8 kJ/mol (bulk MgH_2: 120–142 kJ/mol)	[148]
	Mg + mesoporous Nb_2O_5 catalyst	Absorption E_a	38 kJ/mol (absorption observed down to −50 °C); desorption $E_a \approx 70$ kJ/mol	[148,149]
	MgH_2 + TiF_4 Catalyst	Desorption Initial Temperature (Tonset)	150 °C (vs. 300 °C ball-milled and 400 °C as-received MgH_2)	[148]
	MgH_2 + NiS	Desorption Activation Energy (E_a)	64.71 kJ/mol H_2	[148]
Thermodynamic improvement	MgH_2/Si (Chemical Destabilisation)	Desorption ΔH	36.4 kJ/mol H_2	[143]
	MgH_2–$LiBH_4$ (RHC)	Overall reaction ΔH	46 kJ/mol H_2	[43]
	$Pd_{0.6}Au_{0.4}$ Alloy	Response Time (t_{90})	Five times faster than pure Pd	[150]
Critical size effect	MgH_2 Nanoparticles	Thermodynamic Critical Dimension	below about 10 nm (calculated)	[65]

Compensation Effect:

The linear relationship between apparent activation energy and the pre-exponential factor (Cremer–Constable relationship) suggests a compensation effect in Mg based and $LaNi_5$ hydrides. In the Arrhenius equation, the pre-exponential factor represents the frequency of successful reaction attempts, related to diffusion and surface processes in metal hydrides. However, in Mg-based systems, this effect is largely considered a mathematical consequence of Arrhenius analysis rather than a true physical phenomenon, and therefore changes in the pre-exponential factor should be interpreted with caution [146].

The fundamental challenge with metal hydrides is that high-capacity systems typically possess high thermodynamic stability, which requires temperatures far exceeding the range where waste heat from fuel cells can be utilised for decomposition. Therefore, research efforts have focused on achieving conditions suitable for practical application either by lowering the kinetic barrier (catalyst doping and nanostructuring) or by reducing the reaction enthalpy (alloying and reactive hydride composites) [141,143].

When examining the thermodynamic characteristics of hydrogen storage systems, the binding enthalpy (ΔH) between hydrogen and the metal matrix emerges as the fundamental parameter determining both the stability and practical applicability of the system. Considering the values presented in Table 7, the strength of this chemical bond is directly related to the amount of energy required for hydrogen recovery. For example, when the binding energy is low, such as 20 kJ/mol H_2, the interaction remains weak, causing the system to exhibit an unstable structure that cannot retain hydrogen even at room temperature, leading to leakage. Conversely, high values above 70 kJ/mol H_2, seen in compounds such as MgH_2, indicate that the bond is excessively strong: the equilibrium pressure of MgH_2 reaches 0.1 MPa only at about 285 °C, and in practice temperatures of 300 °C or more are required to release the hydrogen, which poses an operational obstacle in terms of energy efficiency. RHC stands for Reactive Hydride Composite, which refers to a hydrogen storage system

composed of two or more hydrides that chemically interact during hydrogen absorption and desorption to modify thermodynamic properties and improve overall storage performance. The range between these two extremes, about 30–50 kJ mol^{-1} H_2 (see above), is considered the ideal operating window, as it allows hydrogen to be stored safely at near-room temperature and released with minimal energy loss.

Comparative Structure–Property–Performance Relationships of Metal Hydrides

When comparing materials used for hydrogen storage, it is necessary to focus not only on hydrogen storage capacity but also on structure–property relationships. The primary classes of hydrides should be compared using a common framework that encompasses crystal structure and preferred hydrogen sites, equilibrium/plateau pressure, pressure hysteresis, reversible usable capacity, absorption–desorption kinetics, cyclic degradation, and system-level mass and thermal management.

These parameters are strongly interconnected. Crystal structure and hydrogen site occupancy are critical for hydride stability and diffusion characteristics; consequently, they influence equilibrium pressure, kinetics, hysteresis, and usable capacity. A favorable material-level capacity does not necessarily translate into high system-level performance, as containment, heat exchangers, insulation, auxiliary components, and heat transfer during hydrogen absorption and desorption entail additional mass, volume, and energy requirements [94].

Table 8 applies this framework to five representative systems whose crystal structures and hydrogen sites are known from diffraction studies (Section 7) and states the conditions to which each value refers. The examples below show how the structural differences propagate to the equilibrium pressure, hysteresis, usable capacity, kinetics, cycling behaviour and system-level penalties.

Table 8. Structure–property–performance relationships for representative hydrides. Values are material-level values under the stated conditions. Volume changes were calculated from the lattice parameters reported in the cited diffraction studies; the heat per kg H_2 was calculated from $|\Delta H|$ and is also given as a percentage of the lower heating value of hydrogen (119.96 MJ kg^{-1} [3]).

Property	**$LaNi_5$**	**TiFe**	**MgH_2**	**$NaAlH_4$ (Ti-doped)**	**V (VH–VH_2)**
Structure; hydrogen site	$CaCu_5$-type (P6/mmm) retained; interstitial sites [111]	B2 (CsCl-type); octahedral Ti_4Fe_2 sites; γ-$TiFeD_{1.93}$ monoclinic (P2/m) [109,110]	hcp Mg → rutile-type MgH_2 ($P4_2/mnm$); H coordinated by 3 Mg [152]	isolated $[AlH_4]^-$ tetrahedra; release via Na_3AlH_6 and NaH + Al [31,81]	β-VH → fluorite-type VH_2 at higher pressure [123]
Volume change on hydriding	≈25% [111]	≈18% (TiFe → γ) [96,110]	≈30–35% [152]	new phases formed (reconstructive)	–
ΔH (kJ mol^{-1} H_2)	−30.8 [124]	−28.1 [96]	≈−75 [141]	−37 (step 1); −47 (step 2) [81]	≈−40 (VH–VH_2) [123]
Equilibrium conditions	0.15–0.2 MPa at 25 °C (Table 6)	two plateaus (β, γ); ≈0.5 MPa desorption at 25 °C (Table 6)	0.1 MPa at ≈285 °C [69]	0.1 MPa at ≈33 °C (step 1) and ≈110 °C (step 2) [81]	plateau near room temperature [123]
Hysteresis	p_{abs}/p_{des} ≈ 1.3 at 25 °C (Table 6)	larger on the second (β → γ) plateau [96,109]	–	two plateaus [81]	sloping plateaus and large hysteresis in V-based BCC alloys [119]

Table 8. *Cont.*

Property	$LaNi_5$	TiFe	MgH_2	$NaAlH_4$ (Ti-doped)	V (VH–VH_2)
Theoretical → usable capacity (wt.%)	1.49 → ≈1.4 at room temperature below 1 MPa [112]	1.86 → lower when charging pressure is limited [96,109]	7.6 → 6.5–7.0 (R) at 200–300 °C with catalysts (Table 3)	7.4 → 5.6 accessible; 4–5 (R) at 120–150 °C with Ti [29]	3.8 → ≈2.1 (R) near room temperature [123]
Kinetic limitation	fast interstitial diffusion; $E_{a,app}$ 19–38 kJ mol^{-1} [146]	surface oxide; first hydrogenation needs ≈400 °C under H_2 [113]	slow H diffusion through MgH_2 layer and MgO; $E_{a,app}$ 66–308 kJ mol^{-1} [146]	long-range transport of Na/Al species; Ti catalyst required [29,31]	fast (Table 6)
Cycling	decrepitation into fine powder; bed compaction [58]	decrepitation; sensitivity to O_2/H_2O impurities [98,109]	grain growth at operating temperature [65]	capacity decay on long-term cycling [31]	–
Heat per kg H_2 (% of LHV)	15.3 MJ (12.7%)	13.9 MJ (11.6%)	37.2 MJ (31.0%), supplied at ≈300 °C	18.4/23.3 MJ (15.3/19.4%)	19.8 MJ (16.5%)

Interstitial hydrides with moderate stability ($LaNi_5$, TiFe). In $LaNi_5$, hydrogen occupies interstitial sites of the hexagonal $CaCu_5$-type lattice. Neutron and X-ray diffraction of $LaNi_5D_{6.5}$ show that this structure is retained (P6/mmm) while the unit-cell volume increases by about 25% [111]. Because these sites bind hydrogen weakly ($\Delta H = -30.8$ kJ mol^{-1} H_2 [124]), the $\alpha + \beta$ plateau lies at 0.15–0.2 MPa at 25 °C, and the absorption and desorption plateaus differ only by a factor of about 1.3 (Table 6). About 1.4 wt.% can therefore be cycled at room temperature below 1 MPa [112], close to the theoretical value, and interstitial diffusion keeps the apparent activation energy at 19–38 kJ mol^{-1} [146]. The penalty is mechanical: the large lattice expansion breaks the particles into a fine powder during the first cycles [58], which facilitates activation but lowers the effective thermal conductivity of the bed and causes compaction in the tank. TiFe stores hydrogen in octahedral sites formed by four Ti and two Fe atoms, and hydrogenation proceeds through the β monohydride and the γ dihydride, whose monoclinic structure was determined by neutron diffraction of $TiFeD_{1.93}$ [109,110]. The two hydride phases produce two plateaus; the second ($\beta \rightarrow \gamma$) plateau lies at a higher pressure and shows a larger hysteresis [96,109], so that part of the theoretical 1.86 wt.% cannot be used when the charging pressure is limited to a few MPa. In addition, the surface oxide blocks hydrogen uptake, and the first hydrogenation requires heating to about 400 °C under hydrogen pressure [113]. For both alloys, the heat to be removed during charging is only 14–15 MJ per kg H_2 (12–13% of the lower heating value) and can be handled near room temperature, so that the main system-level penalty is the mass of the alloy, vessel and heat exchanger [94].

Reconstructive light hydride (MgH_2). On hydrogenation, hcp Mg transforms into rutile-type MgH_2 ($P4_2/mnm$), in which each hydrogen atom is coordinated by three Mg atoms [152]. This transformation increases the volume by about one third, and the strong Mg–H bond ($\Delta H \approx -75$ kJ mol^{-1} H_2 [141]) shifts the temperature at which the equilibrium pressure reaches 0.1 MPa to about 285 °C [69]. Hydrogen diffuses slowly through the hydride, so that a hydride layer formed on the particle surface hinders further absorption, and the surface MgO layer adds a further barrier; reported apparent activation energies therefore range from 66 to 308 kJ mol^{-1}, depending on the surface state of the samples [146]. Ball milling and catalysts reduce these barriers, and catalysed MgH_2 cycles 6.5–7.0 wt.% at 200–300 °C (Table 3), but grain growth at these temperatures gradually reduces the benefit of nanostructuring [65]. At the system level, the decisive penalty is thermal: about 37 MJ

of heat per kg H_2, equivalent to 31% of the lower heating value of the released hydrogen, must be supplied at close to 300 °C, which cannot be provided by the waste heat of a PEM fuel cell [94,153].

Complex hydride ($NaAlH_4$). In $NaAlH_4$, hydrogen is covalently bound in isolated $[AlH_4]^-$ tetrahedra, so that its release requires the decomposition of the anion and the formation of new phases rather than interstitial diffusion: $NaAlH_4 \rightarrow 1/3\ Na_3AlH_6 + 2/3\ Al + H_2 \rightarrow NaH + Al + 3/2\ H_2$ [81]. The two steps have desorption enthalpies of 37 and 47 kJ mol^{-1} H_2 and reach 0.1 MPa at about 33 and 110 °C, respectively [81]. The isotherm therefore shows two plateaus, and only 5.6 of the stoichiometric 7.4 wt.% is accessible, because NaH decomposes only at much higher temperatures. With 2 mol% Ti, 4–5 wt.% is cycled reversibly at 120–150 °C (Table 4) [29]. Because Na- and Al-containing species must be transported over long distances between the separate phases, the kinetics remain limited by mass transport even in the presence of the catalyst, and the capacity decays during long-term cycling [31]. Time-resolved in situ X-ray diffraction has followed the formation and decomposition of the Na_3AlH_6 intermediate under conditions close to PEM fuel-cell operation [154]. The heat demand of 18–23 MJ per kg H_2 is lower than that of MgH_2, but the second step requires temperatures above the waste-heat level of a PEM fuel cell.

Site-dependent stability in BCC alloys (V–H). In the V–H system, the β monohydride is much more stable than the fluorite-type VH_2 formed at higher hydrogen pressure. Only the VH–VH_2 step has an equilibrium pressure near room temperature ($\Delta H \approx -40$ kJ mol^{-1} H_2), so that only about 2.1 wt.% of the 3.8 wt.% stored can be cycled under these conditions [123]. The same difference between hydrogen sites underlies the sloping plateaus and large hysteresis of V-based BCC solid-solution alloys [119], which reduce the capacity available between practical charging and discharging pressures.

These examples show that the structural origin of storage—interstitial sites with a small or a large volume change, or a reconstructive reaction that forms new phases—determines not only the capacity but also the pressure window, the fraction of the capacity that can be used, the rate-limiting step and the thermal load that the storage system must handle.

The values compiled in Tables 3–7 were obtained under different temperatures, pressures, catalyst loadings and cycling conditions; they can therefore be compared directly only where these conditions are similar, as discussed in Section 7.

6. Hydrogen Storage Standards

Metal hydride (MH) hydrogen storage is a technology that enables hydrogen to be stored at low pressure and with high safety within a solid material. As hydrogen can be stored in gaseous form at high pressures, applications exist to reduce this pressure. Standards in this field are more specific than those for high-pressure gas storage and generally focus on material performance characterisation and system cycle life. [155] The standards relevant to metal hydride storage can be grouped into three distinct levels, and Figure 15 should be read with this distinction in mind. The first level comprises material characterisation standards, which prescribe how the pressure–composition–temperature behaviour, the absorption and desorption rates and the cycle life of hydrogen-absorbing alloys are to be measured; Japan (JIS H 7003 and JIS H 7201–7204) and China (GB/T 33291-2016) have both issued standards at this level [156–161]. The second level comprises standards for complete metal hydride storage systems, which internationally are covered mainly by ISO 16111 [162], specifying the requirements for transportable hydrogen storage devices in which hydrogen is absorbed in a reversible metal hydride; this standard is applied internationally and has been adopted as a national standard in several countries, for example the United Kingdom, Australia and the Republic of Korea. The third level comprises broader hydrogen system regulations, which address compressed gas and liquid hydrogen storage and apply to metal

hydride installations only indirectly. Seen in this way, the United States possesses the most extensive body of hydrogen storage standards overall but addresses metal hydride storage only through system-level and general hydrogen regulations rather than through material-specific documents, whereas Japan is the only country with a complete set of material-level standards dedicated to hydrogen-absorbing alloys. In Canada and France no material-level standard specific to metal hydrides has been issued and national standardisation efforts focus on compressed gas and liquid hydrogen technologies. Overall, global hydrogen storage standards remain shaped around conventional storage methods; metal hydride storage is covered comprehensively at the material level only in Japan, partially in China through GB/T 33291-2016, and elsewhere only through system-level standards such as ISO 16111.

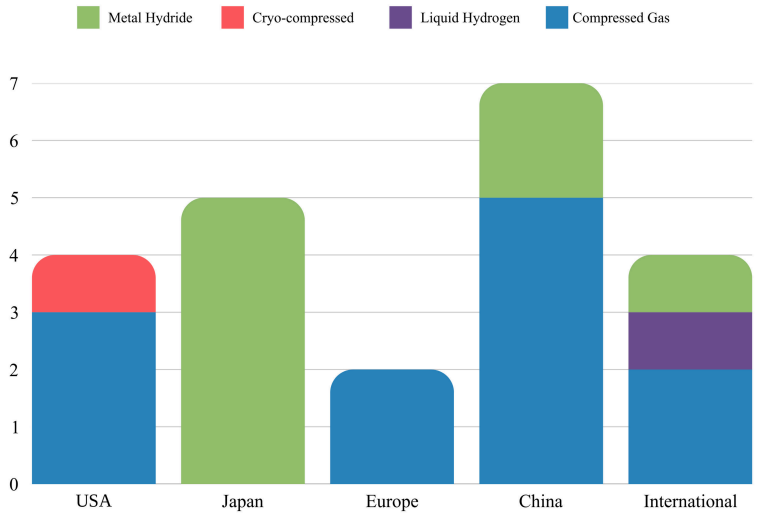


Figure 15. Storage standards for four different hydrogen storage techniques by country. For metal hydride storage the map refers to material-level standards only; system-level coverage through ISO 16111 and its national adoptions is not included in the map.

Table 9 lists the material-level standards issued between 1995 and 2016 for the characterisation of hydrogen-absorbing alloys. Japan accounts for the most complete set of such documents, covering terminology, pressure–composition–temperature relations, reaction rate, cycle characteristics and heat of reaction, while China contributes one standard, GB/T 33291-2016, devoted to pressure–composition–temperature measurement. Standards governing complete metal hydride storage systems, principally ISO 16111 and its national adoptions, and the broader hydrogen-system regulations discussed above are deliberately not listed in Table 9, since they do not address material characterisation. The small number of material-level standards indicates that metal hydride technologies are still at a limited level of commercial and industrial maturity.

Table 9. Material-level standards for the characterisation of hydrogen-absorbing alloys [156–161].

Organization	Standard Code	Name of Standards	Year
Guobiao Standards	GB/T 33291-2016	Measurement method of pressure-composition temperature for reversible hydrogen absorption and desorption of hydrides	2016
Japanese Industrial Standard	JIS H 7003:2007	Glossary of terms used in hydrogen absorbing alloys	2007

Table 9. *Cont.*

Organization	Standard Code	Name of Standards	Year
Japanese Industrial Standard	JIS H 7201:2007	Method for measurement of pressure-composition temperature (PCT) relations of hydrogen absorbing alloys	2007
Japanese Industrial Standard	JIS H 7202:2007	Method for measurement of hydrogen absorption/desorption reaction rate of hydrogen absorbing alloys	2007
Japanese Industrial Standard	JIS H 7203:2007	Method for measurement of hydrogen absorption/desorption cycle characteristic of hydrogen absorbing alloys	2007
Japanese Industrial Standard	JIS H 7204:1995	Method for measuring the heat of hydrating reaction of hydrogen absorbing alloys	1995

7. Metal Hydride Analysis Method

The most common test setup used to determine hydrogen storage performance is Sieverts-type devices, which measure the amount of hydrogen absorbed by the material by monitoring changes in hydrogen pressure in a reactor with a fixed volume [55,159,160,163]. Pressure–Composition–Temperature (PCT) or Pressure–Composition–Isotherm (PCI) curves, which indicate the thermodynamic equilibrium of the material, are created using the data obtained from these devices; these curves reveal the plateau pressure at which the material transitions from the solid solution phase to the hydride phase and its reversible capacity [56,95]. Alternatively, three-electrode electrochemical systems that measure electron/ion transfer during hydrogen absorption and desorption, or Differential Scanning Calorimetry (DSC) and Temperature-Programmed Desorption (TPD) methods that monitor thermal changes, are also used in testing processes [163,164]. When calculating storage capacity, the weight percentage (wt.%) unit is generally used, and this value is obtained by dividing the mass of absorbed hydrogen by the total mass of hydrogen and metal [58]. For the thermodynamic analysis, the van't Hoff equation is used, and mathematical approaches such as the Arrhenius equation for reaction kinetics and activation energy, and the Johnson–Mehl–Avrami–Kolmogorov (JMAK) equation (Equation (3)) defining nucleation-growth models are utilised [56,64].

$$X(t) = 1 - \exp(-k \cdot t^n) \quad (3)$$

$X(t)$, the fraction of transformation at time t (between 0 and 1), k: rate constant (temperature dependent), n: Avrami exponent, indicates the transformation mechanism and nucleation/growth type, t: time.

At the material level, the gravimetric hydrogen capacity is defined as the mass of absorbed hydrogen divided by the mass of the hydrogenated material, that is, by the sum of the mass of the absorbed hydrogen and the mass of the host metal or alloy in its hydrogen-free state. The two mass terms are therefore the mass of hydrogen taken up by the sample and the mass of the host metal or alloy; their sum is, by definition, the mass of the metal hydride, so that no mass is counted twice in the denominator [58,95]. This material-level definition refers exclusively to the storage medium itself and must be kept distinct from the system-level definition given in Equations (6) and (7), in which the mass of the tank, the heat exchanger, the valves and the remaining balance-of-plant components is also included in the denominator [165].

$$\text{Percentage by weight (wt.\%)} = \frac{\text{mass of absorbed hydrogen}}{\text{mass of absorbed hydrogen + mass of host metal or alloy}} \times 100 \quad (4)$$

$$\text{wt.\%} = \frac{m_{H_2}}{m_{H_2} + m_M} \times 100 \quad (5)$$

Theoretical capacity values are generally based solely on the weight of the material itself, whereas in applications such as system targets determined by the DOE, the total weight of the tank and all components is added to the denominator to measure the system's efficiency [166]. The total system mass here includes the metal powder as well as the tank body, the heat exchangers inside it, the valves and the sensors.

$$\text{Percentage by weight (wt.\%)} = \frac{\text{mass of absorbed hydrogen}}{\text{mass of total system}} \times 100 \quad (6)$$

$$\text{wt.\%} = \frac{m_{H_2}}{m_{\text{total system}}} \times 100 \quad (7)$$

The Van't Hoff graph shows the linear relationship between the natural logarithm of the equilibrium pressure (plateau pressure) ($\ln P_{eq}$) and the inverse of the absolute temperature (1/T) in a metal hydride system [58,97]. The slope and intersection points in this graph provide the following critical information about the thermodynamic identity of the material: The slope of the graph is used to determine the enthalpy change (ΔH) of the reaction and mathematically represents the value of $\Delta H/R$ (R: gas constant) [58,97]. Enthalpy is a direct measure of the bond strength between the metal and hydrogen and the thermal stability of the resulting hydride [58,97]. The magnitude of the slope indicates how strongly hydrogen is bonded to the metal; for example, a high enthalpy value indicates that the material is very stable and requires very high temperatures to release hydrogen [58,97].

The point where the graph intersects the vertical axis represents the entropy change in the reaction and is mathematically expressed as $\Delta S/R$. The entropy change (ΔS) describes the change in disorder during the transition of hydrogen from the gas phase to the dissolved state in the solid phase. In metal–hydrogen systems, this value varies only slightly between hydride-forming alloys (about 111 ± 14 J K^{-1} mol^{-1} H_2), because it is dominated by the loss of the entropy of gaseous hydrogen, about 130 J K^{-1} mol^{-1} H_2 [97]. Using these two values, the temperature at which the equilibrium pressure of a material reaches 0.1 MPa (1 bar) is

$$T = \Delta H/\Delta S \quad (8)$$

and can be estimated using the formula [58,97]. This information is vital for understanding whether the storage system can operate with waste heat in applications such as fuel cells and for designing the system's heat management, i.e., how much cooling is required during absorption and how much heating is required during desorption [58].

Figure 16 shows a typical laboratory test rig for metal hydride tanks. Hydrogen is supplied from a cylinder through pressure regulators and gas flow meters, while cold- and hot-water circuits remove the heat released during absorption and supply the heat required for desorption. Thermocouples and pressure gauges on the tank record the data from which the charging time, usable capacity and thermal behaviour of the hydride bed are obtained [165–167].

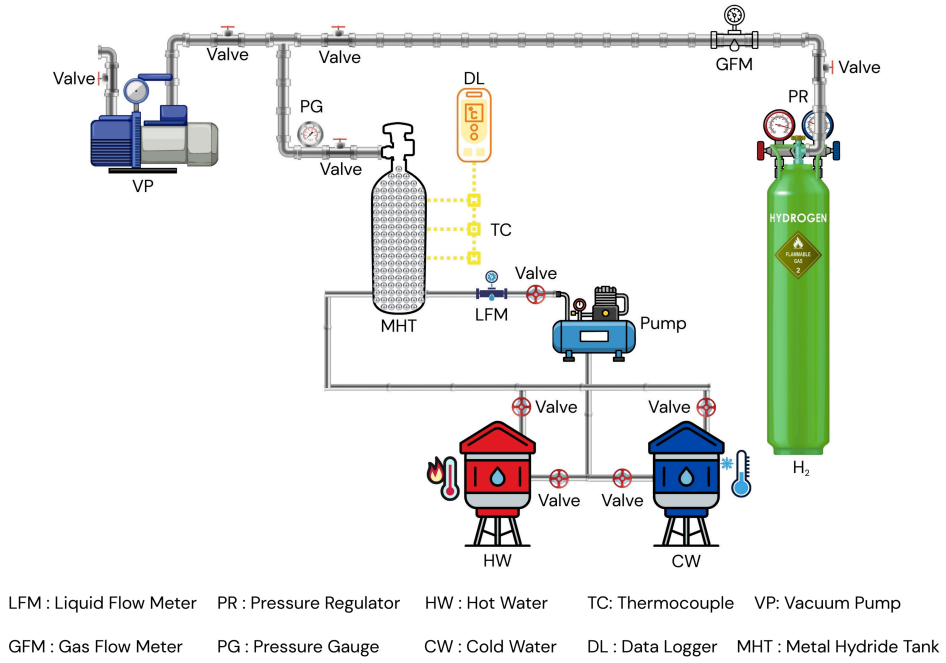


Figure 16. Metal Hydride Storage Test System.

7.1. DTA

In DTA, the temperature difference between the sample and an inert reference is recorded during a controlled temperature programme, so that hydride decomposition appears as an endothermic peak [164].

If DTA is performed at different heating rates, the decomposition activation energy of the hydride can be calculated using the Kissinger method [168]. At the same time, peak shifts, expansions, and the emergence of new phases in the obtained results indicate degradation [58]. The temperature (T_m) corresponding to the maximum hydrogen desorption rate obtained from DTA analyses was determined for different heating rates (β), and the activation energies were calculated using the Kissinger equation according to this method, the linear relationship between $\ln\left(\beta/T_m^2\right)$ and $1000/T_m$ enables the reliable evaluation of the kinetic parameters of the dehydrogenation process [168,169]. Compared to pure MgH_2, the activation energy in MgH_2 samples doped with 16.7% (by weight) MoO_2 and MoS_2 was found to decrease to 101.34 ± 4.32 kJ mol^{-1} and 87.19 ± 4.48 kJ mol^{-1}, respectively. These results indicate that the addition of MoX_2 (X = O, S) significantly reduces the energy barrier in the hydrogen desorption process of MgH_2 and markedly improves the dehydrogenation kinetics [169]. In the same study, the DTA desorption temperature decreased from 662 K for pure MgH_2 to 650 K and 640 K after the addition of MoO_2 and MoS_2, respectively [169]. Schematic pressure–composition isotherms and the corresponding van 't Hoff plot, calculated for an AB_5-type alloy with the $LaNi_5$ parameters used in this review (ΔH_{des} = 30.8 kJ mol^{-1} H_2 [124]; $\Delta S_{des} \approx 108$ J K^{-1} mol^{-1} H_2, obtained from the plateau pressure at 25 °C in Table 6), are shown in Figure 17A,B. The distinct α-phase, α + β two-phase region, and β-phase can be clearly identified, while the temperature dependence of the plateau pressure provides the basis for determining the reaction enthalpy (ΔH) and entropy (ΔS). The crystal structures of hcp Mg and of rutile-type MgH_2, drawn from the structural data in [152], are shown in Figure 17C,D. On hydrogenation, the hexagonal metal lattice is replaced by the tetragonal hydride, in which each Mg atom is octahedrally coordinated by six H atoms and each H atom by three Mg atoms [152]; this reconstructive transformation and the associated volume increase of about one third (Table 8) explain the slow hydrogen diffusion

through the hydride discussed in Section Comparative Structure–Property–Performance Relationships of Metal Hydrides.

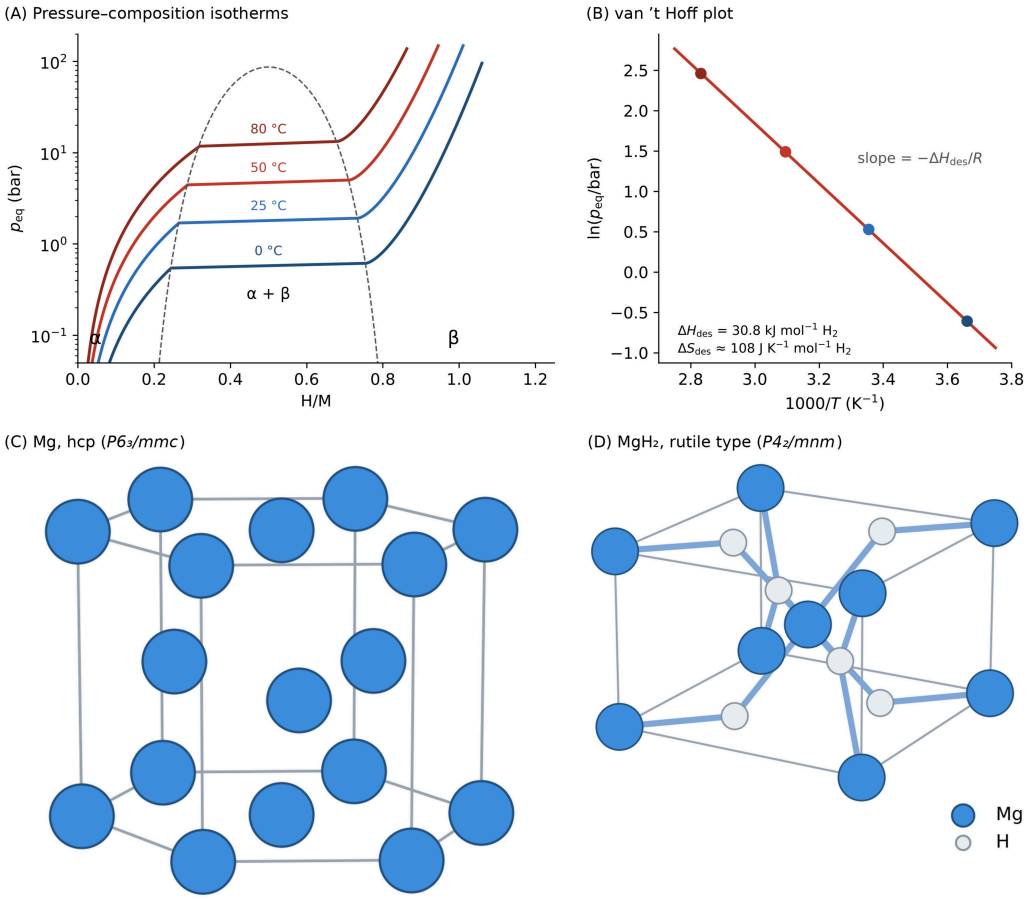


Figure 17. (**A**) Schematic pressure–composition isotherms; (**B**) the corresponding van 't Hoff plot for an AB_5-type alloy; (**C**) crystal structure of hcp Mg; and (**D**) of rutile-type MgH_2. The coloured points in (**B**) are the plateau pressures of the isotherms of the same colour in (**A**).

7.2. DSC

DSC records the difference in heat flow between the sample and a reference. For metal hydrides, the area of the desorption or absorption peak gives the reaction enthalpy, and the peak position gives kinetic information. Under hydrogen atmosphere, isobaric DSC measurements provide a rapid alternative to classical pcT (pressure–composition–temperature) diagrams for determining the relationship between equilibrium pressures and temperatures [164,170].

To determine decomposition temperatures, the onset temperature of hydrogen release (T_{onset}) and the peak temperature at which the reaction rate reaches its maximum (T_{peak}) are identified [171]. For example, this method verifies how much the high decomposition temperature of magnesium hydride (MgH_2) is reduced by catalysts or mechanical grinding [171–174]. Similarly, Kissinger analysis is performed on the data obtained by subjecting the sample to different heating rates (e.g., 20 °C/min) to determine the activation energy [172,175]. This analysis enables the quantitative calculation of the energy barrier that must be overcome for hydrogen release [172,176,177]. In multi-component hydride systems (MgH_2-NaAlH4), the number of stages in which desorption occurs and which phases react in each stage can be tracked via overlapping or separate peaks in the DSC curves [178–180]. In evaluating catalyst activity, the catalytic effect of additives (Ni, Co,

etc.) on the hydride is measured by the shift in DSC peaks to lower temperatures and decreases in enthalpy/activation energy [174,176,177].

Metal hydrides are highly sensitive to air and moisture, so sample preparation and weighing procedures are typically carried out in an inert atmosphere glove box. To determine the type of gas released during DSC analysis, the DSC instrument is usually coupled with a Mass Spectrometer (MS) (DSC-MS). The activation energy (E_a) of the dehydrogenation process of MgH_2 can be calculated from the maximum reaction temperatures (T_m) determined from the DSC curves obtained at different heating rates (β) and the universal gas constant R (8.314 J mol^{-1} K^{-1}) by means of the Kissinger equation (Equation (9)) [168].

$$\ln\left(\frac{\beta}{T_m^2}\right) = \frac{-E_a}{RT_m} + \text{const} \quad (9)$$

The thermal dehydrogenation behaviour of different metal hydride hydrogen storage materials has been examined in detail using DSC curves obtained under various experimental conditions and material compositions [171–183]. Figure 18A compares pure MgH_2 with MgH_2 + 5 wt.% $TiH_{1.971}$ at heating rates of 5–12 K min^{-1}: the catalyst lowers the desorption peak from about 378–397 °C to 281–307 °C [184]. Figure 18B,C show the effect of milling time for MgH_2 catalysed with $ZrNi_5/Nb_2O_5$ (12.5 h and 50 h) under 1 bar He [185].

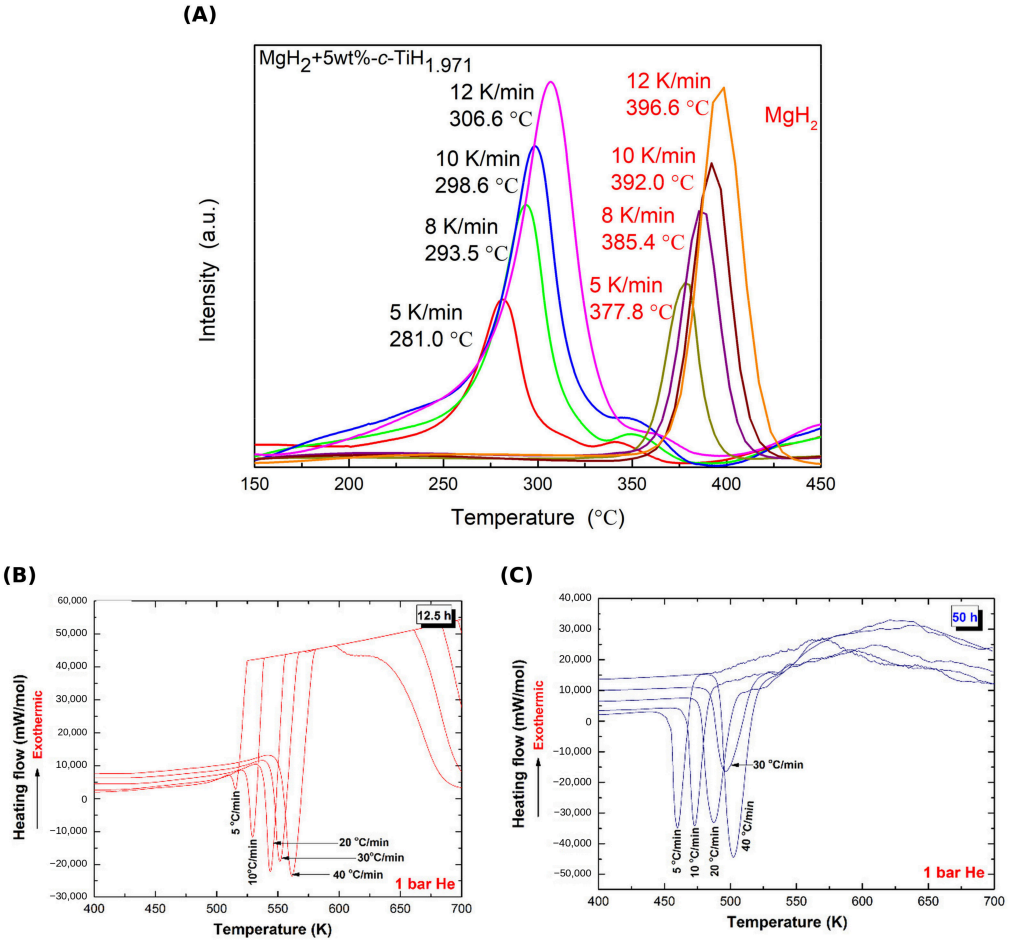


Figure 18. DSC curves of MgH_2-based materials: (**A**) pure MgH_2 and MgH_2 + 5 wt.% $TiH_{1.971}$ at different heating rates; (**B**,**C**) MgH_2/5 wt.% ($ZrNi_5/Nb_2O_5$) milled for 12.5 h and 50 h, measured under 1 bar He. (Adapted from [184,185] under the CC BY 4.0 licence).

7.3. TGA

TGA records the mass of a sample as a function of temperature or time under a controlled atmosphere; for metal hydrides, the mass loss on heating directly gives the amount of hydrogen released [166,186].

In hydrogen storage material research, particularly in the characterisation of metal hydrides, the TGA method plays an important role [187]. The primary application of TGA for metal hydrides is to determine the hydrogen desorption behaviour and the material's total hydrogen storage capacity [164,187]. When the sample is heated, hydrogen gas is released as the hydride phase decomposes, and this is observed as a mass loss in the TGA curve [166]. For example, in the TGA analysis of a metal hydride such as $TiH_{1.9}$, the mass loss is directly related to the hydrogen content of the material. The temperature range at which desorption occurs indicates the thermal stability of the material [188].

The interpretation of mass loss curves is critical for understanding the desorption mechanism of metal hydrides. In materials exhibiting multi-step decomposition (e.g., $NaAlH_4$ or MgH_2-$NaAlH_4$), distinct inflection points corresponding to each step are observed on the TGA curve [178,180]. The first derivative curve, DTG (Derivative Thermogravimetry), displays the temperatures at which mass loss is maximum as peaks, enabling overlapping reactions to be distinguished from one another and kinetic analyses (e.g., activation energy calculations) to be performed more accurately [166,186].

Because TGA alone cannot identify the released gases and is affected by buoyancy at high temperatures, it is usually coupled with DSC or DTA, to separate mass-loss events from transitions without mass change such as melting, and with mass spectrometry, to detect by-products such as NH_3 or B_2H_6 [166,167].

The Thermogravimetric behaviour of different metal hydride hydrogen storage materials has been examined in detail using TGA curves obtained under various experimental conditions and material compositions [170,187,189–192]. Figure 19 compares TGA results for different hydride classes: MgH_2 with and without single-walled carbon nanotubes, measured together with DSC [193]; $LiAlH_4$ with increasing amounts of h-BN, which reduces the mass loss [194]; the isothermal decomposition of γ-$Mg(BH_4)_2$ at 240–400 °C [195]; TiH_2 with Fe and Nb additions, which decomposes above about 500 °C [196]; and, for comparison, ammonia borane and its polymer composites [197].

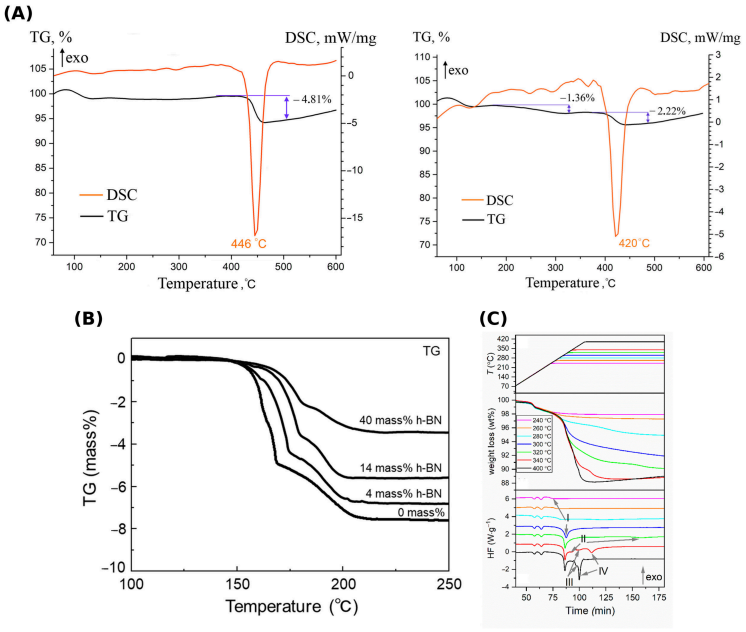


Figure 19. *Cont.*

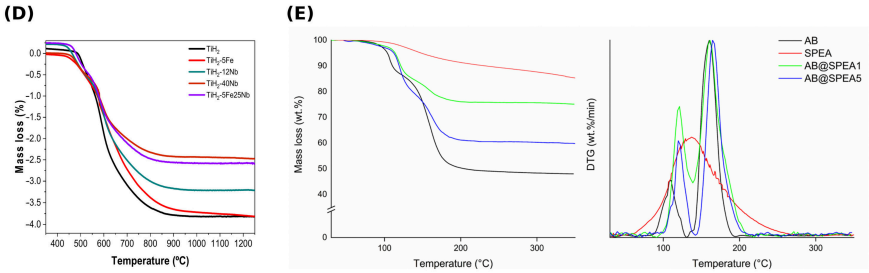


Figure 19. TGA curves of hydrogen storage materials: (**A**) MgH_2 and MgH_2–5 wt.% SWCNT (TG and DSC); (**B**) $LiAlH_4$ with 0–40 mass% h-BN; (**C**) isothermal decomposition of γ-$Mg(BH_4)_2$ at 240–400 °C (temperature programme, mass loss and heat flow); (**D**) TiH_2 and TiH_2 with Fe and Nb additions; (**E**) ammonia borane and its composites with sulphonated poly(ellagic acid) (TGA and DTG). (Adapted from [193–197] under the CC BY 4.0 licence).

7.4. XRD and Neutron Diffraction

X-ray diffraction (XRD) is the standard method for identifying the phases present before and after hydrogenation and for determining lattice parameters, crystallite size and microstrain. For metal hydrides, laboratory XRD is used, for example, to confirm the formation of the hydride phase, to detect the metastable orthorhombic γ-MgH_2 formed during high-energy ball milling of MgH_2 and to follow the decrease in crystallite size with milling time [171]. Rietveld refinement gives phase fractions and lattice parameters. The change in unit-cell volume on hydrogenation, about 25% for $LaNi_5$ → $LaNi_5D_{6.5}$ [111] and about one third for Mg → MgH_2 [152], is directly related to decrepitation, bed compaction and the mechanical stability of the material during cycling (Section Comparative Structure–Property–Performance Relationships of Metal Hydrides, Table 8). Peak broadening after cycling indicates the accumulation of lattice strain and defects, and the appearance of new reflections indicates disproportionation or oxidation.

Because hydrogen has only one electron, it scatters X-rays very weakly, particularly next to heavy atoms such as La or Ni, and its positions cannot normally be determined by XRD. Neutron diffraction overcomes this limitation, because the neutron scattering length of hydrogen is comparable to that of metal atoms. Deuterated samples are generally used, because ordinary hydrogen has a large incoherent scattering cross-section that produces a high background [115]. Neutron diffraction determined, for example, the rutile-type structure of MgD_2 [152], the interstitial deuterium sites in $LaNi_5D_{6.5}$ [111], the monoclinic structure of γ-$TiFeD_{1.93}$ [110] and the occupation of tetrahedral sites in the fluorite-type Group IV A dihydrides [100]; these site assignments provide the structural basis for the comparison in Section Comparative Structure–Property–Performance Relationships of Metal Hydrides. In situ and time-resolved synchrotron XRD combines high intensity with short acquisition times and allows the phase sequence to be followed during heating or under hydrogen pressure. It has been used to follow the polymorphic transitions and decomposition of $Mg(BH_4)_2$ and $Ca(BH_4)_2$ [39] and the formation and decomposition of Na_3AlH_6 during cycling of Ti-doped $NaAlH_4$ [154]. Combined with PCT, DSC or TGA data, such measurements assign each volumetric or thermal event to a specific structural change.

Two limitations of thermal analysis are important for the comparisons made in this review. First, the onset and peak temperatures obtained from DTA, DSC and TGA are kinetic quantities: they shift to higher values with increasing heating rate, which is the basis of the Kissinger method [168], and they also depend on sample mass, particle size, purge gas and hydrogen back-pressure. They are therefore not the same as the thermodynamic equilibrium temperature defined by Equation (8), and desorption temperatures compiled in this review can be compared directly only when they were obtained under similar conditions. Second, thermal analysis does not provide structural information. The identification of

intermediate phases, the phase sequence during hydrogenation and dehydrogenation, and hydrogen site occupancy require the diffraction methods described above, in particular in situ synchrotron X-ray diffraction, as applied, for example, to the phase transitions and thermal decomposition of $Mg(BH_4)_2$ and $Ca(BH_4)_2$ [39], and neutron diffraction, which, for example, located hydrogen on the tetrahedral sites of the fluorite-type Group IV A dihydrides [100].

8. Conclusions

We are entering a new era in which hydrogen is no longer merely a secondary energy carrier but is being recognised as a direct energy source, driven by the discovery of natural reserves and the growing potential for cross-border trade. At the heart of this transformation are innovative storage technologies that will enable hydrogen to be integrated into the system more actively and safely. In contrast to the enormous volume and safety issues created by traditional high-pressure gas or cryogenic liquid storage methods, metal hydrides are a strong candidate, allowing hydrogen to be stored in solid form, at low pressure and with very high volumetric density. The integration of renewable energy sources into the grid and the standardisation and definition of green hydrogen are particularly important for decarbonisation goals. In this new ecosystem, where the need for low-carbon transport and energy-efficient storage is increasing, existing standards must be expanded to cover these solid-state technologies so that metal hydrides can play an active role. The current lack of direct material-based standards for metal hydride storage is slowing down the industrial maturity of these innovative alloys and their full integration into the commercial ecosystem.

The increase in the international trade volume of hydrogen and the reduction in its levelled cost of hydrogen (LCOH) largely depend on the improvement of operational steps and storage processes. Overcoming disadvantages encountered in metal hydride systems, such as high hydrogen desorption temperatures and slow reaction kinetics, through nanostructuring, catalyst addition, and next-generation alloy engineering are key cost-reduction strategies that the academic literature should focus on. Furthermore, optimising initial investment costs (CAPEX) by reducing dependence on rare earth and other critical elements in some heavy metal hydrides [198–200] and resolving industrial scale-up issues for the material will significantly boost the hydrogen ecosystem. Optimising the thermodynamic and kinetic limits of metal hydride-based systems, digitising the hydrogen value chain to become data-driven, and anchoring the entire process in international regulations are essential for sustainable success; life-cycle assessment and life-cycle cost analysis provide the appropriate framework for comparing storage options [201,202]. By taking these steps, metal hydrides will become the fundamental pillar of the future safe, efficient, and low-carbon hydrogen economy.

The success of the hydrogen ecosystem depends on the integration of the production, storage and utilisation stages; however, the intermittent nature of renewable energy sources necessitates the inclusion of storage technologies in the system to ensure reliable and continuous energy supply. Hydrogen storage is considered the bottleneck of this ecosystem, and the efficient storage of energy is vital to achieving net-zero emissions targets.

Hydrogen's low density requires large storage volumes in traditional compressed gas or liquefaction methods, leading to technical challenges. Metal hydrides offer the possibility of solid-state storage by absorbing hydrogen at the atomic level within a metal lattice structure, thereby providing high safety and compactness at low pressures. As discussed in Sections 3 and 4, metal hydrides have the ability to store hydrogen even more densely than in the liquid phase (71 kg/m^3), which makes them particularly attractive where volumetric density, rather than gravimetric density, is the limiting criterion.

Different classes of metal hydrides offer various advantages depending on their application areas. Magnesium-based lightweight metal hydrides hold great potential for portable systems with their high gravimetric capacities of up to 7.6%, but their high hydrogen release temperatures pose an operational challenge. On the other hand, intermetallic hydrides such as $LaNi_5$ and TiFe, despite their low mass capacities, offer a more commercially mature technology by exhibiting fast reaction kinetics and high cycle stability at near-room temperature conditions. The selection of these materials is based on optimising the delicate balance between mass capacity and operating temperature.

The transfer of metal hydrides from laboratory studies to real storage units depends mainly on heat management, because hydrogen absorption is exothermic and desorption is endothermic; the rate at which heat can be removed or supplied through the hydride bed often limits the charging and discharging rate more strongly than the intrinsic kinetics of the material [59,94]. Low-temperature intermetallic hydrides are already used in stationary storage, in hydrogen compressors that exploit the temperature dependence of the plateau pressure [97], and in niche mobile applications such as submarines, where their high weight is not a disadvantage. Their wider use will require improved bed thermal conductivity, control of volume expansion and decrepitation, tank integration with the waste heat of fuel cells, and a reduction in the cost of alloying elements.

The use of hydrogen in the transport sector offers a solution to the long charging times of electric vehicles and provides users with a refuelling experience similar to that of fossil fuels. Vehicle designs require fuel tanks that are lightweight yet durable and compact; the high volumetric efficiency offered by metal hydrides enables seamless integration into vehicle architectures with limited space. In particular, increasing the mass capacity of light metal hydrides and resolving thermal management issues will directly contribute to the goal of zero-emission transport by increasing the range and performance of fuel cell vehicles.

Although metal hydride-based systems offer safe and compact storage solutions, the reaction kinetics and thermodynamic properties need to be improved for practical applications to become widespread. The studies reviewed here indicate that strategies such as nanostructuring, catalyst addition (Nb_2O_5, TiH_2, etc.) and high-entropy alloys have been successful in lowering hydrogen release temperatures and increasing charging rates. Considering the research conducted and standards developed, it is anticipated that metal hydride technology will be the cornerstone of the future hydrogen economy in both stationary energy storage units and mobile applications.

Author Contributions: Writing—original draft, Z.E.; methodology, Z.E.; investigation, Z.E.; data curation, Z.E.; visualization, Z.E.; writing—review and editing, B.D.; conceptualization, B.D.; project administration, B.D.; supervision, A.G.; validation, A.G.; funding acquisition, A.G. All authors have read and agreed to the published version of the manuscript.

Funding: This research was funded by the Gazi University Scientific Research Projects Coordination Unit, grant number FGA-2026-10761. The first author (Z.E.) gratefully acknowledges the Scientific and Technological Research Council of Türkiye (TÜBİTAK) for providing scholarship support throughout this study under the 2210-A National MSc Scholarship Program.

Data Availability Statement: No new data were created in this study; data sharing is not applicable to this article.

Acknowledgments: During the preparation of this manuscript, the authors used AI-based tools (Claude Opus 5.5, Anthropic, web version, 2026; Grammarly and DeepL, web versions, 2026) for language editing and simplification of literature content. The authors have reviewed and edited the output and take full responsibility for the content of this publication.

Conflicts of Interest: The authors declare no conflicts of interest.

Appendix A

Table A1 compiles representative literature values for the main hydride classes compared in Section 4.3. Each entry states the material and, where available, the conditions to which the value refers. The values are given for orientation only and should be compared only where the conditions are similar.

Table A1. Representative literature values for the main hydride classes.

Material Class	Property	Representative Literature Value (Material, Conditions)	Ref.
Light elemental hydrides (e.g., MgH_2)	Gravimetric capacity	MgH_2: 7.6 wt.% H	[57,69]
	Volumetric capacity	MgH_2: 110 kg H_2 m^{-3}	[69]
	Ease of activation	Mg must be exposed to H_2 at higher temperature and pressure than in subsequent operation	[69]
	Kinetics	Very slow kinetics of pure MgH_2; conversion of Mg to MgH_2 difficult below 350 °C; accelerated by milling and catalysts	[69]
	Safety	Activated or nanostructured powders are often pyrophoric	[69]
	Abundance	Mg is highly abundant and relatively inexpensive	[69,198]
Complex hydrides (e.g., $LiBH_4$, $NaAlH_4$)	Gravimetric capacity	$LiBH_4$: 18.5 wt.% (theoretical); $NaAlH_4$: 7.4 wt.% (theoretical), of which 5.6 wt.% is accessible in two steps; 4–5 wt.% reversible with Ti at 120–150 °C	[29,31,88]
	Volumetric capacity	$LiBH_4$: 122 kg H_2 m^{-3}	[88]
	Ease of activation	Rehydrogenation of $LiBH_4$ requires 873 K and 35 MPa for 12 h	[88]
	Kinetics	Multi-step desorption; slow rehydrogenation (see above)	[31,88]
	Safety	Diborane (B_2H_6) release from borohydrides; alanates flammable in air or moisture and ignite in contact with water	[31,88]
	Reversibility	Bulk $LiBH_4$ loses 72% of its capacity over three cycles (about 40% when nanoconfined); long-term capacity decay in doped $NaAlH_4$	[31,88]
	Abundance	Na and Al are major crustal elements; Li and B are trace elements	[198]
Transition metal hydrides (e.g., TiH_2, VH_2, PdH)	Gravimetric capacity	VH–VH_2: about 2 wt.% reversible (Table 6)	[123]
	Volumetric capacity	TiH_2: 9.5×10^{22} H atoms cm^{-3} (about 159 kg H_2 m^{-3})	[100]
	Abundance	Ti is a comparatively abundant crustal element; V, Zr and Pd are less abundant	[198]

Table A1. *Cont.*

Material Class	Property	Representative Literature Value (Material, Conditions)	Ref.
High-entropy hydrides	Gravimetric capacity	0.59–3.5 wt.%; TiVZrNbHf: 2.7 wt.% (H/M = 2.5)	[104]
	Volumetric capacity	H/M close to 2 for most alloys, comparable to transition metal dihydrides	[104]
	Ease of activation	Activation typically by initial hydrogenation and degassing at elevated temperature under dynamic vacuum	[104]
	Kinetics	TiZrNbTa: equilibrium within 1 min at 293 K (after 150 s incubation); $Ti_{0.30}V_{0.25}Zr_{0.10}Nb_{0.25}Ta_{0.10}$: 2 H/M within 2 min at 373 K	[104]
	Reversibility	Limited cycling data: stable over 10 cycles for one alloy, fading within 5 cycles for another	[104]
	Abundance	Ti, V and Zr used in at least 80% of reported alloys; several compositions contain Nb, Hf or Ta	[104]
Intermetallic hydrides (e.g., $LaNi_5$, TiFe)	Gravimetric capacity	$LaNi_5$: 1.40 wt.% at room temperature below 1 MPa	[112]
	Volumetric capacity	$LaNi_5$: 115 kg H_2 m^{-3}; interstitial hydrides up to about 150 kg H_2 m^{-3}	[54]
	Ease of activation	$LaNi_5$ activated by five absorption–desorption cycles and heat treatment at 623 K; TiFe requires several cycles at high temperature and H_2 pressure above 3 MPa	[112,113]
	Reversibility	Stable reversible absorption and desorption at room temperature below 1.0 MPa	[112]
	Abundance	Ti and Fe are abundant; La and Ni are less abundant	[198]

References

1. Züttel, A.; Remhof, A.; Borgschulte, A.; Friedrichs, O. Hydrogen: The future energy carrier. *Philos. Trans. R. Soc. A* **2010**, *368*, 3329–3342. [CrossRef] [PubMed]
2. Trattner, A.; Klell, M.; Radner, F. Sustainable hydrogen society–Vision, findings and development of a hydrogen economy using the example of Austria. *Int. J. Hydrogen Energy* **2022**, *47*, 2059–2079. [CrossRef]
3. Cox, J.D.; Wagman, D.D.; Medvedev, V.A. *CODATA Key Values for Thermodynamics*; Hemisphere Publishing Corp: New York, NY, USA, 1989.
4. Gündoğan, K. Alternatif Yakıtların Benzinli Motor Performansı Üzerine Etkisinin İncelenmesi. Master's Thesis, Kırıkkale Üniversitesi, Kırıkkale, Turkey, 2005. Available online: https://kutuphane.kku.edu.tr/tez/196757.pdf (accessed on 2 May 2026).
5. Molkov, V. *Fundamentals of Hydrogen Safety Engineering, Part I and Part II*; Bookboon: Copenhagen, Denmark, 2012.
6. Boyle, R. *Tracts Written by the Honourable Robert Boyle Containing New Experiments, Touching the Relation Betwixt Flame and Air, and about Explosions*; Richard Davis: London, UK, 1672.
7. Keçebaş, A.; Kayfeci, M. Hydrogen properties. In *Solar Hydrogen Production*; Elsevier: Amsterdam, The Netherlands, 2019; pp. 3–29. [CrossRef]
8. Greenwood, N.N.; Earnshaw, A. *Chemistry of the Elements*; Elsevier: Amsterdam, The Netherlands, 2012. Available online: https://books.google.com/books?hl=tr&lr=&id=EvTI-ouH3SsC&oi=fnd&pg=PP1&dq=N.+N.+Greenwood+ve+A.+Earnshaw&ots=pRaTQAgsF9&sig=o33McpMquRCCQTILpFPa9MYz3r4 (accessed on 3 February 2026).

9. Hydrogen|Properties, Uses, & Facts|Britannica. Available online: https://www.britannica.com/science/hydrogen (accessed on 20 April 2025).
10. Dincer, I.; Acar, C. Review and evaluation of hydrogen production methods for better sustainability. *Int. J. Hydrogen Energy* **2015**, *40*, 11094–11111. [CrossRef]
11. Dresselhaus, M.S.; Thomas, I.L. Alternative energy technologies. *Nature* **2001**, *414*, 332–337. [CrossRef] [PubMed]
12. Abanades, S.; Poinsot, C.; Charvin, P.; Flamant, G. Hydrogen storage: From conventional methods to emerging opportunities. *Energy Environ. Sci.* **2020**, *13*, 1264–1281.
13. Orhan, M.F.; Dincer, I.; Rosen, M.A.; Kanoglu, M. Integrated hydrogen production options based on renewable and nuclear energy sources. *Renew. Sustain. Energy Rev.* **2012**, *16*, 6059–6082. [CrossRef]
14. Staffell, I.; Scamman, D.; Velazquez Abad, A.; Balcombe, P.; Dodds, P.E.; Ekins, P.; Shah, N.; Ward, K.R. The role of hydrogen and fuel cells in the global energy system. *Energy Environ. Sci.* **2019**, *12*, 463–491. [CrossRef]
15. Zgonnik, V. The occurrence and geoscience of natural hydrogen: A comprehensive review. *Earth-Sci. Rev.* **2020**, *203*, 103140. [CrossRef]
16. International Renewable Energy Agency. *Green Hydrogen: A Guide to Policy Making*; International Renewable Energy Agency: Abu Dhabi, United Arab Emirates, 2020.
17. DOE. *Hydrogen Storage Targets*; U.S. Department of Energy (DOE): Washington, DC, USA, 2020.
18. Materials-Based Hydrogen Storage. Available online: https://www.energy.gov/eere/fuelcells/materials-based-hydrogen-storage (accessed on 9 September 2025).
19. Gross, K.J.; Spatz, P.; Züttel, A.; Schlapbach, L. Mechanically milled Mg composites for hydrogen storage the transition to a steady state composition. *J. Alloys Compd.* **1996**, *240*, 206–213. [CrossRef]
20. Simple Metal and Intermetallic Hydrides. In *Nanomaterials for Solid State Hydrogen Storage*; Fuel Cells and Hydrogen Energy; Springer: Boston, MA, USA, 2009; pp. 83–193. [CrossRef]
21. Barkhordarian, G.; Klassen, T.; Bormann, R. Fast hydrogen sorption kinetics of nanocrystalline Mg using Nb_2O_5 as catalyst. *Scr. Mater.* **2003**, *49*, 213–217. [CrossRef]
22. Kesarwani, R.; Bhatnagar, A.; Verma, S.K.; Hudson, M.S.L.; Shaz, M.A. Enhancement in hydrogen sorption behaviour of MgH_2 catalyzed by graphene quantum dots. *Int. J. Hydrogen Energy* **2024**, *67*, 1026–1032. [CrossRef]
23. Shao, H.; Felderhoff, M.; Schüth, F. Hydrogen storage properties of nanostructured MgH_2/TiH_2 composite prepared by ball milling under high hydrogen pressure. *Int. J. Hydrogen Energy* **2011**, *36*, 10828–10833. [CrossRef]
24. Liang, G.; Huot, J.; Boily, S.; Van Neste, A.; Schulz, R. Catalytic effect of transition metals on hydrogen sorption in nanocrystalline ball milled MgH_2–Tm (Tm = Ti, V, Mn, Fe and Ni) systems. *J. Alloys Compd.* **1999**, *292*, 247–252. [CrossRef]
25. Xu, Y.; Li, Y.; Hou, Q.; Hao, Y.; Ding, Z. Ball Milling Innovations Advance Mg-Based Hydrogen Storage Materials Towards Practical Applications. *Materials* **2024**, *17*, 2510. [CrossRef] [PubMed]
26. Lu, X.; Zhang, L.; Yu, H.; Lu, Z.; He, J.; Zheng, J.; Wu, F.; Chen, L. Achieving superior hydrogen storage properties of MgH_2 by the effect of TiFe and carbon nanotubes. *Chem. Eng. J.* **2021**, *422*, 130101. [CrossRef]
27. Messer, C.E. *A Survey Report on Lithium Hydride*; United States Atomic Energy Commission, Technical Information Service: Oak Ridge, TN, USA, 1960; Volume 9470. Available online: https://books.google.com/books?hl=tr&lr=&id=HY_rl6BAtegC&oi=fnd&pg=PR7&dq=C.+E.+Messer,+%22A+survey+report+on+lithium+hydride,%22+U.S.+Atomic+Energy+Commission,+NYO-9470,+1960.&ots=U6JT7kE6nV&sig=mM7Pytjeq0wMXx_OTIGCOcdfEG8 (accessed on 27 January 2026).
28. Brower, F.M.; Matzek, N.E.; Reigler, P.F.; Rinn, H.W.; Roberts, C.B.; Schmidt, D.L.; Snover, J.A.; Terada, K. Preparation and properties of aluminum hydride. *J. Am. Chem. Soc.* **1976**, *98*, 2450–2453. [CrossRef]
29. Bogdanović, B.; Schwickardi, M. Ti-doped alkali metal aluminium hydrides as potential novel reversible hydrogen storage materials. *J. Alloys Compd.* **1997**, *253–254*, 1–9. [CrossRef]
30. Bogdanović, B.; Felderhoff, M.; Pommerin, A.; Schüth, F.; Spielkamp, N. Advanced hydrogen-storage materials based on Sc-, Ce-, and Pr-doped $NaAlH_4$. *Adv. Mater.* **2006**, *18*, 1198–1201. [CrossRef]
31. Suárez-Alcántara, K.; Tena-Garcia, J.R.; Guerrero-Ortiz, R. Alanates, a Comprehensive Review. *Materials* **2019**, *12*, 2724. [CrossRef] [PubMed]
32. Wang, L.; Aguey-Zinsou, K.-F. Synthesis of $LiAlH_4$ Nanoparticles Leading to a Single Hydrogen Release Step upon Ti Coating. *Inorganics* **2017**, *5*, 38. [CrossRef]
33. Morioka, H.; Kakizaki, K.; Chung, S.-C.; Yamada, A. Reversible hydrogen decomposition of $KAlH_4$. *J. Alloys Compd.* **2003**, *353*, 310–314. [CrossRef]
34. Mamatha, M.; Bogdanović, B.; Felderhoff, M.; Pommerin, A.; Schmidt, W.; Schüth, F.; Weidenthaler, C. Mechanochemical preparation and investigation of properties of magnesium, calcium and lithium–magnesium alanates. *J. Alloys Compd.* **2006**, *407*, 78–86. [CrossRef]
35. Züttel, A.; Wenger, P.; Rentsch, S.; Sudan, P.; Mauron, P.; Emmenegger, C. $LiBH_4$ a new hydrogen storage material. *J. Power Sources* **2003**, *118*, 1–7. [CrossRef]

36. Ngene, P.; Adelhelm, P.; Beale, A.M.; De Jong, K.P.; De Jongh, P.E. $LiBH_4$/SBA-15 Nanocomposites Prepared by Melt Infiltration under Hydrogen Pressure: Synthesis and Hydrogen Sorption Properties. *J. Phys. Chem. C* **2010**, *114*, 6163–6168. [CrossRef]
37. Chłopek, K.; Frommen, C.; Léon, A.; Zabara, O.; Fichtner, M. Synthesis and properties of magnesium tetrahydroborate, $Mg(BH_4)_2$. *J. Mater. Chem.* **2007**, *17*, 3496. [CrossRef]
38. Soloveichik, G.L. Metal borohydrides as hydrogen storage materials. *Mater. Matters* **2007**, *2*, 11–14. Available online: https://www.sigmaaldrich.com/technical-documents/technical-article/materials-science-and-engineering/batteries-supercapacitors-and-fuel-cells/metal-borohydrides (accessed on 27 January 2026).
39. Riktor, M.D.; Sørby, M.H.; Chłopek, K.; Fichtner, M.; Buchter, F.; Züttel, A.; Hauback, B.C. In situ synchrotron diffraction studies of phase transitions and thermal decomposition of $Mg(BH_4)_2$ and $Ca(BH_4)_2$. *J. Mater. Chem.* **2007**, *17*, 4939. [CrossRef]
40. Yan, Y.; Li, H.-W.; Sato, T.; Umeda, N.; Miwa, K.; Towata, S.-I.; Orimo, S.-I. Dehydriding and rehydriding properties of yttrium borohydride $Y(BH_4)_3$ prepared by liquid-phase synthesis. *Int. J. Hydrogen Energy* **2009**, *34*, 5732–5736. [CrossRef]
41. Jeon, E.; Cho, Y. Mechanochemical synthesis and thermal decomposition of zinc borohydride. *J. Alloys Compd.* **2006**, *422*, 273–275. [CrossRef]
42. Pinkerton, F.E.; Meyer, M.S.; Meisner, G.P.; Balogh, M.P.; Vajo, J.J. Phase Boundaries and Reversibility of $LiBH_4$/MgH_2 Hydrogen Storage Material. *J. Phys. Chem. C* **2007**, *111*, 12881–12885. [CrossRef]
43. Karimi, F.; Pranzas, P.K.; Puszkiel, J.A.; Riglos, M.V.C.; Milanese, C.; Vainio, U.; Pistidda, C.; Gizer, G.; Klassen, T.; Schreyer, A.; et al. A comprehensive study on lithium-based reactive hydride composite (Li-RHC) as a reversible solid-state hydrogen storage system toward potential mobile applications. *RSC Adv.* **2021**, *11*, 23122–23135. [CrossRef] [PubMed]
44. Kumar, S.; Nakajima, K.; Singh, A.; Kojima, Y.; Dey, G.K. Assessment of hydrogen storage property of Ca Mg B H system using NMR and thermal analysis techniques. *Int. J. Hydrogen Energy* **2017**, *42*, 26007–26012. [CrossRef]
45. Chen, P.; Xiong, Z.; Luo, J.; Lin, J.; Tan, K.L. Interaction of hydrogen with metal nitrides and imides. *Nature* **2002**, *420*, 302–304. [CrossRef] [PubMed]
46. Leng, H.; Ichikawa, T.; Hino, S.; Hanada, N.; Isobe, S.; Fujii, H. Synthesis and decomposition reactions of metal amides in metal–N–H hydrogen storage system. *J. Power Sources* **2006**, *156*, 166–170. [CrossRef]
47. Luo, W. ($LiNH_2$–MgH_2): A viable hydrogen storage system. *J. Alloys Compd.* **2004**, *381*, 284–287. [CrossRef]
48. Hino, S.; Ichikawa, T.; Leng, H.; Fujii, H. Hydrogen desorption properties of the Ca–N–H system. *J. Alloys Compd.* **2005**, *398*, 62–66. [CrossRef]
49. Baitalow, F.; Baumann, J.; Wolf, G.; Jaenicke-Rößler, K.; Leitner, G. Thermal decomposition of B–N–H compounds investigated by using combined thermoanalytical methods. *Thermochim. Acta* **2002**, *391*, 159–168. [CrossRef]
50. Xiong, Z.; Chua, Y.S.; Wu, G.; Xu, W.; Chen, P.; Shaw, W.; Karkamkar, A.; Linehan, J.; Smurthwaite, T.; Autrey, T. Interaction of lithium hydride and ammonia borane in THF. *Chem. Commun.* **2008**, *43*, 5595. [CrossRef] [PubMed]
51. Chua, Y.S.; Wu, H.; Zhou, W.; Udovic, T.J.; Wu, G.; Xiong, Z.; Wong, M.W.; Chen, P. Monoammoniate of Calcium Amidoborane: Synthesis, Structure, and Hydrogen-Storage Properties. *Inorg. Chem.* **2012**, *51*, 1599–1603. [CrossRef] [PubMed]
52. Dornheim, M.; Doppiu, S.; Barkhordarian, G.; Boesenberg, U.; Klassen, T.; Gutfleisch, O.; Bormann, R. Hydrogen storage in magnesium-based hydrides and hydride composites. *Scr. Mater.* **2007**, *56*, 841–846. [CrossRef]
53. Schlapbach, L.; Züttel, A. Hydrogen-storage materials for mobile applications. *Nature* **2001**, *414*, 353–358. [CrossRef] [PubMed]
54. Züttel, A. Materials for hydrogen storage. *Mater. Today* **2003**, *6*, 24–33. [CrossRef]
55. Osman, A.I.; Ayati, A.; Farrokhi, M.; Khadempir, S.; Rajabzadeh, A.R.; Farghali, M.; Krivoshapkin, P.; Tanhaei, B.; Rooney, D.W.; Yap, P.-S. Innovations in hydrogen storage materials: Synthesis, applications, and prospects. *J. Energy Storage* **2024**, *95*, 112376. [CrossRef]
56. Blagojević, V.A.; Minić, D.G.; Grbović Novaković, J.; Minić, D.M. Hydrogen Economy: Modern Concepts, Challenges and Perspectives. In *Hydrogen Energy—Challenges and Perspectives*; Minic, D., Ed.; InTech: London, UK, 2012. [CrossRef] [PubMed]
57. Sakintuna, B.; Lamaridarkrim, F.; Hirscher, M. Metal hydride materials for solid hydrogen storage: A review. *Int. J. Hydrogen Energy* **2007**, *32*, 1121–1140. [CrossRef]
58. Sandrock, G. A panoramic overview of hydrogen storage alloys from a gas reaction point of view. *J. Alloys Compd.* **1999**, *293–295*, 877–888. [CrossRef]
59. Scarpati, G.; Frasci, E.; Di Ilio, G.; Jannelli, E. A comprehensive review on metal hydrides-based hydrogen storage systems for mobile applications. *J. Energy Storage* **2024**, *102*, 113934. [CrossRef]
60. Abe, J.O.; Popoola, A.P.I.; Ajenifuja, E.; Popoola, O.M. Hydrogen energy, economy and storage: Review and recommendation. *Int. J. Hydrogen Energy* **2019**, *44*, 15072–15086. [CrossRef]
61. Walker, G.S.; Grant, D.M.; Price, T.C.; Yu, X.; Legrand, V. High capacity multicomponent hydrogen storage materials: Investigation of the effect of stoichiometry and decomposition conditions on the cycling behaviour of $LiBH_4$–MgH_2. *J. Power Sources* **2009**, *194*, 1128–1134. [CrossRef]
62. Orimo, S.; Nakamori, Y.; Eliseo, J.R.; Züttel, A.; Jensen, C.M. Complex Hydrides for Hydrogen Storage. *Chem. Rev.* **2007**, *107*, 4111–4132. [CrossRef] [PubMed]

63. Jain, I.P.; Lal, C.; Jain, A. Hydrogen storage in Mg: A most promising material. *Int. J. Hydrogen Energy* **2010**, *35*, 5133–5144. [CrossRef]
64. Ren, L.; Li, Y.; Zhang, N.; Li, Z.; Lin, X.; Zhu, W.; Lu, C.; Ding, W.; Zou, J. Nanostructuring of Mg-Based Hydrogen Storage Materials: Recent Advances for Promoting Key Applications. *Nano-Micro Lett.* **2023**, *15*, 93. [CrossRef] [PubMed]
65. Schneemann, A.; White, J.L.; Kang, S.; Jeong, S.; Wan, L.F.; Cho, E.S.; Heo, T.W.; Prendergast, D.; Urban, J.J.; Wood, B.C.; et al. Nanostructured Metal Hydrides for Hydrogen Storage. *Chem. Rev.* **2018**, *118*, 10775–10839. [CrossRef] [PubMed]
66. Alobaid, A.; Kamil, M.; Khalil, K.A. Metal hydrides for solid hydrogen storage: Experimental insights, suitability evaluation, and innovative technical considerations for stationary and mobile applications. *Int. J. Hydrogen Energy* **2025**, *128*, 432–456. [CrossRef]
67. Christensen, C.H.; Sørensen, R.Z.; Johannessen, T.; Quaade, U.J.; Honkala, K.; Elmøe, T.D.; Køhler, R.; Nørskov, J.K. Metal ammine complexes for hydrogen storage. *J. Mater. Chem.* **2005**, *15*, 4106. [CrossRef]
68. Grochala, W.; Edwards, P.P. Thermal Decomposition of the Non-Interstitial Hydrides for the Storage and Production of Hydrogen. *Chem. Rev.* **2004**, *104*, 1283–1316. [CrossRef] [PubMed]
69. Baran, A.; Polański, M. Magnesium-Based Materials for Hydrogen Storage—A Scope Review. *Materials* **2020**, *13*, 3993. [CrossRef] [PubMed]
70. Graetz, J. New approaches to hydrogen storage. *Chem. Soc. Rev.* **2009**, *38*, 73–82. [CrossRef] [PubMed]
71. Zhang, X.; Zhang, X.; Zhang, L.; Huang, Z.; Yang, L.; Gao, M.; Gu, C.; Sun, W.; Pan, H.; Liu, Y. Nb_2O_5 Nanostructures as Precursors of Cycling Catalysts for Hydrogen Storage in MgH_2. *ACS Appl. Nano Mater.* **2023**, *6*, 14527–14539. [CrossRef]
72. Jangir, M.; Jain, I.P.; Gattia, D.M. Effect of Ti-Based Additives on the Hydrogen Storage Properties of MgH_2: A Review. *Hydrogen* **2023**, *4*, 523–541. [CrossRef]
73. Edalati, K.; Akiba, E.; Botta, W.J.; Estrin, Y.; Floriano, R.; Fruchart, D.; Grosdidier, T.; Horita, Z.; Huot, J.; Li, H.-W.; et al. Impact of severe plastic deformation on kinetics and thermodynamics of hydrogen storage in magnesium and its alloys. *J. Mater. Sci. Technol.* **2023**, *146*, 221–239. [CrossRef]
74. Grill, A.; Horky, J.; Panigrahi, A.; Krexner, G.; Zehetbauer, M. Long-term hydrogen storage in Mg and ZK60 after Severe Plastic Deformation. *Int. J. Hydrogen Energy* **2015**, *40*, 17144–17152. [CrossRef]
75. Mauron, P.; Bielmann, M.; Remhof, A.; Züttel, A.; Shim, J.-H.; Cho, Y.W. Stability of the $LiBH_4/CeH_2$ composite system determined by dynamic PCT measurements. *J. Phys. Chem. C* **2010**, *114*, 16801–16805. [CrossRef]
76. Ali, N.A.; Sazelee, N.A.; Ismail, M. An overview of reactive hydride composite (RHC) for solid-state hydrogen storage materials. *Int. J. Hydrogen Energy* **2021**, *46*, 31674–31698. [CrossRef]
77. Puszkiel, J.; Gasnier, A.; Amica, G.; Gennari, F. Tuning $LiBH_4$ for Hydrogen Storage: Destabilization, Additive, and Nanoconfinement Approaches. *Molecules* **2019**, *25*, 163. [CrossRef] [PubMed]
78. Yartys, V.; Lototskyy, M.; Akiba, E.; Albert, R.; Antonov, V.; Ares, J.; Baricco, M.; Bourgeois, N.; Buckley, C.; von Colbe, J.B.; et al. Magnesium based materials for hydrogen based energy storage: Past, present and future. *Int. J. Hydrogen Energy* **2019**, *44*, 7809–7859. [CrossRef]
79. Reilly, J.J.; Wiswall, R.H. Reaction of hydrogen with alloys of magnesium and nickel and the formation of Mg_2NiH_4. *Inorg. Chem.* **1968**, *7*, 2254–2256. [CrossRef]
80. Milanese, C.; Garroni, S.; Gennari, F.; Marini, A.; Klassen, T.; Dornheim, M.; Pistidda, C. Solid State Hydrogen Storage in Alanates and Alanate-Based Compounds: A Review. *Metals* **2018**, *8*, 567. [CrossRef]
81. Bogdanović, B.; Brand, R.A.; Marjanović, A.; Schwickardi, M.; Tölle, J. Metal-doped sodium aluminium hydrides as potential new hydrogen storage materials. *J. Alloys Compd.* **2000**, *302*, 36–58. [CrossRef]
82. Vajeeston, P.; Ravindran, P.; Kjekshus, A.; Fjellvåg, H. Crystal structure of $KAlH_4$ from first principle calculations. *J. Alloys Compd.* **2004**, *363*, L8–L12. [CrossRef]
83. Majdalawieh, A.F.; Viswanathan, R.; Abu-Yousef, I.A.; Das, P.E.; Narasimhan, S. Efficient and simple protocol employing borohydride systems to design a selective osthol-zirconium (OST-Zr) library from potential natural products. *Mediterr. J. Chem.* **2016**, *5*, 450–457. [CrossRef]
84. Kitano, M.; Yamagata, K.; Hosono, H. Why Ca_2NH works as an efficient and stable support of Ru catalyst in ammonia synthesis. *Res. Chem. Intermed.* **2021**, *47*, 235–248. [CrossRef]
85. Nakamori, Y.; Orimo, S. Destabilization of Li-based complex hydrides. *J. Alloys Compd.* **2004**, *370*, 271–275. [CrossRef]
86. Kojima, Y.; Kawai, Y.; Ohba, N. Hydrogen storage of metal nitrides by a mechanochemical reaction. *J. Power Sources* **2006**, *159*, 81–87. [CrossRef]
87. Hu, Y.H.; Ruckenstein, E. Ultrafast Reaction between LiH and NH_3 during H_2 Storage in Li_3N. *J. Phys. Chem. A* **2003**, *107*, 9737–9739. [CrossRef]
88. Li, H.-W.; Yan, Y.; Orimo, S.; Züttel, A.; Jensen, C.M. Recent Progress in Metal Borohydrides for Hydrogen Storage. *Energies* **2011**, *4*, 185–214. [CrossRef]
89. Rafiee, M.A. Comparison of high pressure-induced phases of $Mg(AlH_4)_2$ as hydrogen storage using ab initio calculated NQCC parameters. *J. Phys. Sci.* **2017**, *28*, 69–79. [CrossRef]

90. Huang, Y.; Zheng, Y.; Li, J.; Bao, X.; Guo, J.; Shen, J.; Guo, Y.; Zhang, Q.; Li, J.; Lei, W.; et al. Li- and Mg-based borohydrides for hydrogen storage and ionic conductor. *J. Mater. Sci. Technol.* **2023**, *153*, 181–204. [CrossRef]
91. Liu, Y.; Chen, W.; Ju, S.; Yu, X.; Xia, G. Stable hydrogen storage of lithium borohydrides via the catalytic effect of Ni_2B induced by thermodynamic destabilization reaction. *J. Mater. Sci. Technol.* **2024**, *202*, 192–200. [CrossRef]
92. Johannessen, T.; Sorensen, R.Z.; Christense, C.H.; Quaade, U.; Norskov, J.K. Metal Ammine Complexes for High-Density Storage of Hydrogen-Bridging the Hydrogen and Ammonia Economy. 2005. Available online: https://www.osti.gov/etdeweb/biblio/20758146 (accessed on 9 October 2025).
93. Rehman, A.U.; Khan, S.A.; Mansha, M.; Iqbal, S.; Khan, M.; Abbas, S.M.; Ali, S. MXenes and MXene-Based Metal Hydrides for Solid-State Hydrogen Storage: A Review. *Chem. Asian J.* **2024**, *19*, e202400308. [CrossRef] [PubMed]
94. Larpruenrudee, P.; Bennett, N.S.; Luo, Z.; Hossain, M.J.; Haque, N.; Sauret, E.; Fitch, R.; Islam, M.S. A Review on the Overall Performance of Metal Hydride-Based Hydrogen Storage Systems. *Energies* **2025**, *18*, 1291. [CrossRef]
95. Bowman, R.C.; Fultz, B. Metallic Hydrides I: Hydrogen Storage and Other Gas-Phase Applications. *MRS Bull.* **2002**, *27*, 688–693. [CrossRef]
96. Reilly, J.J.; Wiswall, R.H. Formation and properties of iron titanium hydride. *Inorg. Chem.* **1974**, *13*, 218–222. [CrossRef]
97. Lototskyy, M.V.; Yartys, V.A.; Pollet, B.G.; Bowman, R.C. Metal hydride hydrogen compressors: A review. *Int. J. Hydrogen Energy* **2014**, *39*, 5818–5851. [CrossRef]
98. Sujan, G.K.; Pan, Z.; Li, H.; Liang, D.; Alam, N. An overview on TiFe intermetallic for solid-state hydrogen storage: Microstructure, hydrogenation and fabrication processes. *Crit. Rev. Solid State Mater. Sci.* **2020**, *45*, 410–427. [CrossRef]
99. McGrady, G.S.; Guilera, G. The multifarious world of transition metal hydrides. *Chem. Soc. Rev.* **2003**, *32*, 383. [CrossRef] [PubMed]
100. Libowitz, G.G. The nature and properties of transition metal hydrides. *J. Nucl. Mater.* **1960**, *2*, 1–22. [CrossRef]
101. Norton, J.R.; Sowa, J. Introduction: Metal Hydrides. *Chem. Rev.* **2016**, *116*, 8315–8317. [CrossRef] [PubMed]
102. Wiedner, E.S.; Chambers, M.B.; Pitman, C.L.; Bullock, R.M.; Miller, A.J.M.; Appel, A.M. Thermodynamic Hydricity of Transition Metal Hydrides. *Chem. Rev.* **2016**, *116*, 8655–8692. [CrossRef] [PubMed]
103. Adams, R.E.; Grusenmeyer, T.A.; Griffith, A.L.; Schmehl, R.H. Transition metal hydride complexes as mechanistic models for proton reduction catalysis. *Coord. Chem. Rev.* **2018**, *362*, 44–53. [CrossRef]
104. Marques, F.; Balcerzak, M.; Winkelmann, F.; Zepon, G.; Felderhoff, M. Review and outlook on high-entropy alloys for hydrogen storage. *Energy Environ. Sci.* **2021**, *14*, 5191–5227. [CrossRef]
105. Yadav, T.P.; Kumar, A.; Verma, S.K.; Mukhopadhyay, N.K. High-Entropy Alloys for Solid Hydrogen Storage: Potentials and Prospects. *Trans. Indian Natl. Acad. Eng.* **2022**, *7*, 147–156. [CrossRef] [PubMed]
106. Somo, T.R.; Lototskyy, M.V.; Yartys, V.A.; Davids, M.W.; Nyamsi, S.N. Hydrogen storage behaviours of high entropy alloys: A Review. *J. Energy Storage* **2023**, *73*, 108969. [CrossRef]
107. Qureshi, T.; Khan, M.M.; Pali, H.S. The future of hydrogen economy: Role of high entropy alloys in hydrogen storage. *J. Alloys Compd.* **2024**, *1004*, 175668. [CrossRef]
108. Wei, M.; Liu, Y.; Xing, X.; Zhang, Z.; Liu, T. $(TiVZrNb)_{83}Cr_{17}$ high-entropy alloy as catalyst for hydrogen storage in MgH_2. *Chem. Eng. J.* **2023**, *476*, 146639. [CrossRef]
109. Liu, H.; Zhang, J.; Sun, P.; Zhou, C.; Liu, Y.; Fang, Z.Z. An overview of TiFe alloys for hydrogen storage: Structure, processes, properties, and applications. *J. Energy Storage* **2023**, *68*, 107772. [CrossRef]
110. Thompson, P.; Reilly, J.J.; Reidinger, F.; Hastings, J.M.; Corliss, L.M. Neutron diffraction study of gamma iron titanium deuteride. *J. Phys. F Met. Phys.* **1979**, *9*, L61–L66. [CrossRef]
111. Percheron-Guégan, A.; Lartigue, C.; Achard, J.C.; Germi, P.; Tasset, F. Neutron and X-ray diffraction profile analyses and structure of $LaNi_5$, $LaNi_{5-x}Al_x$ and $LaNi_{5-x}Mn_x$ intermetallics and their deuterides. *J. Less Common Met.* **1980**, *74*, 1–12. [CrossRef]
112. Sato, T.; Saitoh, H.; Utsumi, R.; Ito, J.; Nakahira, Y.; Obana, K.; Takagi, S.; Orimo, S.-I. Hydrogen Absorption Reactions of Hydrogen Storage Alloy $LaNi_5$ under High Pressure. *Molecules* **2023**, *28*, 1256. [CrossRef] [PubMed]
113. Emami, H.; Edalati, K.; Matsuda, J.; Akiba, E.; Horita, Z. Hydrogen storage performance of TiFe after processing by ball milling. *Acta Mater.* **2015**, *88*, 190–195. [CrossRef]
114. Shaltiel, D.; Jacob, I.; Davidov, D. Hydrogen absorption and desorption properties of AB2 laves-phase pseudobinary compounds. *J. Less Common Met.* **1977**, *53*, 117–131. [CrossRef]
115. Broom, D.P. Hydrogen Storage Materials: The Characterisation of Their Storage Properties. In *Green Energy and Technology*; Springer: London, UK, 2011. [CrossRef]
116. Ovshinsky, S.R.; Fetcenko, M.A.; Ross, J. A Nickel Metal Hydride Battery for Electric Vehicles. *Science* **1993**, *260*, 176–181. [CrossRef] [PubMed]
117. Kohno, T.; Yoshida, H.; Kawashima, F.; Inaba, T.; Sakai, I.; Yamamoto, M.; Kanda, M. Hydrogen storage properties of new ternary system alloys: La_2MgNi_9, $La_5Mg_2Ni_{23}$, La_3MgNi_{14}. *J. Alloys Compd.* **2000**, *311*, L5–L7. [CrossRef]

118. Willems, J. Metal Hydride Electrodes Stability of $LaNi_5$-Related Compounds. Ph.D. Thesis, Technische Hogeschool Eindhoven, Eindhoven, The Netherlands, 1984.
119. Akiba, E.; Iba, H. Hydrogen absorption by Laves phase related BCC solid solution. *Intermetallics* **1998**, *6*, 461–470. [CrossRef]
120. Pericoli, E.; Barzotti, A.; Mazzaro, R.; Moury, R.; Cuevas, F.; Pasquini, L. Synthesis and Hydrogen Storage Properties of Mg-Based Complex Hydrides with Multiple Transition Metal Elements. *ACS Appl. Energy Mater.* **2025**, *8*, 4993–5003. [CrossRef] [PubMed]
121. Martínez-Amariz, A.; Bellon, D. Effect of adding ZrM (M = Fe, Ni) intermetallic compounds on the hydrogen absorption/desorption properties of $TiCr_{1.1}V_{0.9}$ alloy. *Heliyon* **2022**, *8*, e09042. [CrossRef] [PubMed]
122. Liu, J.; Sun, L.; Yang, J.; Guo, D.; Chen, D.; Yang, L.; Xiao, P. Ti–Mn hydrogen storage alloys: From properties to applications. *RSC Adv.* **2022**, *12*, 35744–35755. [CrossRef] [PubMed]
123. Reilly, J.J.; Wiswall, R.H. Higher hydrides of vanadium and niobium. *Inorg. Chem.* **1970**, *9*, 1678–1682. [CrossRef]
124. Murray, J.J.; Post, M.L.; Taylor, J.B. The thermodynamics of the $LaNi_5$-H_2 system by differential heat flow calorimetry I: Techniques; the $\alpha + \beta$ two-phase region. *J. Less Common Met.* **1981**, *80*, 201–209. [CrossRef]
125. Pasturel, A.; Chatillon-Colinet, C.; Guégan, A.P.; Achard, J.C. Thermodynamic properties of $LaNi_4M$ compounds and their related hydrides. *J. Less Common Met.* **1982**, *84*, 73–78. [CrossRef]
126. Van Mal, H.H.; Buschow, K.H.J.; Miedema, A.R. Hydrogen absorption in $LaNi_5$ and related compounds: Experimental observations and their explanation. *J. Less Common Met.* **1974**, *35*, 65–76. [CrossRef]
127. Liang, G.; Huot, J.; Schulz, R. Mechanical alloying and hydrogen storage properties of $CaNi_5$-based alloys. *J. Alloys Compd.* **2001**, *321*, 146–150. [CrossRef]
128. Shang, H.; Li, Y.; Zhang, Y.; Zhao, D.; Qi, Y.; Xu, X. Investigations on hydrogen storage performances and mechanisms of as-cast $TiFe_{0.8}Ni_{0.2}Co$ (m = 0, 0.03, 0.05 and 0.1) alloys. *Int. J. Hydrogen Energy* **2021**, *46*, 17840–17852. [CrossRef]
129. Liu, B.-H.; Kim, D.-M.; Lee, K.-Y.; Lee, J.-Y. Hydrogen storage properties of $TiMn_2$-based alloys. *J. Alloys Compd.* **1996**, *240*, 214–218. [CrossRef]
130. Gamo, T.; Moriwaki, Y.; Yanagihara, N.; Iwaki, T. Life properties of TiMn alloy hydrides and their hydrogen purification effect. *J. Less Common Met.* **1983**, *89*, 495–504. [CrossRef]
131. Pourarian, F.; Wallace, W.E. Hydrogen sorption characteristics of $Zr1-xTix(Cr1-yFey)_2$ alloys. *J. Less Common Met.* **1985**, *107*, 69–78. [CrossRef]
132. Zaluski, L.; Zaluska, A.; Ström-Olsen, J.O. Nanocrystalline metal hydrides. *J. Alloys Compd.* **1997**, *253–254*, 70–79. [CrossRef]
133. Wicke, E.; Brodowsky, H.; Züchner, H. Hydrogen in palladium and palladium alloys. In *Hydrogen in Metals II*; Alefeld, G., Völkl, J., Eds.; Springer: Berlin/Heidelberg, Germany, 1978; Volume 29, pp. 73–155. [CrossRef] [PubMed]
134. Warf, J.C. *Chemical Properties of Uranium Hydride*; Iowa State University: Ames, IA, USA, 1946. Available online: https://search.proquest.com/openview/32f20295082dd6cd41fca3fc6df01104/1.pdf?pq-origsite=gscholar&cbl=18750&diss=y (accessed on 28 January 2026).
135. San-Martin, A.; Manchester, F.D. The H−Ti (Hydrogen-Titanium) system. *Bull. Alloy Phase Diagr.* **1987**, *8*, 30–42. [CrossRef]
136. Montero, J.; Zlotea, C.; Ek, G.; Crivello, J.-C.; Laversenne, L.; Sahlberg, M. TiVZrNb Multi-Principal-Element Alloy: Synthesis Optimization, Structural, and Hydrogen Sorption Properties. *Molecules* **2019**, *24*, 2799. [CrossRef] [PubMed]
137. Sahlberg, M.; Karlsson, D.; Zlotea, C.; Jansson, U. Superior hydrogen storage in high entropy alloys. *Sci. Rep.* **2016**, *6*, 36770. [CrossRef] [PubMed]
138. Zepon, G.; Leiva, D.; Strozi, R.; Bedoch, A.; Figueroa, S.; Ishikawa, T.; Botta, W. Hydrogen-induced phase transition of MgZr-$TiFe_{0.5}Co_{0.5}Ni_{0.5}$ high entropy alloy. *Int. J. Hydrogen Energy* **2018**, *43*, 1702–1708. [CrossRef]
139. Bérubé, V.; Radtke, G.; Dresselhaus, M.; Chen, G. Size effects on the hydrogen storage properties of nanostructured metal hydrides: A review. *Int. J. Energy Res.* **2007**, *31*, 637–663. [CrossRef]
140. Michel, K.J.; Ozoliņš, V. Recent advances in the theory of hydrogen storage in complex metal hydrides. *MRS Bull.* **2013**, *38*, 462–472. [CrossRef]
141. Kim, K.C. A review on design strategies for metal hydrides with enhanced reaction thermodynamics for hydrogen storage applications. *Int. J. Energy Res.* **2018**, *42*, 1455–1468. [CrossRef]
142. Wang, H.; Li, J.; Wei, X.; Zheng, Y.; Yang, S.; Lu, Y.; Ding, Z.; Luo, Q.; Li, Q.; Pan, F. Thermodynamic and Kinetic Regulation for Mg-Based Hydrogen Storage Materials: Challenges, Strategies, and Perspectives. *Adv. Funct. Mater.* **2024**, *34*, 2406639. [CrossRef]
143. Yang, H.; Ding, Z.; Li, Y.; Li, S.; Wu, P.; Hou, Q.; Zheng, Y.; Gao, B.; Huo, K.; Du, W.; et al. Recent advances in kinetic and thermodynamic regulation of magnesium hydride for hydrogen storage. *Rare Met.* **2023**, *42*, 2906–2927. [CrossRef]
144. Wu, X.; Wang, X.; Cao, G.; Li, S.; Ge, H.; Chen, L.; Yan, M. Hydrogen storage properties of $LiBH_4$–Li_3AlH_6 composites. *J. Alloys Compd.* **2012**, *517*, 127–131. [CrossRef]
145. Ershova, O.G.; Dobrovolsky, V.D.; Solonin, Y.M.; Khyzhun, O.Y.; Koval, A.Y. The effect of Al on thermal stability and kinetics of decomposition of MgH_2 prepared by mechanochemical reaction at different conditions. *Mater. Chem. Phys.* **2015**, *162*, 408–416. [CrossRef]

146. Andreasen, A.; Vegge, T.; Pedersen, A.S. Compensation Effect in the Hydrogenation/Dehydrogenation Kinetics of Metal Hydrides. *J. Phys. Chem. B* **2005**, *109*, 3340–3344. [CrossRef] [PubMed]
147. Van Hung, B.; Van, L.A.; Tam, N.H. Advancements in Solid Hydrogen Storage: Enhancing The Performance of MgH_2-Based Materials. In *2025 10th International Conference on Applying New Technology in Green Buildings (ATiGB)*; IEEE: Piscataway, NJ, USA, 2025; pp. 764–770. [CrossRef]
148. Jain, A.; Agarwal, S.; Ichikawa, T. Catalytic Tuning of Sorption Kinetics of Lightweight Hydrides: A Review of the Materials and Mechanism. *Catalysts* **2018**, *8*, 651. [CrossRef]
149. Kimura, T.; Miyaoka, H.; Ichikawa, T.; Kojima, Y. Hydrogen absorption of catalyzed magnesium below room temperature. *Int. J. Hydrogen Energy* **2013**, *38*, 13728–13733. [CrossRef]
150. Bannenberg, L.J.; Boshuizen, B.; Nugroho, F.A.A.; Schreuders, H. Hydrogenation Kinetics of Metal Hydride Catalytic Layers. *ACS Appl. Mater. Interfaces* **2021**, *13*, 52530–52541. [CrossRef] [PubMed]
151. Yao, X.; Zhu, Z.H.; Cheng, H.M.; Lu, G.Q. Hydrogen diffusion and effect of grain size on hydrogenation kinetics in magnesium hydrides. *J. Mater. Res.* **2008**, *23*, 336–340. [CrossRef]
152. Zachariasen, W.H.; Holley, C.E.; Stamper, J.F. Neutron diffraction study of magnesium deuteride. *Acta Crystallogr.* **1963**, *16*, 352–353. [CrossRef]
153. Pasini, J.M.; Corgnale, C.; Van Hassel, B.A.; Motyka, T.; Kumar, S.; Simmons, K.L. Metal hydride material requirements for automotive hydrogen storage systems. *Int. J. Hydrogen Energy* **2013**, *38*, 9755–9765. [CrossRef]
154. Gross, K.J.; Sandrock, G.; Thomas, G.J. Dynamic in situ X-ray diffraction of catalyzed alanates. *J. Alloys Compd.* **2002**, *330–332*, 691–695. [CrossRef]
155. Yang, Y.; Xu, H.; Lu, Q.; Bao, W.; Lin, L.; Ai, B.; Zhang, B. Development of Standards for Hydrogen Storage and Transportation. *E3S Web Conf.* **2020**, *194*, 02018. [CrossRef]
156. *GB/T 33291-2016*; Measurement Method of Pressure-Composition Temperature for Reversible Hydrogen Absorption & Desorption of Hydrides. China Standards Press: Beijing, China, 2016.
157. *JIS H 7003:2007*; Glossary of Terms Used in Hydrogen Absorbing Alloys. Japanese Standards Association: Tokyo, Japan, 2007.
158. *JIS H 7201:2007*; Method for Measurement of Pressure-Composition Temperature (PCT) Relations of Hydrogen Absorbing Alloys. Japanese Standards Association: Tokyo, Japan, 2007.
159. *JIS H 7202:2007*; Method for Measurement of Hydrogen Absorption/Desorption Reaction Rate of Hydrogen Absorbing Alloys. Japanese Standards Association: Tokyo, Japan, 2007.
160. *JIS H 7203:2007*; Method for Measurement of Hydrogen Absorption/Desorption Cycle Characteristic of Hydrogen Absorbing Alloys. Japanese Standards Association: Tokyo, Japan, 2007.
161. *JIS H 7204:1995*; Measuring Methodology for Hydrogenation Thermal Energy of Metal Hydrides. Japanese Standards Association: Tokyo, Japan, 1995.
162. *ISO 16111:2018*; Transportable Gas Storage Devices—Hydrogen Absorbed in Reversible Metal Hydride. International Organization for Standardization: Geneva, Switzerland, 2018.
163. Kwak, Y.J.; Song, M.Y. How to Analyse Metal Hydride Decomposition Temperatures Using a Sieverts' Type Hydriding-Dehydriding Apparatus and Hydrogen-Storage Characteristics for an MgH_2–Based Alloy. *Mater. Sci.* **2018**, *24*, 24–28. [CrossRef]
164. Brown, M.E. (Ed.) *Introduction to Thermal Analysis: Techniques and Applications*; Hot Topics in Thermal Analysis and Calorimetry; Kluwer Academic Publishers: Dordrecht, The Netherlands, 2004; Volume 1. [CrossRef]
165. Nivedhitha, K.; Beena, T.; Banapurmath, N.; Umarfarooq, M.; Ramasamy, V.; Soudagar, M.E.M.; Ağbulut, Ü. Advances in hydrogen storage with metal hydrides: Mechanisms, materials, and challenges. *Int. J. Hydrogen Energy* **2024**, *61*, 1259–1273. [CrossRef]
166. Krishna, R.; Titus, E.; Salimian, M.; Okhay, O.; Rajendran, S.; Rajkumar, A.; Sousa, J.M.G.; Ferreira, A.L.C.; Campos, J.; Gracio, J. Hydrogen Storage for Energy Application. In *Hydrogen Storage*; Liu, J., Ed.; InTech: London, UK, 2012. [CrossRef] [PubMed]
167. Nemukula, E.; Mtshali, C.B.; Nemangwele, F. Metal Hydrides for Sustainable Hydrogen Storage: A Review. *Int. J. Energy Res.* **2025**, *2025*, 6300225. [CrossRef]
168. Kissinger, H.E. Reaction Kinetics in Differential Thermal Analysis. *Anal. Chem.* **1957**, *29*, 1702–1706. [CrossRef]
169. Jia, Y.; Han, S.; Zhang, W.; Zhao, X.; Sun, P.; Liu, Y.; Shi, H.; Wang, J. Hydrogen absorption and desorption kinetics of MgH_2 catalyzed by MoS_2 and MoO_2. *Int. J. Hydrogen Energy* **2013**, *38*, 2352–2356. [CrossRef]
170. Menczel, J.D.; Prime, R.B. *Thermal Analysis of Polymers: Fundamentals and Applications*; John Wiley: Hoboken, NJ, USA, 2009.
171. Czujko, T.; Oleszek, E.E.; Szot, M. New Aspects of MgH_2 Morphological and Structural Changes during High-Energy Ball Milling. *Materials* **2020**, *13*, 4550. [CrossRef] [PubMed]
172. Mustafa, N.S.; Ismail, M. Hydrogen sorption improvement of MgH_2 catalyzed by CeO_2 nanopowder. *J. Alloys Compd.* **2017**, *695*, 2532–2538. [CrossRef]
173. Ismail, M. Effect of $LaCl_3$ addition on the hydrogen storage properties of MgH_2. *Energy* **2015**, *79*, 177–182. [CrossRef]

174. Juahir, N.; Mustafa, N.S.; Sinin, A.M.; Ismail, M. Improved hydrogen storage properties of MgH_2 by addition of Co_2NiO nanoparticles. *RSC Adv.* **2015**, *5*, 60983–60989. [CrossRef]
175. Ismail, M. The Hydrogen Storage Properties of Destabilized MgH_2–AlH_3 (2:1) System. *Mater. Today Proc.* **2016**, *3*, S80–S87. [CrossRef]
176. Zhao, Y.; Zhu, Y.; Liu, J.; Ma, Z.; Zhang, J.; Liu, Y.; Li, Y.; Li, L. Enhancing hydrogen storage properties of MgH_2 by core-shell CoNi@C. *J. Alloys Compd.* **2021**, *862*, 158004. [CrossRef]
177. Yu, H.; Fu, Y.; Jian, C.; Xi, S.; Han, Z.; Fu, M.; Chen, W.; Yang, Y.; Ning, L.; Gao, M. Exploring the Hydrogen Storage Performance of MgH_2 Catalyzed by Two Transition Metals Ni and Co by In-situ Calorimetry and Density Functional Theory Calculations. *ChemistrySelect* **2023**, *8*, e202303280. [CrossRef]
178. Ismail, M.; Zhao, Y.; Yu, X.B.; Mao, J.F.; Dou, S.X. The hydrogen storage properties and reaction mechanism of the MgH_2–$NaAlH_4$ composite system. *Int. J. Hydrogen Energy* **2011**, *36*, 9045–9050. [CrossRef]
179. Ismail, M.; Zhao, Y.; Yu, X.B.; Dou, S.X. Improved hydrogen storage performance of MgH_2–$NaAlH_4$ composite by addition of TiF_3. *Int. J. Hydrogen Energy* **2012**, *37*, 8395–8401. [CrossRef]
180. Ismail, M. Study on the hydrogen storage properties and reaction mechanism of $NaAlH_4$–MgH_2–$LiBH_4$ ternary-hydride system. *Int. J. Hydrogen Energy* **2014**, *39*, 8340–8346. [CrossRef]
181. Borgschulte, A.; Bösenberg, U.; Barkhordarian, G.; Dornheim, M.; Bormann, R. Enhanced hydrogen sorption kinetics of magnesium by destabilized $MgH_2-\delta$. *Catal. Today* **2007**, *120*, 262–269. [CrossRef]
182. Liu, H.; Wang, X.; Liu, Y.; Dong, Z.; Ge, H.; Li, S.; Yan, M. Hydrogen Desorption Properties of the MgH_2–AlH_3 Composites. *J. Phys. Chem. C* **2014**, *118*, 37–45. [CrossRef]
183. Sazelee, N.A.; Ali, N.A.; Ismail, M. The role of MgH_2 in improving the hydrogen storage performance of the KBH_4–$LiAlH_4$ system. *Int. J. Hydrogen Energy* **2026**, *199*, 152863. [CrossRef]
184. Zhang, L.; Lu, X.; Ji, L.; Yan, N.; Sun, Z.; Zhu, X. Catalytic Effect of Facile Synthesized $TiH_{1.971}$ Nanoparticles on the Hydrogen Storage Properties of MgH_2. *Nanomaterials* **2019**, *9*, 1370. [CrossRef] [PubMed]
185. El-Eskandarany, M.S.; Banyan, M.; Al-Ajmi, F. Synergistic Effect of New $ZrNi_5/Nb_2O_5$ Catalytic Agent on Storage Behavior of Nanocrystalline MgH_2 Powders. *Catalysts* **2019**, *9*, 306. [CrossRef]
186. Saadatkhah, N.; Garcia, A.C.; Ackermann, S.; Leclerc, P.; Latifi, M.; Samih, S.; Patience, G.S.; Chaouki, J. Experimental methods in chemical engineering: Thermogravimetric analysis—TGA. *Can. J. Chem. Eng.* **2020**, *98*, 34–43. [CrossRef]
187. Kleperis, J.; Grinberga, L.; Ergle, M.; Chikvaidze, G.; Klavins, J. Thermogravimetric research of hydrogen storage materials. *J. Phys. Conf. Ser.* **2007**, *93*, 012027. [CrossRef]
188. Chen, Y.; Williams, J.S. Formation of metal hydrides by mechanical alloying. *J. Alloys Compd.* **1995**, *217*, 181–184. [CrossRef]
189. Ibikunle, A.; Goudy, A.J.; Yang, H. Hydrogen storage in a $CaH_2/LiBH_4$ destabilized metal hydride system. *J. Alloys Compd.* **2009**, *475*, 110–115. [CrossRef]
190. Choi, Y.J.; Xu, Y.; Shaw, W.J.; Rönnebro, E.C.E. Hydrogen Storage Properties of New Hydrogen-Rich BH_3 NH_3-Metal Hydride (TiH_2, ZrH_2, MgH_2, and/or CaH_2) Composite Systems. *J. Phys. Chem. C* **2012**, *116*, 8349–8358. [CrossRef]
191. Dilts, J.A.; Ashby, E.C. Thermal decomposition of complex metal hydrides. *Inorg. Chem.* **1972**, *11*, 1230–1236. [CrossRef]
192. García De León, M.E.; Téllez-Vázquez, O.; Patiño-Carachure, C.; Rosas Trejo, G.A. DSC-TGA Hydrogen Evaluation during Mechanical Milling of AlFe Intermetallic. *MSF* **2013**, *755*, 105–110. [CrossRef]
193. Kudiyarov, V.N.; Elman, R.R.; Kurdyumov, N.E. The Effect of High-Energy Ball Milling Conditions on Microstructure and Hydrogen Desorption Properties of Magnesium Hydride and Single-Walled Carbon Nanotubes. *Metals* **2021**, *11*, 1409. [CrossRef]
194. Nakagawa, Y.; Isobe, S.; Ohki, T.; Hashimoto, N. Unique Hydrogen Desorption Properties of $LiAlH_4$/h-BN Composites. *Inorganics* **2017**, *5*, 71. [CrossRef]
195. Dahal, R.; Vitillo, J.G.; Åsland, A.C.; Frommen, C.; Deledda, S.; Zavorotynska, O. X-ray and Synchrotron FTIR Studies of Partially Decomposed Magnesium Borohydride. *Energies* **2022**, *15*, 7998. [CrossRef]
196. Chirico, C.; Tsipas, S.A.; Wilczynski, P.; Gordo, E. Beta Titanium Alloys Produced from Titanium Hydride: Effect of Alloying Elements on Titanium Hydride Decomposition. *Metals* **2020**, *10*, 682. [CrossRef]
197. Astorino, C.; De Nardo, E.; Lettieri, S.; Ferraro, G.; Bartoli, M.; Etzi, M.; Chiodoni, A.M.; Pirri, C.F.; Bocchini, S. Investigation of Solid-State Thermal Decomposition of Ammonia Borane Mix with Sulphonated Poly(ellagic Acid) for Hydrogen Release. *Polymers* **2024**, *16*, 3471. [CrossRef] [PubMed]
198. Taylor, S.R.; McLennan, S.M. *The Continental Crust: Its Composition and Evolution*; Blackwell Scientific: Oxford, UK, 1985.
199. Valero, A.; Valero, A. Physical geonomics: Combining the exergy and Hubbert peak analysis for predicting mineral resources depletion. *Resour. Conserv. Recycl.* **2010**, *54*, 1074–1083. [CrossRef]
200. Eggert, R.G. Critical minerals and emerging technologies. *Issues Sci. Technol.* **2010**, *26*, 49–58.

201. Guinée, J.B. *Handbook on Life Cycle Assessment: Operational Guide to the ISO Standards*; Springer Science & Business Media: New York, NY, USA, 2002; Volume 7. Available online: https://books.google.com/books?hl=tr&lr=&id=Q1VYuV5vc8UC&oi=fnd&pg=PR7&dq=J.+B.+Guin%C3%A9e+vd.,+%22Handbook+on+life+cycle+assessment+operational+guide+to+the+ISO+standards,%22+The+International+Journal+of+Life+Cycle+Assessment,+cilt+7,+ss.+311%E2%80%93313,+2002&ots=mYdXijzGLM&sig=YdXmHuH9iwnMfuurfc2eJgCKufI (accessed on 3 February 2026).
202. Schoenung, S.; Hassenzahl, W. *Long- vs. Short-Term Energy Storage Technologies Analysis: A Life-Cycle Cost Study: A Study for the DOE Energy Storage Systems Program*; SAND2003-2783, 918358; Sandia National Laboratories: Albuquerque, NM, USA, 2003. [CrossRef] [PubMed]

Disclaimer/Publisher's Note: The statements, opinions and data contained in all publications are solely those of the individual author(s) and contributor(s) and not of MDPI and/or the editor(s). MDPI and/or the editor(s) disclaim responsibility for any injury to people or property resulting from any ideas, methods, instructions or products referred to in the content.